INSTITUTE FOR AEROSPACE STUDIES

UNIVERSITY OF TORONTO

RESEARCH INTO AIR CUSHION STABILITY: 1978 REPORT

Prepared by

P. A. Sullivan, M. J. Hinchey, P. V. Hartmann and A. Dupuis

for

Transportation Development Centre
Transport Canada
Montreal, Quebec

TP 1760

TDC File D-500-431-1

JANUARY 1981

CA1
DTC 801
81
R21
c.

RESEARCH INTO AIR CUSHION STABILITY: 1978 REPORT

Prepared by

P. A. Sullivan, M. J. Hinchey, P. V. Hartmann and A. Dupuis

for

Transportation Development Centre
Transport Canada
Montreal, Quebec

TP 1760

TDC File D-500-431-1

Library and Information Centre/
Centre de Documentation (GSLA)
RECEIVED - REÇU LE
MAY 4 1983
Transport Canada/Transports Canada

January, 1981

The contents of this report reflect the views of the Contractor and not necessarily the official views or policies of the Transportation Development Centre.

REPORT DOCUMENTATION FORM

1. Transport Canada Report No.	2. TDC Project No.	3. Recipient's Catalogue No.
TP1760	7479	

4. Title and Subtitle	5. Report Date
RESEARCH INTO AIR CUSHION STABILITY 1978 REPORT	January 1981
	6. Performing Organization Report No.
7. Author(s)	8. Transport Canada File No.
P.A. Sullivan, M.J. Hinchey, P.V. Hartmann & A. Dupuis	D1460-125
9. Performing Organization Name and Address University of Toronto Institute for Aerospace Studies 4925 Dufferin Street Downsview, Ontario M3H 5T6	10. DSS File No. T8200-7-7513
	11. DSS or Transport Canada Contract No. OSU-77-00208
12. Sponsoring Agency Name and Address Transportation Development Centre (TDC) 1000 Sherbrooke Street West P.O. Box 549 Montreal, Quebec H3A 2R3	13. Type of Report and Period Covered Yearly - 1978
	14. Sponsoring Agency Code 7479
15. Supplementary Notes	16. TDC Project Officer J.E. Laframboise

17. Abstract

This is the first of two reports which describe research on selected topics in air cushion vehicle (ACV) dynamics undertaken from July 1977 to April 1980. The work had three objectives: (i) investigation of the dynamical properties of an uncompartmented segmented skirt cushion, (ii) development of methods for prediction of the onset of self-excited oscillations and (iii) investigation of structural stability characteristics of flexible skirts. In this report a linear analysis of the effect of ducting on stability of a single plenum chamber shows that even short ducts may have a major destabilizing effect, associated with the inertia of the duct air. The general structure of the stability boundaries in terms of cushion pressure and cushion volume flow is established. A nonlinear analysis of fan-duct plenum systems also shows that ducting has a major effect on the dynamics. A second nonlinear analysis shows that the motion in a linearly unstable regime is usually a limit cycle oscillation. A preliminary investigation of the effect of orifice-cavity combinations on cushion dynamics suggests that they may be destabilizing. A finite difference programme for the computation of turbulent recirculating flows is used to study the steady-state internal flow mechanism within a cushion volume; however a stability analysis based on this mechanism shows that for most cushion geometries flow effects should be insignificant. The development of a computer programme for the analysis of ACV flight tests is described. Finally the effect of wrinkling phenomena and skirt-ground contact on the structural stability of a single conical cell is explored.

18. Key Words	19. Distribution Statement
Air Cushion Stability, Flexibly Skirted Air Cushion, Hovercraft Dynamics Pneumatic Instability	Limited number of copies available at TDC

20. Security Classification (of this report)	21. Security Classification (of this page)	22. No. of Pages	23. Price
None	None		-

TDC CDT 79-005

FORMULE DE DOCUMENTATION POUR RAPPORT

1. N° du rapport Transports Canada	2. N° de l'étude — CDT	3. N° de catalogue du destinataire
TP1760	7479	

4. Titre et sous-titre	5. Date du rapport
RESEARCH INTO AIR CUSHION STABILITY 1978 REPORT	Janvier 1981
	6. N° du rapport de l'organisme exécutant

7. Auteur(s)	8. N° de dossier Transports Canada
P.A. Sullivan, M.J. Hinchey, P.V. Hartmann & A. Dupuis	D1460-125

9. Nom et adresse de l'organisme exécutant	10. N° de dossier — ASC
University of Toronto Institute for Aerospace Studies 4925 rue Dufferin Downsview, Ontario M3H 5T6	T8200-7-7513
	11. N° de contrat — ASC ou Transports Canada OSU-77-00208

12. Nom et adresse de l'organisme parrain	13. Genre de rapport et période visée
Centre de développement des transports (CDT) 1000, rue Sherbrooke ouest C.P. 549 Montréal, Québec H3A 2R3	Annuel - 1978
	14. Code de l'organisme parrain 7479

15. Remarques additionnelles	16. Agent de projet — CDT
	J.E. Laframboise

17. Resumé

Ce document est le premier des deux rapports qui décrit les recherches dans certains domaines du comportement dynamique des véhicules à coussin d'air (VCA) entreprises de juillet 1977 à avril 1980. La recherche visait trois objectifs: (i) recherches sur les propriétés dynamiques d'un coussin d'air unicellulaire à jupe segmentée, (ii) étude des méthodes de prédiction de l'amorce des oscillations auto-entretenues, (iii) recherche sur la stabilité mécanique des jupes souples. Une analyse linéaire de la stabilité dynamique d'une cellule unique, tenant compte de l'inertie de l'air, démontre que des conduits, même courts, peuvent rendre le système instable. Cette analyse définit les limites de stabilité en fonction de la pression et du débit dans le coussin. Une analyse non-linéaire du système ventilateur - conduit - cellule confirme cet effet du conduit sur la dynamique du système. Une seconde analyse non-linéaire montre que le mouvement en régime instable définit par l'analyse linéaire est de type oscillatoire à amplitude limitée. Une étude préliminaire des combinaisons orifice - cavité sur la stabilité du coussin fait croire que ces dispositifs peuvent être déstabilisateurs. Une étude par incréments discrets de l'écoulement turbulent dans une cellule a démontré que pour les cas usuels cet écoulement interne était sans effet sur la stabilité du coussin.

Le rapport décrit ensuite la préparation d'un programme d'analyse d'essais de VCA. Le rapport se termine sur l'étude du plissement des jupes en contact avec le sol et sa conséquence sur la stabilité structurelle d'une cellule conique.

18. Mots-clés	19. Diffusion
Stabilité des coussins d'air, coussin d'air à jupes souples, dynamique des aéroglisseurs, instabilité pneumatique	Nombre limité de copies disponibles auprès du CDT

20. Classification de sécurité (de ce rapport)	21. Classification de sécurité (de cette page)	22. Nombre de pages	23. Prix
Aucune	Aucune		-

CDT/TDC 79-005

PREFACE AND ACKNOWLEDGEMENTS

This is the first of two reports which describe research on some basic aspects of air cushion vehicle (ACV) technology initiated at this Institute as part of a contract with the Transportation Development Centre (TDC) during the period 1 July, 1977 to 1 January, 1980, (TDC File D-500-431). As for previous research for TDC completed at this Institute, although the research was broad ranging in nature, it was oriented towards projects of current Canadian interest. For example, a major emphasis in the present programme has been the investigation of the dynamical properties of an uncompartmented segmented skirt cushion which has been developed in Canada for application to low speed cross-river ferries. The work described in this and the second report (TP3109E) was also partly funded by the first author's Natural Sciences and Engineering Research Council (NSERC) Operating Grant (A3378) and Core Grant (A0982). In general, although NSERC funds have been used to support work of a basic nature, no clear cut distinction has been made between specific projects supported by TDC and those supported by NSERC.

As in past work for TDC, examination of cushion geometries of specific interest to TDC has led to the definition of work of a more fundamental nature. Understanding of these basic questions is often essential to development of design and testing methods, in addition to having intrinsic academic interest. We are very grateful to TDC for allowing us the flexibility to explore these basic questions.

Finally the first author would like to note that since about 1968, he has been attempting to build up a high quality research programme in this new field, one that is recognized as both having the intellectual challenge characteristic of the research tradition at UTIAS and yet at the same time being perceived as relevant to TDC's mission. At the start in 1968 he knew nothing about air cushion technology, and the task has been very difficult; at times it has seemed to be impossible. The present report (TP 1760) reflects to some extent the process of establishing competence in certain techniques, rather than achieving specific results. However, it now seems fair to say that, at the time of writing of this preface, the programme is well established. This is particularly evident in the TP 3109E report, in which three major achievements are described.

The first author would like to express his deep gratitude to Mr. P. L. Eggleton and Mr. J. E. Laframboise of TDC for their sustained financial support, encouragement, and flexibility in allowing him to meet the two success criteria noted above, especially since at times they seemed to be in conflict. The encouragement of his academic colleagues and the efforts of his students have been instrumental in achieving this success. However, most of all, the author would like to record here his deep gratitude to Dr. Michael Hinchey for his efforts, skill and perseverence, first as a student, then as a colleague.

CONTENTS

		Page
1.	INTRODUCTION	1
2.	EFFECT OF DUCTING ON THE HEAVE STABILITY OF PLENUM AIR CUSHIONS	7
	2.1 Introduction	7
	2.2 Geometry of Cushion Model	7
	2.3 Equations for Mathematical Model	8
	2.4 Linear Stability Analysis	11
	2.5 Results	13
	2.5.1 Lumped Capacitance Boundaries	13
	2.5.2 Limiting Behaviour of Lumped Capacitance Boundaries at High and Low Volume Flow	15
	2.5.3 Source of the Instability	15
	2.5.4 Duct Effects Obtained from Finite Element Analysis	16
	2.6 Discussion	16
	2.6.1 Major Feature of the Duct Effect	16
	2.6.2 Behaviour at Very Low Cushion Flows: Helmholtz Resonator Effect	19
	2.6.3 Behaviour of the Stability Boundaries in the Absence of a Duct	20
	2.7 Nonlinear Analysis	21
	2.7.1 Nonlinear Stability Difficulties	21
	2.7.2 Method of Characteristics Analysis	21
	2.7.3 Nonlinear Results	23
	2.8 Transmission Line Analysis Based on the Acoustic Wave Equation	23
	2.9 Conclusions	23
3.	EFFECT OF DUCTING ON THE DYNAMIC FAN CHARACTERISTICS OF AIR CUSHIONS	27
	3.1 Introduction	27
	3.2 Analytical Model	27
	3.3 Results	27
	3.4 Conclusions	30
4.	LIMIT CYCLE OSCILLATIONS OF AIR CUSHIONS	31
	4.1 Introduction	31
	4.2 Nonlinearities in Air Cushion Dynamics	32
	4.3 Air Cushion Model and Equations	34

Contents - Continued

		Page
4.4	Approximate Methods	39
4.5	Illustration of Galerkin Procedure Applied to ACV Problems: The Box Supply Case	43
4.6	Typical Results	46
4.6.1	Box Plenum Model	46
4.6.2	Duct-Plenum Model	46
4.7	Limit Cycle Suppression	54
4.8	Conclusions	58
5.	USE OF ORIFICE-CAVITY COMBINATIONS TO CONTROL STABILITY AND DAMPING	59
5.1	Introduction	59
5.2	Basic Problem	59
5.3	Application to Air Cushion Stability Analysis	64
5.3.1	Formulation	64
5.3.2	Linear Stability Analysis	67
5.3.3	Typical Results	70
5.3.4	Discussion	70
5.4	Conclusion	70
6.	COMPUTATION OF TURBULENT FLOW PATTERNS IN AIR CUSHIONS	73
6.1	Introduction	73
6.2	Problem Formulations	73
6.2.1	Vorticity Transport-Stream Function (ω-ψ) Formulation	74
6.2.2	Stream Function (ψ)	76
6.2.3	Primitive Variable (u,v,p)	76
6.3	Turbulence Modelling	77
6.3.1	Fundamental Problem	77
6.3.2	Eddy Viscosity and Mixing Length Models	77
6.3.3	More Sophisticated Models of Turbulence	78
6.3.4	Equations for the k-ϵ Turbulence Model	79
6.3.5	Limitations of Two-Equation Models	80
6.4	Finite Difference Numerical Procedure	81
6.4.1	Description of Teach T Programme	81
6.4.2	Upwind Difference Schemes	84
6.4.3	Procedure Adopted for the Present Work	85
6.4.4	Application to Single Cell Plenum Chamber	86

Contents - Continued

		Page
6.5	Results	88
6.6	Conclusions: Implications for Dynamic Stability Calculations	91
7.	DEVELOPMENT OF A COMPUTER PROGRAMME FOR ANALYSIS OF CIRCULAR TRACK EXPERIMENTS	103
7.1	Basic Purpose	103
7.2	Description of the Selected Method	106
7.2.1	Overall Concept	106
7.2.2	Formulation of Mathematical Model	107
7.2.3	Criterion Function	108
7.2.4	Parameter Adjustment Algorithm	110
7.3	Development of SPI and Test Programmes	113
7.3.1	Development	113
7.3.2	Simulation Test Programme	113
7.3.3	Example of Test of SPI Programme	114
7.4	Conclusions	120
8.	BUCKLING OF SKIRT MATERIAL	121
8.1	Introduction	121
8.1.1	Discussion of Previous Work	121
8.1.2	Effects of Wrinkling on Membrane Structures	122
8.1.3	Distinction Between Wrinkling and Buckling For the Cone Problem	124
8.1.4	Comments on the Importance of Material Bending Effects	129
8.1.5	Principal Objectives of the Present Work	129
8.2	Effect of a Small Uniform Tension at the Bottom of a Conical Cell	130
8.2.1	Introduction	130
8.2.2	Analysis	130
8.2.3	Results	137
8.2.4	Conclusions	138
REFERENCES		141
APPENDIX A		149

LIST OF FIGURES

		Page
Fig. 1.1	Photograph of the 4.2m x 2.03m Vampire I equipped with uncompartmented segmented skirt cushion and in flight on the 43m diameter circular track	3
Fig. 2.1	Fan-duct-plenum model for finite element heave stability analysis	9
Fig. 2.2	Application of finite element technique to duct problem	12
Fig. 2.3	Lumped capacitance stability boundaries	14
Fig. 2.4	Typical finite element heave stability results. Cases 1 to 6 have values of L_d/D_d = 0.125, 4.0, 8.0, 16.0, 64.0, respectively	17
Fig. 2.5	Comparison of finite element and lumped inertance results for Cases 3 and 6	18
Fig. 2.6	Characteristic lines in the "x-t" plane	22
Fig. 2.7	An illustration of a practical stability calculation for the duct-plenum system	24
Fig. 2.8	Transmission line results for Case 6	25
Fig. 3.1	Dynamic fan characteristics for a duct length of 3.03 metres	28
Fig. 3.2	Dynamic fan characteristics for a duct length of 7.62 metres	28
Fig. 4.1	Basic air cushion geometries studied	33
Fig. 4.2	Assumed behaviour of skirt for $x < 0$	36
Fig. 4.3	Canonical block diagram with one linear element	40
Fig. 4.4	A block diagram for the Vander Pol oscillator	40
Fig. 4.5	Linear heave stability boundary for box-plenum system	47
Fig. 4.6	Runge-Kutta numerical integration results for box-plenum system	49
Fig. 4.7	Linear heave stability boundary for duct-plenum system	51
Fig. 4.8	Amplitude of limit cycle for duct-plenum system	53
Fig. 4.9	Runge-Kutta results for duct-plenum systems	55

List of Figures - Continued

		Page
Fig. 5.1	Geometry of hinged lip TACV cushion tested at UTIAS	60
Fig. 5.2	Typical measured amplitude response of hinged-lip cushion at two damper inlet areas. The heave table ground input is Z and the vehicle response is Y	61
Fig. 5.3	Comparison of theory and experiment for hinged lip cushion with $A_D/A_C = 1/10$	62
Fig. 5.4	Comparison of theory and experiment for hinged lip cushion with $A_D/A_C = 3$	63
Fig. 5.5	Illustrating the Helmholtz resonator model	65
Fig. 5.6	Basic cushion with orifice-cavity attached	65
Fig. 5.7	Typical theoretical stability results for orifice-cavity damper. The hatched line results for $V_o = 3.82\ m^3$ are for V_D lumped with V_C	71
Fig. 5.8	Illustration of possible damping mechanisms that may be important for orifice-cavity resonators	72
Fig. 6.1	Staggered grid-cell arrangement for finite difference calculations	83
Fig. 6.2	Illustrating upwind difference schemes	83
Fig. 6.3	Typical air cushion geometry used for internal flow studies	87
Fig. 6.4	Application of outlet flow boundary condition	87
Fig. 6.5	Wall functions and wall boundary condition	87
Fig. 6.6A	Velocity-vector plot for a simple air cushion. Gap $h = 0.1h_s$ and the laminar Reynolds number R_L based on inlet diameter = 10^5	89
Fig. 6.6B	Velocity-vector plot for a simple air cushion. Gap $h = 0.025h_s$ and $R_L = 10^4$	90
Fig. 6.7	Computed pressure distributions on ground-board for $Re_L = 10^4$ (A) $h = 0.025$ and 0.05	92
	(B) $h = 0.10$ and 0.20	93
Fig. 6.8	Measurements of ground-board pressure distributions on cushion having geometry given in Fig. 6.3. $R_L = 2.8 \times 10^5$	94

List of Figures - Continued

		Page
Fig. 6.9A	Computed pressure profiles at lip for three values of h, $R_L = 10^4$	95
Fig. 6.9B	Computed radial velocity profiles at lip for three values of h, $R_L = 10^4$	95
Fig. 6.10	Radial distribution of axial component of velocity for h = 0.05 and 0.025 with $R_L = 10^4$. Profiles are located approximately at $x = 0.6\ h_s$, see Fig. 6.3. The weak viscous vortex is visible	96
Fig. 6.11	Computed axial distribution for radial component of velocity for three values of h, $R_L = 10^4$	97
Fig. 6.12	Velocity vector plot on air cushion with a baffle plate, $R_L = 10^5$, h = 0.1	98
Fig. 6.13	Postulated simplified models for internal flow effects	100
Fig. 6.14	Radial wall-jet effect on stability	100
Fig. 7.1	Typical outputs of a rate gyro and an accelerometer in Vampire I instrumentation package	104
Fig. 7.2	Block diagram of response matching method of system parameter identification	106
Fig. 7.3	Control inputs used in simulation programme	115
Fig. 7.4	Typical outputs $Z_1(t)$ and $Z_6(t)$ of simulation programme in the absence of noise, generated by the control input of Fig. 7.3 (Case 1)	116
Fig. 7.5	Typical outputs $Z_1(t)$ and $Z_6(t)$ of simulation programme for high noise case	117
Fig. 7.6	Typical outputs for initial condition input (Case 2) for zero noise and high noise respectively	118
Fig. 7.7	Cost function J as a function of number of iterations for runs 1 to 5	119
Fig. 8.1	N-string-beam analogue of wrinkling	123
Fig. 8.2	Stiffness characteristics of string-beam	123
Fig. 8.3	Effect of total weight on roll angle at which wrinkling and buckling first occurs	126
Fig. 8.4	Photographs of polyethylene cell used in tests described in figure 8.3. Large wrinkled regions are clearly visible	127

List of Figures - Continued

		Page
Fig. 8.5	Details of failure process for conical cell. Buckling occurs when points C of the two diamond shaped regions meet	128
Fig. 8.6	Details of skirt-ground contact	131
Fig. 8.7	Coordinate system for conical cell geometry	134
Fig. 8.8	Bottom edge boundary condition with uniform tension applied	134
Fig. 8.9	Geometrical features of conical cell	136
Fig. 8.10	Effect of small uniform tension at bottom edge on onset of wrinkling	139

List of Tables

		Page
Table 4.1	Typical Galerkin results for plenum-box model with first order harmonics only	48
Table 4.2	Initial estimates for iteration: box supply case	48
Table 4.3	Fourier decomposition of numerical simulation for plenum-box model	50
Table 4.4	Galerkin results for point "a" with second harmonics included	50
Table 4.5	Typical Galerkin results for duct-plenum model with first order harmonics only	52
Table 4.6	Initial estimates for iteration: duct supply case	54
Table 4.7	Fourier decomposition of numerical simulation for duct-plenum model	56
Table 4.8	Galerkin limit cycle quenching results for box-plenum system	57
Table 4.9	Galerkin limit cycle suppression results for box plenum system	57
Table 7.1	Matrices $\underset{\sim}{A}$ and $\underset{\sim}{B}$ used in simulations	114
Table 7.2	Matrices $\underset{\sim}{A}$ and $\underset{\sim}{B}$ recovered for runs (2) and (3) Case 1 only	120

NOTATION

Section 2

Arabic

A	Area
a	Sound Speed in Air
C^+ C^-	Characteristic Lines in x-t Plane
C	Fan Slope = $dPf/dQf\big\|_e$
C_M	Orifice Flow Discharge Coefficient
C_i	Capacitance (Volume i)
C_{QC}	Flow Coefficient
D	Diameter
f	Duct Flow Friction Factor
g	Gravitational Acceleration
h	Hover-gap
L	Length
ℓ	Skirt Perimeter at Ground Level
m	Suspension Mass
n	Polytropic Exponent
P	Absolute Pressure
p	Gauge Pressure
Q	Volume Flow of Air
R(x,t)	Residual in Galerkin Solution
R	Orifice Flow Resistance
R	Gas Constant for Air
S_a	Support Area
S	Laplace Transform
T	Temperature of Air

t	Time
V	Volume
v	Flow Velocity in Duct
W	Weight
x	Distance Along Duct from Fan
$Y_n(x)$	Shape Function
Z	Complex Impedance

Greek

α	Orifice Flow Resistance
γ	Ratio of Specific Heats; Isentropic Flow
Δ	Small Perturbation from an Equilibrium State
ρ	Air Density
ω	Oscillation Frequency

Subscripts

a	Lip of Skirt
c	Cushion or Plenum
d	Duct
dc	Duct at Cushion Inlet
df	Duct at Fan
e	Equilibrium Condition
f	Fan
o	Orifice
p	Plenum or Cushion
ref	Reference

NOTATION

Section 3

Arabic

C_p	Pressure coefficient
C_Q	Flow coefficient
D	Fan wheel diameter
f	Frequency hz
N	Fan speed
p	Gauge pressure
Q	Volume flow rate

Greek

ρ	Air density

Subscripts

d	Duct
h	Helmholtz
p	Pressure
$\dot{Q}$	Flow

NOTATION

Section 4

Arabic

A	Area
A	Limit cycle amplitude
a	Isentropic sound speed
A_n, B_n	Coefficients in Galerkin approximation
C_d	Amplitude of volume oscillation (dither)
C_i	Capacitance (volume i)
D	Diameter
e(t)	Error or residual in Galerkin approximation
f(t)	Input to Van der Pol oscillator
g	Gravitational acceleration
h	Hover-gap
j	$\sqrt{-1}$
$L(j\omega)$	Linear part of system
L	Length
m	Mass
$\dot{m}$	Mass flow rate
$N_s(A, \omega)$	Describing function for nonlinear element
n	Polytropic exponent
P	Absolute pressure
p	Gauge pressure
Q	Volume flow rate
S_a	Support area
t	Time
V	Volume
x(t)	Input to nonlinearity

$y(t)$	Output of Van der Pol oscillator

Greek

α, β	Parameters in Van der Pol's equation
γ	Ratio of specific heats
λ	Relaxation factor
π	3.14159
ϕ	Phase angle
ψ	Angle $0 < \psi < 2\pi$
ω	Frequency of limit cycle

Subscripts

a	Approximate
b	Box
c	Cushion
d	Dither
d	Duct
dc	Duct at cushion
df	Duct at fan
e	Equilibrium
f	Fan
o	Bias
p	Plenum

NOTATION

Section 5

Arabic

A	Area
a	Sound speed in air
C	Coefficient
C_A	Slug inertance
C_i	Capacitance (volume i)
C_m	Discharge coefficient
d	Diameter
g	Gravitational acceleration
h	Hover-gap
K_D	Ratio of damper bag feed area to cushion feed area
L	Perimeter
ℓ	Orifice thickness
ℓ'	Slug length = ℓ + end corrections
M	Suspension mass
m	Slug mass
p	Gauge pressure
Q	Volume flow rate
R	Orifice flow resistance
S_a	Support area
s	Laplace transform
t	Time
V	Volume

Greek

α	Gap flow parameter
Δ	Perturbation
π	3.14159
ρ	Air density

Subscripts

a	Atmosphere
b	Box
c	Cushion or plenum
d	Damper
e	Equilibrium
f	Fan
p	Cushion or plenum

NOTATION

Section 6

Arabic

A	Area
C_1, C_2, C_D, C_μ	Constants in turbulence transport equations
C_c	Cushion capacitance
C_p	Specific heat at constant pressure
E	Constant of integration in wall region analysis
f	Characteristic frequency of turbulence
G	Production function
G	Flow
g	Gravitational acceleration
h	Hover-gap
i	Turbulence intensity
k	Kinetic energy of turbulence
k	Thermal conductivity
L	Characteristic length
ℓ	Perimeter
m	Suspension mass
n	Distance from wall
Pe	Peclet number
p	Gauge pressure
δp	Pressure correction
Q	Volume flow rate

Re	Reynolds number
r	Radial coordinate
S_a	Support area
S(u), S(v)	Extra source terms in momentum equations
T	Temperature
t	Time
U	Characteristic velocity
u	Axial velocity
u^t	Tangential velocity
u*	Friction velocity
V	Characteristic velocity
v	Radial velocity
x, y	Cartesian coordinates

Greek

Δ	Perturbation
ϵ	Dissipation rate of turbulence
ϵ	Effective viscosity
κ	Von Karman's constant
μ	Viscosity
ρ	Density
σ_k, σ_ϵ	Turbulent Prandtl numbers
τ	Shear stress
ψ	Stream function
ω	Vorticity

Subscripts

e	Equilibrium
ef	Effective
in	Inlet
jet	Radial wall jet
ℓ, L	Laminar
o	Orifice
out	Outlet
P N S E W	Node labels: north N, south S, east E, west W
t	Turbulent
W	wall

NOTATION

Section 7

Arabic

$\underset{\sim}{A}$	System matrix
$\underset{\sim}{B}$	Control matrix
c	Damping coefficient
$\underset{\sim}{C}$	Unknown coefficients vector
$\underset{\sim}{F}$	State transformation matrix
$\underset{\sim}{G}$	Control transformation matrix
J	Cost function to be minimized
k	Spring constant
m	Mass
$\underset{\sim}{n}(t)$	Measurement noise vector
$\underset{\sim}{u}(t)$	Input vector
$\underset{\sim}{W}$	Weighting matrix: expresses the confidence in various measurements
x(t)	Displacement
$\underset{\sim}{X}(t)$	Experimental response vector
$\underset{\sim}{X}_e(t)$	Calculated response vector
$\underset{\sim}{Z}(t)$	Measured response vector

Greek

$\underset{\sim}{\gamma}(t)$	Difference between measured and calculated response

NOTATION

Section 8

Arabic

C_{ST}	Skirt thickness divided by suitable reference dimension
D	Diameter
H	Height from apex of cone
k_s	String stiffness
M	Moment
N	Stress
P	Load
p	Pressure
s	Generator coordinate

Greek

α	Cone included angle ($90°-\beta$)
β	Taper angle of cone
θ	Critical angle
θ	Angular coordinate
ϕ	Rotation deflection

Subscripts

B	Buckling
W	Wrinkling

1. INTRODUCTION

This report is the first of two which describe the results of research on selected topics in the dynamics of air cushion vehicles (ACV) undertaken as part of a contract with the Transportation Development Centre (TDC - File D-500-431). The work has been focussed mainly on the effects of flexible skirts on the stability and other aspects of the overall vehicle dynamics. However, other basic cushion dynamical problems identified during previous TDC contracts have also been investigated. The period covered by the two reports is approximately July, 1977 to April, 1980.

The research undertaken at the Institute (UTIAS) on cushion dynamics since 1974 has generally been aimed at providing a basic understanding of cushion geometries of current interest to TDC. Work under previous contracts reflected TDC's involvement in projects using multicell type cushions, originally based on the designs of SEDAM et Cie of France, and Jones, Kirwan and Associates of Canada. During the tenure of the present Contract, the cushion system of current interest has been that developed by Hoverlift Systems of Calgary (HSL). This is a variant of the uncompartmented loop and segment skirt cushion developed originally by Hovercraft Development Limited (HDL) of Britain. The objectives of the present Contract reflected this perspective. They were:

(i) To provide information on the stability and other dynamical characteristics of vehicles equipped with the HSL skirt, both when hovering at rest and in motion over certain obstacles such as a ramp,

(ii) To provide mathematical criteria for prediction of the onset of self-excited oscillations,

(iii) To provide a description and mathematical treatment of the structural stability of flexible skirts with specific reference to a conical cell.

The second and third objectives are essentially continuations of work undertaken as part of the immediately preceding Contract (TDC File No. D-500-308). It is noted that these are all particular aspects of the more general problem of formulating mathematical models of the dynamics of flexible skirt cushions for engineering prediction purposes. As such, progress in the understanding of any one of them may shed light on the others. For example, the second objective requires a linear stability analysis of certain features of the models developed for the first objective.

It should also be noted that the present work is intended to develop aids to design and development, and it therefore attempts to investigate questions of perceived practical significance. However, the processes involved in air cushion vehicle dynamics can be very complex, so that some judgement has to be used in selecting the aspects for detailed investigation. Hence the success of the work depends critically on the choice of relevant problems. Furthermore it is intended that the mathematical models developed should be no more complex than is necessary to achieve a desired level of accuracy of prediction.

This point may be illustrated by discussing briefly a phenomenon encountered during previous work on multicell cushions for TDC. The experimentally measured static roll and pitch stiffness characteristics of certain

cushions exhibitied a very large hysteresis. This is believed to be associated with the viscoelastic or stress relaxation phenomena characteristics of some of the elastomer-fabric materials used to build these model skirts. It can have a major effect on the vehicle dynamics, but can be made negligible by using sufficiently thin material. The crucial question is: Can such hysteresis phenomena be significant on full scale vehicles and for other skirt geometries? No information on either point has been made available to the authors of this report and, even though the phenomenon is intrinsically interesting, work on it has usually been postponed until some indications of its practical significance have been obtained.

The first objective of the present Contract involved construction of HSL skirt systems according to specifications supplied by H. S. Fowler of the National Research Council of Canada (NRC) for both the UTIAS 43m diameter Circular Track test vehicle, Vampire I, and the UTIAS cushion dynamics facility. For the Vampire I model, which has a 4.2 x 2.03m planform, the individual segments were the same size and made of the same material as NRC's 4.0 x 2.5m HEX 4. This material has a 0.46 mm thick neoprene-coated nylon fabric supplied by Uniroyal of Canada. The segments for the 2.44 x 1.22m cushion dynamics facility were scaled down appropriately, and two sets constructed, each of different material. The first material was recommended by J. E. Rapson (HDL) as suitable for model tests; it was a 0.10mm thick urethane coated nylon supplied by B and M Coatings of Britain. The second was 0.12 mm thick extruded polyethylene film. Because the HSL skirt on Vampire 1 was found to exhibit significant hysteresis in pitch and roll, towards the end of the Contract, a second set of segments for this vehicle was manufactured from the nylon/urethane material. Figure 1.1 is a photograph of the Vampire I in flight on the Track.

The programme for the cushion dynamics facility model was the same as that adopted for multicell models investigated previously, that is, development of a theory for the static pitch and roll stiffness characteristics of the HSL cushion and comparison with experimental measurements. However, the programme for the Vampire I model was much more ambitious than anything undertaken previously using the Circular Track facility; it was the first attempt to use the overall system, including vehicle, dynamics instrumentation and data acquisition system (DAS), to explore vehicle dynamics. The basic experimental concept was very simple, namely, to record the response of accelerometers, angular rate gyros and other transducers carried on board the vehicle when it was flown over a ramp disturbance at various forward speeds and for a range of cushion air flow rates. It was intended that the ramp would excite only the combined pitch-heave dynamics, this being the simplest case possible. The results were to be analyzed for comparison with a suitable theory.

The Circular Track programme required, in addition to construction of a new base for Vampire I, two major developments. The first involved a redesign of the DAS in order to facilitate a large reduction of the weight of the cable that tethered the vehicle to the centre-post of the Track. The second was the development of a computer programme for the analysis of the Circular Track test data. The reasons for these requirements are described briefly in turn.

The original DAS, designed prior to 1974, had a total of sixteen transducers carried on board the vehicle. The outputs from these transducers were amplified on board, and then transmitted in analog form to the facility Control Room, where they were digitized and then stored by a small digital computer on magnetic tape. The signal cable, which was attached to the main tether cable,

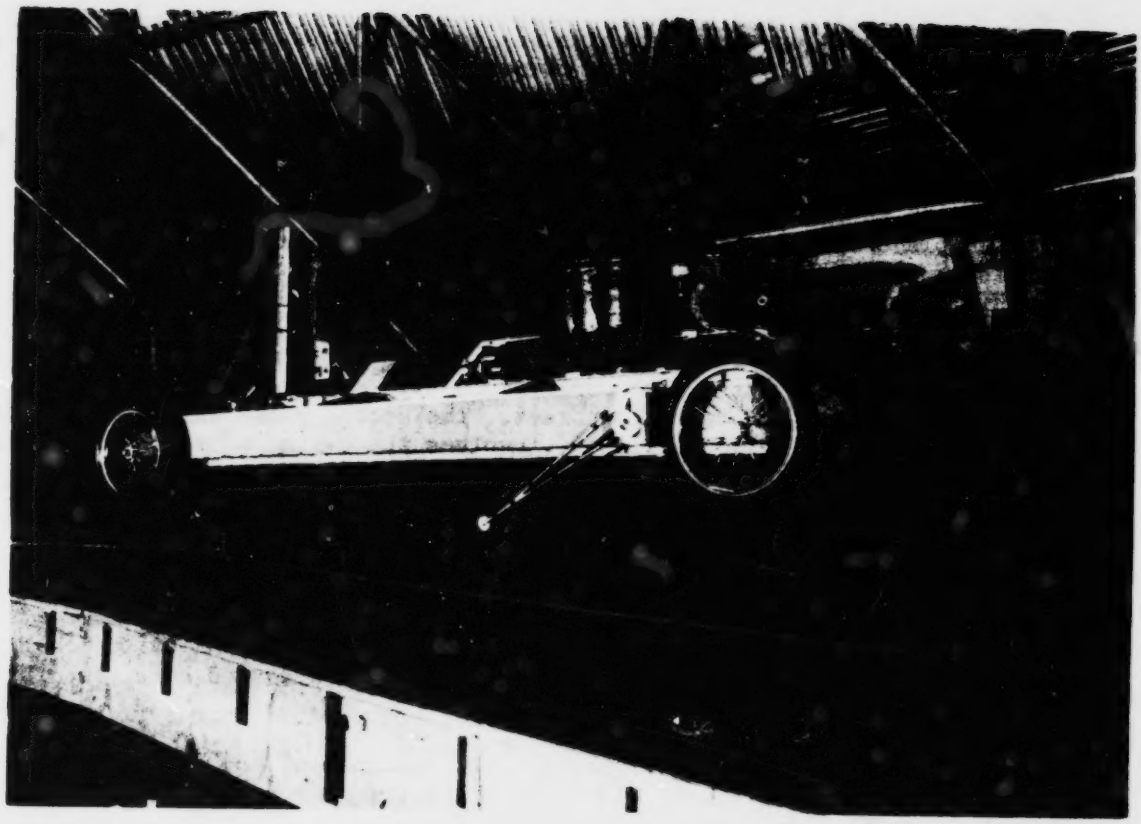

FIGURE 1.1 PHOTOGRAPH OF THE 4.2m x 2.03m VAMPIRE 1 EQUIPPED WITH UNCOMPARTMENTED SEGMENTED SKIRT CUSHION AND IN FLIGHT ON THE 43m DIAMETER CIRCULAR TRACK

consisted of sixteen twisted, shielded pairs of wires. The weight of the entire cable, comprising tether cable, signal cable, and power supply cable, was so high that the cable dynamics coupled strongly with the vehicle dynamics. Typically, flight over a disturbance would cause cable oscillations which, in turn, could induce a pronounced, lightly damped yaw oscillation in the vehicle motion. The high cable weight also caused another difficulty: it imposed a minimum operating speed which was well above that required to allow proper scaling of certain experiments. The signal cable contributed the major component of the cable weight. The presence of large cable effects was a significant departure from the original elegant concept envisaged by B. Etkin of UTIAS, which was to use a cable which was so light that it behaved quasistatically, and thus avoid the necessity of measuring cable dynamic behaviour in order to separate these from true air cushion phenomena.

During the tenure of the present contract, advantage of recent developments in integrated circuits and microprocessor technology was taken to eliminate the analog signal cable. Implementation of the replacement system has taken place in two phases. Both involve simultaneous sampling all sixteen channels of data every 1/100 second and digitizing by a unit carried on board the vehicle. The data is encoded for serial transmission along a single very light cable to a second unit in the control room. This unit then transmits the data to the data acquisition computer for storage on magnetic tape and subsequent analysis. This phase was completed in 1978 and was used for the experiments performed for the present Contract. The second phase which, at the time of writing, is still being developed, involves the use of a dedicated microprocessor to perform certain elementary data processing functions. This includes adjustable signal gain and automatic zeroing of channels.

This work was completed by D. Ribner under the general direction of A. J. Cousin, a member of the staff of the Department of Electrical Engineering at the University of Toronto. Mr. Ribner undertook the project as part of a Master's Degree programme, and was supported by a TDC Transportation Scholarship. A detailed report on this system has not been included here, but is available as a UTIAS Technical Note.

The computer programme developed for the analysis of the data obtained from the Circular Track experiments was essentially the same as that used for the interpretation of flight test experiments of aircraft. In this procedure, experimentally measured histories of such quantities as accelerations are not compared directly with the theoretical predictions. The very large quantity of data makes a systematic comparison in this form very difficult to obtain. Instead, a mathematical model for the cushion processes of interest is postulated. This model is normally derived from theoretical considerations but, in contrast to a theoretical analysis, coefficients in the differential equations are assumed to be unknowns. The data processing procedure then searches for the coefficients of this system of equations which enable their theoretical predictions to best fit the data. The comparison between the experiment and theory is done in terms of the coefficients obtained by theory and by fitting the data. Such a procedure may be termed "system parameter identification" (SPI) and its philosophy and use is well

---

*Ribner, D., "A Remote Data Acquisition and Control System", UTIAS TN (to be published)

known in many fields of engineering. However, it is believed that this Contract represents the first time that such a procedure has been used in ACV technology development. Also, development of a suitable programme is not a simple task. Consequently, a description of the basic concept finally chosen and of the way in which it was tested before being used on the Circular Track data is given in Section 7 of this report.

The results of the work undertaken on the HSL cushion are described in Sections 3 and 4 of the second report. Section 3 describes the theory developed for the static pitch and roll stiffness characteristics of the HSL cushion, and the experimental results obtained on the 2.44 x 1.22 cushion facility. Section 4 describes the results obtained from the Circular Track tests.

Work at UTIAS on the problem of predicting the onset of self-excited oscillations of ACV's, the second objective of the present Contract, started prior to the commencement of the preceding Contract (D500-308). It was motivated originally by problems encountered by a Canadian company. More generally, it appears that they may pose a serious difficulty for certain applications, such as large platforms operating over land or water. Some exploratory measurements undertaken at the Company's facilities had suggested that, of the factors affecting stability not apparently included in analyses of the problem available at that time, one seemed to have the most practical significance. This was the effect of internal flow structure within a given cell on stability. Consequently, in an attempt to understand this phenomenon, it was decided to explore the use of numerical methods for prediction of recirculating turbulent flow structure in a cushion cell. In view of the complexity of even this first step, it was also decided to develop the appropriate numerical methods by applying them to the much simpler problem of the effect of ducting on stability. For this problem, the fluid mechanics could be modelled by the equations for one-dimensional unsteady flow. The numerical results obtained suggested that even moderately short ducting could have a major effect on stability, greatly exceeding anything attributable to internal flow structure. These results had been obtained just prior to the termination of Contract D-500-308. Consequently, a major effort to interpret them and to provide physical insights into this duct effect has been made, and the results are given in Section 2 of this report. The structure of the stability boundaries is discussed in terms of the two quantities of basic interest to the designer, cushion pressure and cushion volume flow, and it is believed it is the first to do this in any detail. An excellent experimental confirmation has been obtained by using a very large volume between the air supply fan and the test duct to uncouple fan dynamics. This is described in Section 2 of the second report.

Some work on other aspects of the self excited oscillation problem has also been completed. Section 3 demonstrates the very large effect that ducting may have on the equivalent fan characteristic that the cushion experiences during such oscillations. A question of fundamental interest which is not addressed by a linear stability analysis is: what is the nature of the motion that ultimately occurs as a result of instability? A nonlinear analysis of two simple geometries confirms inferences made from experiments, which is that the resultant motion is usually a stable finite amplitude oscillation or limit cycle. A practical motivation for this work is the interest in the possibility that such oscillations

might be used to generate oscillatory pressure signals on ground for geological survey purposes, but the main interest is that measurements of the dynamical properties of these oscillations may be used as a sensitive test of nonlinear aspects of mathematical models of cushion processes.

Development of methods of suppressing self-excited oscillations has considerable practical significance, and one suggested technique is the application of orifice-cavity combinations, or "Helmholtz Resonators". Section 5 describes a linear stability analysis of a simple cushion equipped with such a device. Contrary to expectations, it suggested that such devices would have a destabilizing effect. However, some limitations of the analysis are identified, although no further work has been attempted.

Section 6 describes the theoretical work that was ultimately done on the effect of internal flow structure on stability. The numerical predictions of the steady state flow patterns inside a cushion cell, obtained by application of a finite difference technique to the equations commonly used to describe turbulent flows, did suggest a mechanism by which a significant internal flow effect might occur. A stability analysis based on this idea is also described in Section 6; it is shown that the effect would only occur for particular geometries, and then would only be significant at relatively high cushion flow rates. The experiments described in Section 2 of the second report confirm the existence of this mechanism.

The work done towards the third objective of the present Contract - investigation of structural stability of flexible skirt systems - is much more limited in scope than that done for the first two. It is the continuation of an investigation of the buckling properties of a conical cell of the type first used in the SEDAM multicell cushion. A simple theory for the buckling of this cell that occurs when it is rolled to a sufficiently large angle was developed during the tenure of the preceding Contract (D-500-308). However experiments indicated that the phenomenon could be considerably more complex, and raised several fundamental questions. It is believed that these questions may have practical significance for any skirt geometry, and the research described in this and the second report addresses them. A problem encountered in the investigation of skirt systems is that the complexity of some cushion geometries, such as the segments of the HSL skirt investigated here, makes them unsuitable for simple mathematical analysis. Hence the work has continued to use the conical cell geometry, because it is about the simplest possible that has the features intrinsic to a flexible skirt. The work completed is described in Section 8 of this report and Section 5 of the second report.

2 EFFECT OF DUCTING ON THE HEAVE STABILITY OF PLENUM AIR CUSHIONS

2.1 Introduction

While some important insights into the factors that affect heave stability have been obtained by using lumped capacitance and resistance concepts [Refs. 2.1 to 2.4], only recently have other factors such as the distributed properties of ducting and lift fan dynamics been considered. Sweet, Richardson, and Wormley Ref. 2.5 used a linear model, based on the one dimensional wave equation and the well known transmission line solution techniques [Ref. 2.6, 2.7], to show the effect of ducting on overall system frequency response. They used a product expansion technique [Ref. 2.6] to approximate the infinite order duct transfer function by a finite order model and recommended that, although in certain restricted circumstances the duct might be represented by a lumped capacitance or a lumped inertance, their first order model should be used, since this involved only a slight increase in model complexity. This first order model may be thought of as a combined capacitance-inertance model. They concluded that duct dynamics could increase or decrease stability, but observed that, in a situation where the cushion is a primary suspension and the vehicle is connected to the cushion by a suitable secondary suspension, duct dynamics would have only a minor influence on the vehicle behaviour but would have a major influence on the primary suspension behaviour. This is typical of a TLV application. Goldschmied and Wormley [Ref. 2.8] extended the above work to include the effect of blower dynamics on frequency response.

Very little attention has been paid in the literature to the nonlinear aspects of cushion dynamics and stability. An important exception is the analysis by Leatherwood [Ref. 2.9], who, among other things, showed that small transient disturbances could trigger large subharmonic responses. On the other hand, Wormley, Garg, and Boghani [Ref. 2.10] compared the linear and nonlinear responses to transient disturbances of a TLV type suspension and concluded that a linear model should provide a good initial basis for design purposes.

In this section, both linear and nonlinear analyses of the heave stability of a fan-duct-plenum air cushion suspension system are presented. The linear analysis uses a quasi-static pressure-flow relationship for the fan, a finite element discretization for one dimensional unsteady duct flow, and a lumped capacitance model for the plenum. Its results indicate that even relatively short ducts can have a significant effect on the stability of cushion systems typically used on amphibious and overland vehicles. The nonlinear analysis uses the method of characteristics for the duct flow and the nonlinear orifice flow relationships. Its results suggest that the linear analysis should be adequate for practical stability calculations.

2.2 Geometry of Cushion Model

Since the purpose of the present work is to provide an insight into the very large duct effects first encountered during the previous TDC contract [Ref. 2.11] the same cushion geometry is used here. It is a single

cell plenum chamber, the walls of which are made from a slightly tapered cone. Although this geometry was originally chosen because it formed part of a multicell cushion being tested for TDC [Ref. 2.12], its main advantage here is its simplicity. In addition to facilitating the required insights, it is also amenable to experimental confirmation.

The model is shown in Figure 2.1. A fan with a known characteristic for pressure p_f is a function of volume flow Q_f supplies air through an orifice with area A_f into a straight rigid duct having a variable length to diameter ratio L_d/D_d but constant total volume $V_d = 1.415\ m^3$. The duct in turn feeds the cushion cell which has a diameter $D_p = 1.83m$ and a height $L_p = 0.915m$ through an orifice with area A_c. The cell is free to move in heave while the duct is fixed in the inertial reference frame. Although in practice the cell wall is flexible, the flexibility is ignored.

2.3 Equations for Mathematical Model

The well known lumped parameter equations for the basic cushion are used [Refs. 2.1, 2.5]. These are: (1) Newton's law for forces on the cushion

$$m \frac{d^2h}{dt^2} = S_a p_c - mg \tag{1}$$

where m is the cushion mass, t is time, h is the hovergap, S_a is the pressurized support area, and p_c is the gauge cushion pressure; and (2) the compressible unsteady mass conservation equation for the cushion volume

$$C_c \frac{dp_c}{dt} = (Q_c - Q_a) - S_a \frac{dh}{dt} \tag{2}$$

In the latter equation, Q_c is the volume flow into the cushion, Q_a is the flow under the cushion lip to atmosphere, and C_c is the cushion capacitance. It is usual to assume that the cushion thermodynamic compression-expansion processes can be described by a polytropic equation of state, P/ρ^n = constant, so that, if V_c is the total cushion volume, $C_c = V_c/nP_c$ for pressure perturbations which are small compared to the absolute pressure P_c. For the present analysis, it is assumed that the oscillation frequencies are sufficiently high that the compression-expansion processes can be taken to be isentropic, in which case $n = \gamma$, the specific heat ratio, and

$$C_c = \frac{V_c}{\rho a^2} \tag{3}$$

where $a = \sqrt{\gamma RT}$ is the sound speed and ρ is the air density. The flows Q_c and Q_a is assumed to be inviscid, incompressible and quasi-steady. Thus

$$Q_c = C_m A_c \left(\frac{2(p_{dc} - p_c)}{\rho} \right)^{1/2} \tag{4}$$

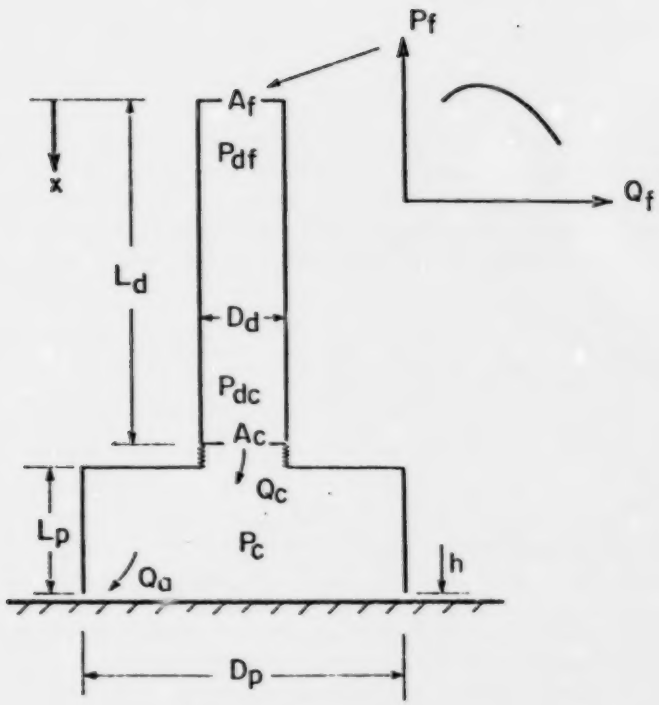

FIG. 2.1 FAN-DUCT-PLENUM MODEL FOR FINITE ELEMENT HEAVE STABILITY ANALYSIS.

$$Q_a = C_m \ell h \left[\frac{2p_c}{\rho}\right]^{1/2} \tag{5}$$

where C_m is the usual discharge coefficient and ℓ is the cushion perimeter at ground level. For the stability analysis, the above equations are linearized about an equilibrium or operating point [Ref. 2.1] to obtain

$$m \frac{d^2\Delta h}{dt^2} = S_a \Delta p_c \tag{6}$$

$$C_c \frac{d\Delta p_c}{dt} = (\Delta Q_c - \Delta Q_a) - S_a \frac{d\Delta h}{dt} \tag{7}$$

$$C_c = \frac{V_{ce}}{\rho a^2} \tag{8}$$

$$\Delta Q_c = \frac{\Delta p_{dc} - \Delta p_c}{R_c} \tag{9}$$

$$\Delta Q_a = \frac{\Delta p_c}{R_a} + \frac{\Delta h}{\alpha_a} \tag{10}$$

where

$$R_f = \frac{2(p_{ce} - p_{dfe})}{Q_e}, \quad R_c = \frac{2(p_{dce} - p_{ce})}{Q_e}, \quad R_a = \frac{2p_{ce}}{Q_e}, \quad \alpha_a = \frac{h_e}{Q_e} \tag{11}$$

where the subscript "e" indicates an equilibrium value and the symbol Δ indicates a small disturbance from equilibrium.

To include the duct properties, the partial differential equations for one dimensional unsteady duct flow with friction, namely continuity and momentum, combined with a polytropic equation of state, are used [Ref. 2.7].

Momentum

$$\frac{\partial v}{\partial t} + v \frac{\partial v}{\partial x} + \frac{fv|v|}{2D_d} + \frac{1}{\rho} \frac{\partial p}{\partial x} = 0 \tag{12}$$

Continuity

$$\rho \frac{\partial v}{\partial x} + \frac{\rho}{nP_d} \left(v \frac{\partial p}{\partial x} + \frac{\partial p}{\partial t}\right) = 0 \tag{13}$$

where x is the distance along the duct measured from the fan, v is the flow velocity, and f is a turbulent flow friction factor. These in turn are linearized in the usual way to obtain

Momentum

$$\frac{\partial \Delta v}{\partial t} + v_e \frac{\partial \Delta v}{\partial x} + \frac{f v_e}{D_d} \Delta v + \frac{1}{\rho} \frac{\partial \Delta p}{\partial x} = 0 \qquad (14)$$

Continuity

$$\rho \frac{\partial \Delta v}{\partial x} + \frac{\rho}{n P_d} \left(\frac{dp_e}{dx} \Delta v + v_e \frac{\partial \Delta p}{\partial x} + \frac{\partial \Delta p}{\partial t} \right) = 0 \qquad (15)$$

The upstream boundary condition on the duct flow is also linearized appropriately.

2.4 Linear Stability Analysis

Equations (14) and (15) govern the pressure and flow velocity perturbations which occur along the duct during small amplitude unsteady operation. Here, a finite element Galerkin procedure is used to reduce these partial differential equations to ordinary differential equations in time. The perturbations in pressure and flow velocity are assumed to be given by

$$\Delta p(x,t) = \sum_{n=1}^{m} \Delta p_n(t) Y_n(x) \qquad (16a)$$

$$\Delta v(x,t) = \sum_{n=1}^{m} \Delta v_n(t) Y_n(x) \qquad (16b)$$

where, here, the coefficients $\Delta p_n(t)$ and $\Delta v_n(t)$ are approximations to the pressure and velocity perturbations which occur at specific positions along the duct. Following the usual finite element procedure, normalized piecewise continuous roof functions [Ref. 2.13] are used for the basis functions $Y_n(x)$, typical examples of which are shown in Figure 2.2. When the assumed solution forms (16.a) and (16.b) are substituted into the differential equations (14) and (15), two residuals, $R_m(x,t)$ and $R_c(x,t)$ respectively, are obtained. By using the basis functions as weighting functions and writing

$$\int_0^{L_d} Y_i(x) R_m(x,t) dx = \int_{x_{i-1}}^{x_{i+1}} Y_i(x) R_m(x,t) dx = 0 \qquad (17a)$$

$$\int_0^{L_d} Y_i(x) R_c(x,t) dx = \int_{x_{i-1}}^{x_{i+1}} Y_i(x) R_c(x,t) dx = 0 \qquad (17b)$$

these residuals are made orthogonal to m members of a complete set of functions [Refs. 2.13, 2.14]. One advantage of the finite element procedure, when compared to the more usual Galerkin procedure, is that the formal

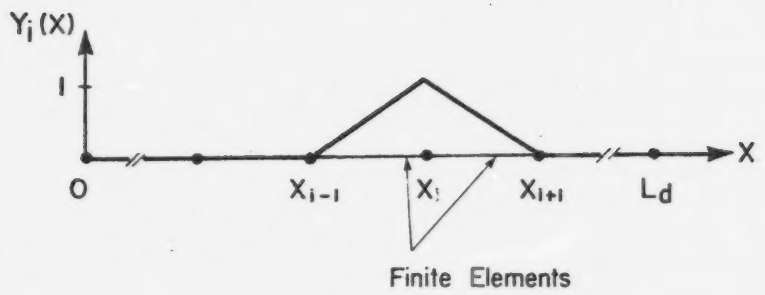

TYPICAL PIECEWISE LINEAR SHAPE FUNCTION

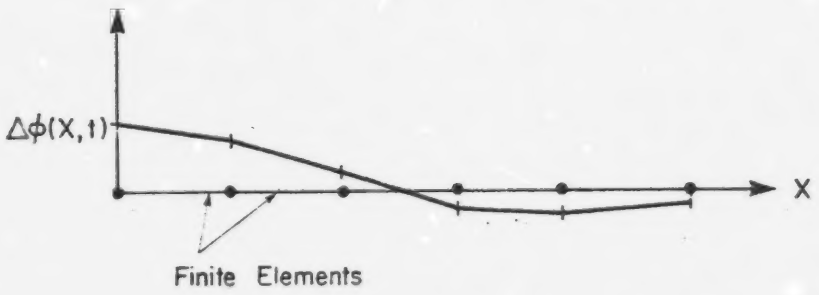

TYPICAL PIECEWISE LINEAR VARIATION ALONG THE DUCT

FIG. 2.2 APPLICATION OF FINITE ELEMENT TECHNIQUE TO DUCT PROBLEM

integrations (17) are greatly simplified. The duct is in effect broken into finite elements as shown in Figure 2.2. Each element is then considered in turn and its contributions to the global weighted integral expressions (17.a) and (17.b) are calculated and assembled according to standard procedures [Ref. 2.15]. The model obtained by using just one element for the duct discretization is, if friction is omitted, equivalent to the capacitance-inertance model given in [Ref. 2.5].

The downstream orifice boundary condition couples the duct equations to the equations for the basic cushion. When assembled, a system of equations of the form

$$\underset{\sim}{A}\,\dot{\underline{x}} = \underset{\sim}{B}\,\underline{x} \tag{18}$$

is obtained. Stability boundaries and the source of the instability are ascertained from an examination of the system eigenvalues and their associated eigenvectors [Ref. 2.19].

2.5 Results

2.5.1 Lumped Capacitance Boundaries

Inspection of the Routh-Hurwitz criteria for the lumped capacitance model of the duct-plenum system indicates that heave stability boundaries should be plotted in the form of nondimensional cushion pressure, p_{ce}/P_a, versus the nondimensional hovergap, h_e/D_p. Here, results are presented in this manner. Now h_e/D_p is a measure of the equilibrium air flow rate through the cushion. In fact, for a circular cushion, if the well known inviscid flow law for volume flow discharge is used, then

$$\frac{h_e}{D_p} = \frac{C_{QC}}{4C_m} \tag{19a}$$

where

$$C_{QC} = Q_e \left(\frac{\rho}{2WA_{ref}} \right)^{1/2} \tag{19b}$$

and Q_e is the cushion flow at equilibrium, C_{QC} is a nondimensional cushion flow coefficient [Refs. 2.11, 2.12], W is the gross weight carried by the cushion, and $A_{ref} = (\pi/4)D_p^2$. The range $0.0005 \le h/D_p \le 0.01$ corresponds to volume flow rates which are typical of those chosen for overland and amphibious operations [Ref. 2.20].

Figure 2.3 shows stability boundaries obtained when the duct is treated as a lumped capacitance, where the hatched side of the curves indicates the unstable region. These provide a convenient reference for describing the effect of ducting. Results are given for two values of A_c/D_p^2 and with $A_f = A_c$. Also, for $A_c/D_p^2 = 0.0218$, the three cases corresponding to $C = (dp_f/dQ_f)\big|_e = 0$, $-.767$ and $-\infty$ span the practical limit of the supply fan characteristics, with $C = 0$ corresponding to a constant pressure source, and $C = -\infty$ corresponding to a constant volume flow source. In engineering terms the constant pressure source relates to a very large fan while the constant

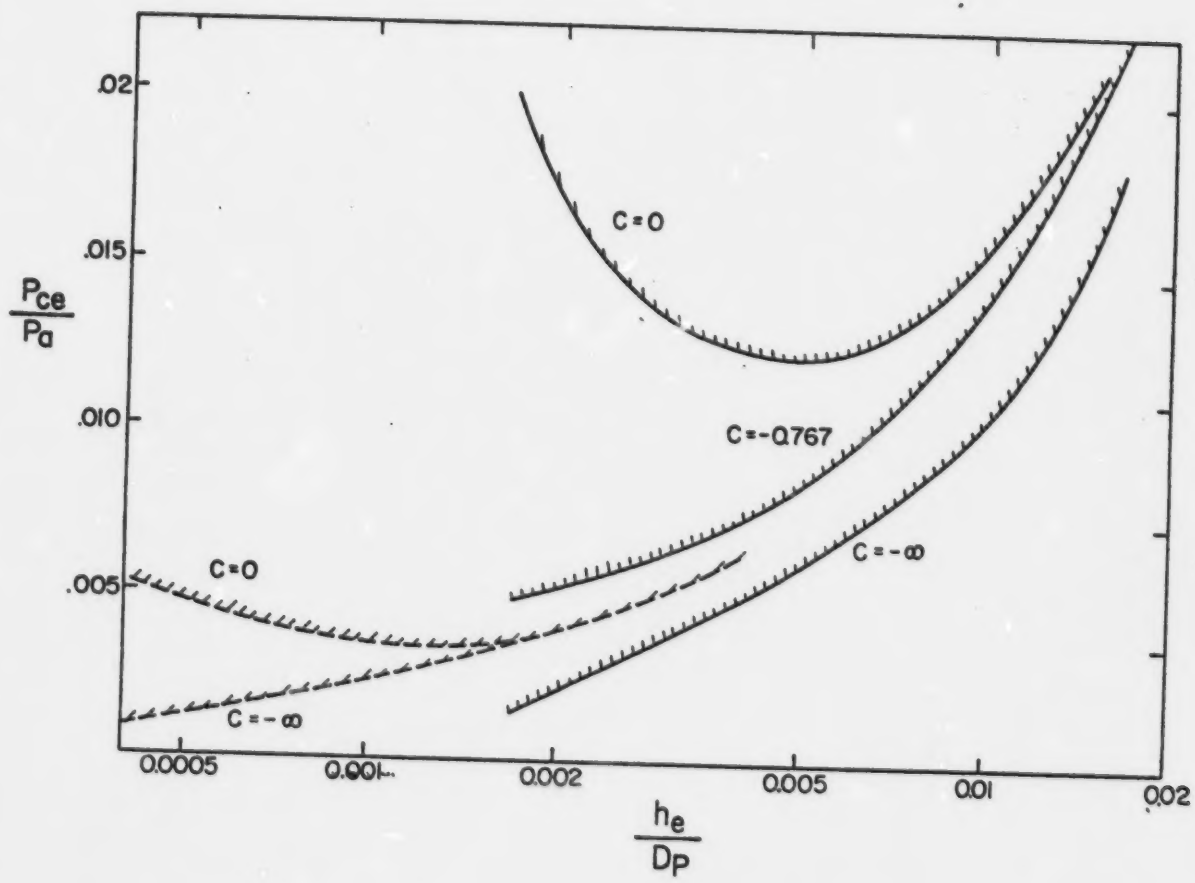

FIG. 2.3 LUMPED CAPACITANCE STABILITY BOUNDARIES.

volume flow source relates to a very small fan. The results demonstrate that the choice of the basic quasi-steady fan characteristic can have a considerable effect on system stability, as has been pointed out previously [Ref. 2.1].

2.5.2 Limiting Behaviour of Lumped Capacitance Boundaries at High and Low Volume Flow

As is shown below, the duct capacitance has very little effect on the stability boundaries presented. Thus, one can study the effects shown in Figure 2.3 by considering the characteristic equation for the simpler system consisting of a plenum separated from a source by an orifice:

$$C_c s^3 + \left(\frac{1}{R_c - C} + \frac{1}{R_a} \right) s^2 + \frac{S_a^2}{m} s + \frac{S_a}{\alpha_a m} = 0 \qquad (20)$$

The Routh-Hurwitz criteria indicate that for stability

$$\left(\frac{1}{R_c - C} + \frac{1}{R_a} \right) S_a - \frac{C_c}{\alpha_a} > 0 \qquad (21)$$

In the limit as $h_e/D_p \to 0$, $1/R_a \to 0$ and $R_c \to 0$. So, the equation for the stability boundary reduces to

$$- \frac{S_a}{C} - \frac{C_c}{\alpha_a} = 0 \qquad (22)$$

As $C \to 0$ from C negative, $\alpha_a \to 0$ or $p_{ce} \to \infty$, whereas as $C \to -\infty$, $\alpha_a \to \infty$ or $p_{ce} \to 0$. The characteristic equation also shows that, in the limit as $h_e/D_p \to \infty$, the stability boundaries for $C = 0$ and $C = -\infty$ converge, and the cushion pressure for instability tends to infinity. These trends can be seen in Figure 2.3. Of course, as h_e/D_p increases, internal flows within the cushion volume would become important, and the lumped parameter assumption would not be justified.

2.5.3 Source of the Instability

The unstable regions in Figure 2.3 are associated with plenum air compressibility. This can be seen by substituting $s = j\omega$ into equation (20). This argument, which was first presented in [Ref. 2.18] shows that the coefficient of s^3, which is directly proportional to C_c, is equivalent to a negative damping which, in turn, is proportional to $\omega^2 C_c$. Now when $C = 0$, the spring stiffness tends to zero as $h_e/D_p \to 0$. That is, $\omega \to 0$ and the negative damping goes to zero. When $C = -\infty$, the spring stiffness and $\omega \to \infty$ as $h_e/D_p \to 0$, so that the negative damping also tends to infinity. Note that if the air is incompressible, so that $a = \infty$, the negative damping term would always be zero.

2.5.4 Duct Effects Obtained From Finite Element Analysis

Typical results showing a duct effect are given in Figure 2.4. For these the 1.415 m^3 volume is stretched into a series of straight ducts. Because each duct-plenum system considered has the same total duct volume, each had the same stability boundary when the duct is modelled as a lumped capacitance. This common boundary is included in Figure 2.4 for constant pressure and constant volume flow sources. All finite element results presented in Figure 2.4 were obtained with a constant pressure source separated from the duct by an orifice with area $A_f/D_p^2 = 0.0218$ and with $A_c = A_f$, $n = \gamma$ and $f = 0$. The effect of discretization was checked in certain cases by increasing the number of finite elements from five to ten, and the difference between the results so obtained was found to be negligible. Case 1 was included purely to check the internal consistency of the calculations. Cases 2 to 6 are typical of the range of L_d/D_d found on a practical vehicle. Case 1, as expected, gave results which were effectively identical to the lumped capacitance calculation with $C = 0$. The results for cases 2 to 6 show that ducting can significantly increase or decrease stability and that, in the limit as C_{QC} or $h_e/D_p \rightarrow 0$, the duct effects become very large.

Some results were obtained with a friction factor $f = 0.07$, which corresponds to a very rough duct. For the duct lengths considered, the the differences between corresponding smooth and rough duct stability boundaries were found to be a few percent at most. Also, some results obtained with C equal to a typical value other than $C = 0$ showed that the duct effect was still significant.

2.6 Discussion

2.6.1 Major Feature of the Duct Effect

In an effort to understand the duct effects, the eigenvalues and associated eigenvectors for particular cases were examined. In many cases when the ducting had a destabilizing effect, a real root with low stability margin was found to be present. The corresponding eigenvector showed that this real root was associated primarily with the velocity of the duct flow. Thus it appeared that air inertance had a destabilizing influence. To check this, some results were obtained by using a purely lumped inertance model for the duct; that is, the compressible unsteady mass conservation equation for the duct volume used in the lumped capacitance model was replaced with Newton's law for oscillations of the slug of air in the duct about its mean velocity:

$$\frac{d\Delta Q_d}{dt} = \frac{A_d}{L_d \rho} (\Delta p_{df} - \Delta p_{dc}) \qquad (23)$$

where A_d is the duct cross sectional area. The plenum was modelled as a lumped capacitance, and a constant pressure fan source was used. Typical results are shown in Figure 2.5 for cases 3 and 6. The qualitative agreement between the lumped inertance and the finite element results shows that the duct destabilizing effect does indeed manifest itself primarily through the inertia of the air in the duct. However, the results

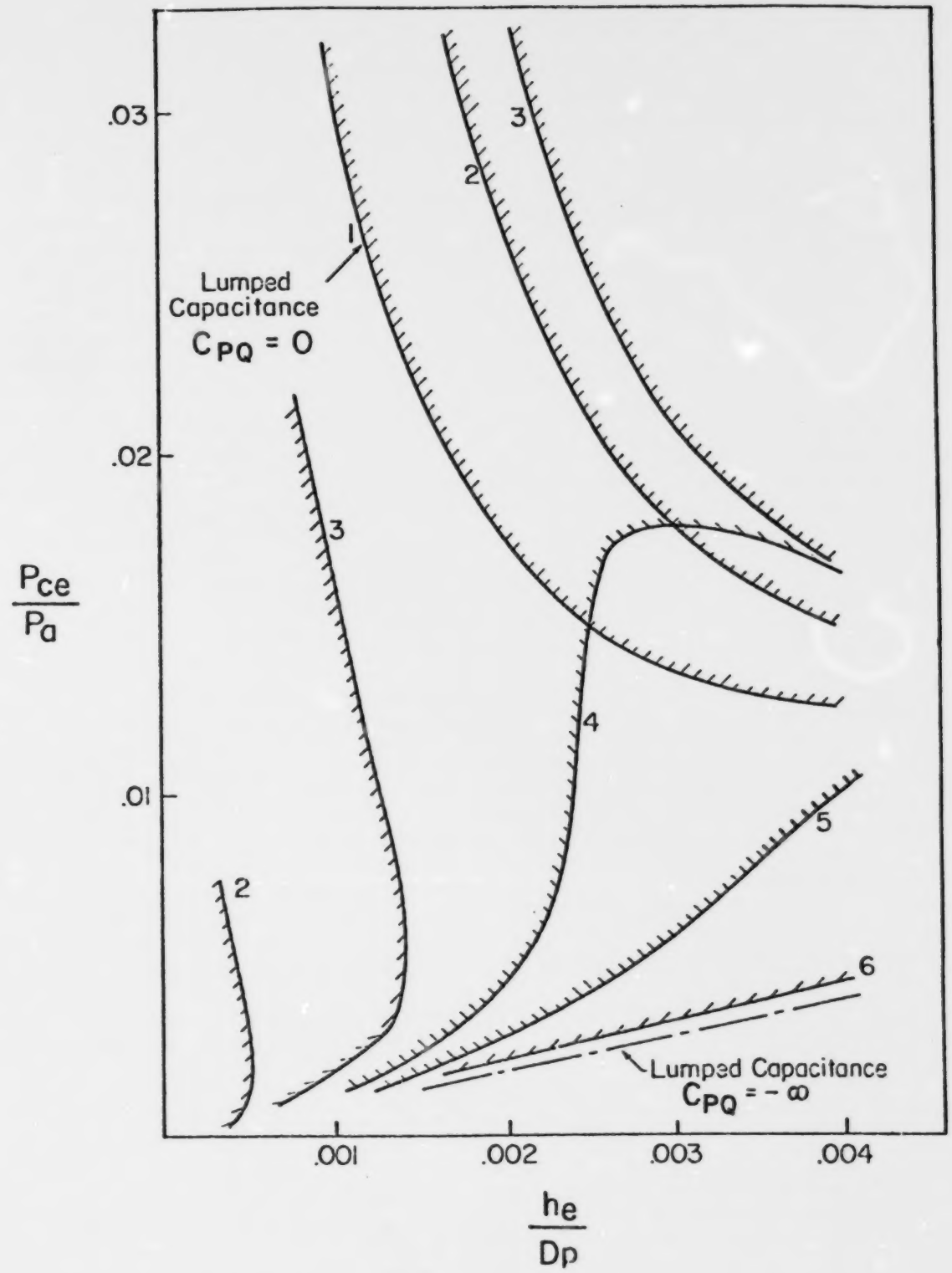

FIG. 2.4 TYPICAL FINITE ELEMENT HEAVE STABILITY RESULTS. CASES 1 TO 6 HAVE VALUES OF L_d/D_d = 0.125, 4,0, 8.0, 16.0, 64.0, RESPECTIVELY.

also show that air inertance can provide a stabilizing influence. The difference between the inertance and finite element results is presumably associated with the duct capacitance.

Given the reasonably accurate predictions made by the lumped inertance model, it can be exploited to obtain further insights into the present results. The characteristic equation for this simplified model in terms of the Laplace variable s is:

$$\left[\frac{L_d \rho}{A_d} s + R_f + R_c\right]\left[C_c s^3 + \frac{s^2}{R_a} + \frac{S_a^2}{m} s + \frac{S_a}{\alpha_a m}\right] + s^2 = 0 \quad (24)$$

For the results presented, the duct volume is fixed. This implies that if $L_d/D_d \to \infty$ or $D_d \to 0$, then $A_d \to 0$. The latter in turn implies that the pressure forces at either end of the duct and the duct flow variations would also tend to zero, and one could expect the plenum to behave as if it had a constant volume flow source. Now, in the limit as $L_d\rho/A_d \to \infty$, equation (24) reduces to

$$s\left[C_c s^3 + \frac{s^2}{R_a} + \frac{S_a^2}{m} s + \frac{S_a}{\alpha_a m}\right] = 0 \quad (25)$$

The $s = 0$ root implies that the duct flow is critically stable. The cubic equation in brackets is the characteristic equation for a plenum with a constant flow source. Of course, in the limit being considered, wave propagation effects associated with duct air compressibility could be very significant. The lumped inertance model ignores such effects. Also, in the limit as $L_d/D_d \to 0$, with the duct volume fixed, $A_d \to \infty$. In this case, the time constant for the duct flow would be zero, and one could expect the duct effect to disappear and the system to behave as a plenum separated from a constant pressure source by two orifices in series. The characteristic equation (24) can be shown to reduce to this situation.

2.6.2 Behaviour at Very Low Cushion Flows: Helmholtz Resonator Effect

In the limit as $h_e/D_p \to 0$, $(R_f + R_c) \to 0$ and $1/R_a \to 0$. So, the characteristic equation reduces to

$$s\left[C_c s^3 + \left(\frac{A_d}{L_d \rho} + \frac{S_a^2}{m}\right) s + \frac{S_a}{\alpha_a m}\right] = 0 \quad (26)$$

The $s = 0$ root and the absence of an s^2 term for the cubic in brackets imply that in this limit the system can never be asymptotically stable. Application of the Routh Hurwitz criteria to the cubic leads to the critical stability requirement

$$-S_a C_c/\alpha_a m > 0 \quad (27)$$

In a practical situation, this inequality can never be satisfied, so that the maximum cushion pressure for stability with $C = 0$ tends toward zero

as $h_e/D_p \to 0$, in contrast to the prediction of the lumped capacitance model. The finite element calculations also show this trend. Now in the limit as $h_e/D_p \to 0$, $C_{QC} \to 0$, and it is reasonable to expect that the system would act as an Helmholtz resonator. In other words, the air in the duct would oscillate as a single lumped mass on the plenum air spring, as the damping provided by the orifices at either end of the duct would be effectively zero. If this argument is valid, then the frequency associated with a critically stable eigenvalue, as obtained by either finite element or lumped inertance analysis, should agree reasonably well with the value given by the well known formula for a Helmholtz resonator [Ref. 2.16].

$$\omega_h^2 = \frac{a^2}{L_d V_{ce}} A_d \tag{28}$$

This is found to be the case. For example, for system 3 and for the points d and e shown in Figure 2.5, the frequencies as obtained by the finite element eigenvalue analysis are respectively 52.3 rad/sec and 57.9 rad/sec. The frequency ω_h as determined by equation (28) is 54.3 rad/sec. Now at a stability boundary, $s = j\omega$ so that the real part of equation (26) gives for ω

$$\omega^2 = \frac{a^2}{L_d V_{ce}} A_d + \frac{S_a^2}{mC_c} \tag{29}$$

Note that, when the second term on the right-hand side is small relative to the first term, equation (29) reduces to equation (28).

2.6.3 Behaviour of the Stability Boundaries in the Absence of a Duct

It should also be noted that, even when duct effects are not important and $C = 0$, the stability limit for p_{ce} will not tend to infinity as $h_e/D_p \to 0$, as is suggested by the lumped capacitance model. The reason is that the quasisteady orifice flow equation, which is used to describe the flow into the cushion, will not be valid in this limit. That is, the local or unsteady terms in the differential equations describing the flow become important. Hence, for the very low hovergaps, a lumped reactance-resistance model [Ref. 2.17] for the flow is more appropriate. With this model for the inlet flow, and a purely resistive model for the outlet flow, the characteristic equation for a plenum separated from a constant pressure source by an orifice is

$$(C_a s + C_b)\left(C_c s^3 + \frac{1}{R_a} s^2 + \frac{S_a^2}{m} s + \frac{S_a}{\alpha_a m}\right) + s^2 = 0 \tag{30}$$

where $C_b \cong R_c$ and $C_a \cong \ell_o \rho / A_c$ where ℓ_o is the effective length of the slug of air which oscillates in the orifice region. For the outlet flow, C_b is usually much larger than C_a so a purely resistive model for this flow can be used. In fact, in the limit as $h_e/D_p \to 0$, it can be shown that $C_a \to 0$ and $C_b \to \infty$. Now equation (30) is of the form of equation (24). Thus, the upper limit of p_{ce} for stability would again go to zero as $h_e/D_p \to 0$, and the orifice-plenum system would tend to behave as an Helmholtz resonator.

2.7 Nonlinear Analysis

2.7.1 Nonlinear Stability Difficulties

Because the linear calculations described above indicate that even relatively short ducts could have a major influence at practical values of h_e/D_p or C_{QC}, it was decided to examine the nonlinear behaviour of the system, since it is known that a nonlinear analysis provides insights into the practical importance of linear predictions. For example, it is conceivable that a nonlinear system which is unstable in a linear sense could enter a limit cycle which is of sufficiently small amplitude that it could be described as "practically" stable [Ref. 2.19]. It is also conceivable that a nonlinear system which is stable in a linear sense could be "practically" unstable.

2.7.2 Method of Characteristics Analysis

The nonlinear analysis used the method of characteristics to reduce the two nonlinear hyperbolic partial differential equations (12) and (13) to the ordinary differential equations [Ref. 2.7].

$$\rho \frac{dv}{dt} + \frac{1}{a}\frac{dp}{dt} + \rho \frac{fv|v|}{2D_d} = 0 \tag{31a}$$

on

$$\left.\frac{dx}{dt}\right|_{C^+} = v + a \tag{31b}$$

$$\rho \frac{dv}{dt} - \frac{1}{a}\frac{dp}{dt} + \rho \frac{fv|v|}{2D_d} = 0 \tag{31c}$$

on

$$\left.\frac{dx}{dt}\right|_{C^-} = v - a \tag{31d}$$

Equations (31b) and (31d) describe families of characteristic lines in the x-t plane (Figure 2.6). The ordinary differential equations (31a) and (31c) were integrated numerically along these lines using an Euler type integration known as the method of specified time intervals [Ref. 2.7] to obtain

$$v_P - v_R + \frac{1}{\rho}\frac{(p_P - p_R)}{a} + \frac{fv_R|v_R|}{2D_d}\Delta t = 0 \tag{32a}$$

$$x_P - x_R = (v_R + a)\Delta t \tag{32b}$$

$$v_P - v_S - \frac{1}{\rho}\frac{(p_P - p_S)}{a} + \frac{fv_S|v_S|}{2D_d}\Delta t = 0 \tag{32c}$$

$$x_P - x_S = (v_S - a)\Delta t \tag{32d}$$

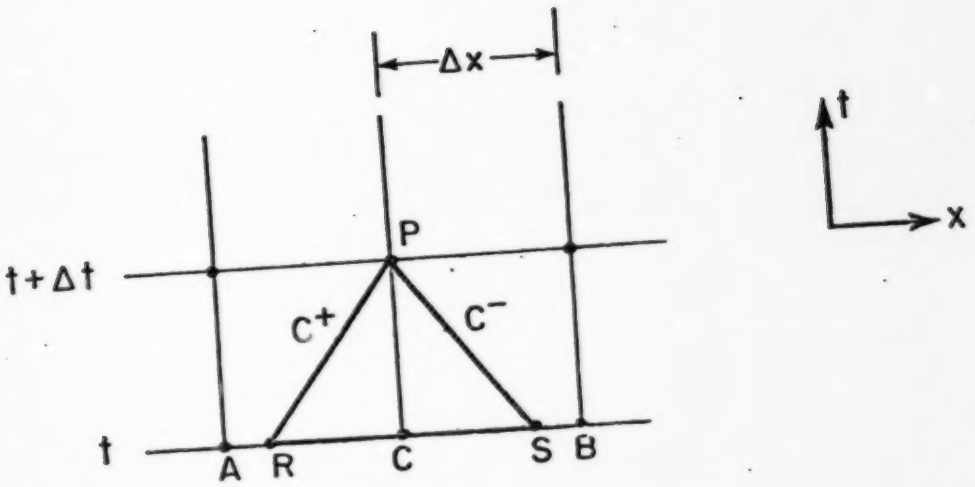

FIG. 2.6 CHARACTERISTIC LINES IN THE "x-t" PLANE

For a point P where $0 < x(P) < L_d$, manipulations of equations (32a) and (32c) gave

$$v_P = .5\left[v_R + v_S + \frac{1}{\rho}\frac{(p_R - p_S)}{a} - \frac{f\Delta t}{2D_d}(v_R|v_R| + v_S|v_S|)\right] \quad (33a)$$

$$p_p = .5\left[p_R + p_S + \rho a(v_R - v_S) - \frac{\rho f a\Delta t}{2D_d}(v_R|v_R| - v_S|v_S|)\right] \quad (33b)$$

where conditions at positions R and S were obtained from known conditions at A, C and B by a linear interpolation which made use of equations (32a) and (32c). For a point P at either end of the duct, where boundary conditions had to be applied, procedures described in [Ref. 2.7] were used. The nonlinear equations for the plenum were integrated numerically using a fourth order Runge-Kutta procedure.

2.7.3 Nonlinear Results

Typical results for case 6 are given in Figure 2.7, where the letters b and c refer to the equilibrium points shown in Figure 2.5, and where a 100% reduction in hovergap at t = 0 was used to disturb the system. These results suggest that the linear analysis should be adequate for practical stability calculations. For example, for the point c which lies in the linear stable region, the oscillation resulting from a large disturbance from equilibrium is a decaying one. The nonlinear results also confirm the accuracy of the finite element calculations. Typically, for the critically stable equilibrium a, the finite element analysis gives the oscillation frequency as 32.9 rad/sec whereas the nonlinear analysis gives 32.6 rad/sec.

2.8 Transmission Line Analysis Based on the Acoustic Wave Equation

As mentioned in the Introduction, a linear stability analysis for the duct-plenum problem based on a transmission-line formulation of the acoustic wave equation and the Nyquist criterion was presented in [Refs. 2.5, 2.18]. The details of this analysis are quite involved and will not be repeated here.

Figure 2.8 shows an application of the theory to case 6, where Z_p and Z_d are complex impedances relating cushion pressure and cushion inlet flow [Ref. 2.18]. Figure (2.8a) is for equilibrium b. As outlined in [Ref. 2.18], the loci intersections indicate that, with A_d fixed, the system is unstable for L_d/D_p ratios in the range 3.55 to and 13.82. Note that for case 6, $L_d/D_p \cong 10.5$. Figure 2.8b is for equilibrium c. The theory of [Ref. 2.18] shows that because $Z_p(j\omega)/R$ does not make any clockwise encirclements of $-Z_d(j\omega)/R$ and because $Z_p(s)$ does not have any poles in the right half of the complex plane, the system is stable.

2.9 Conclusions

The calculations reported here show that even relatively short ducts can have a major effect on the heave stability of cushion systems used for amphibious and overland operations. Comparisons with lumped parameter models show that duct air inertance is the dominant destabilizing mechanism, although in general, the simplest duct model used in practical calculations

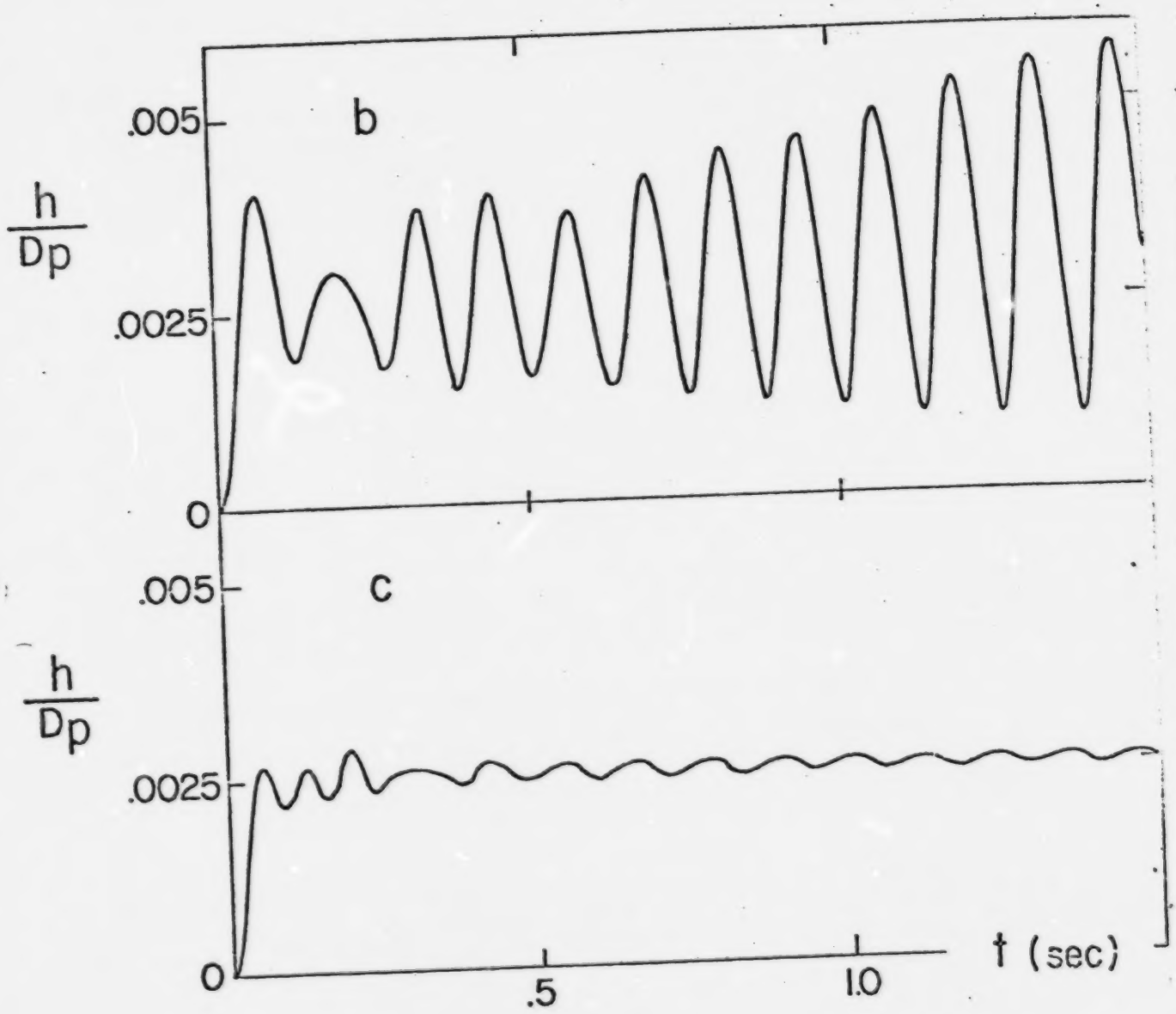

FIG. 2.7 AN ILLUSTRATION OF A PRACTICAL STABILITY CALCULATION FOR THE DUCT-PLENUM SYSTEM.

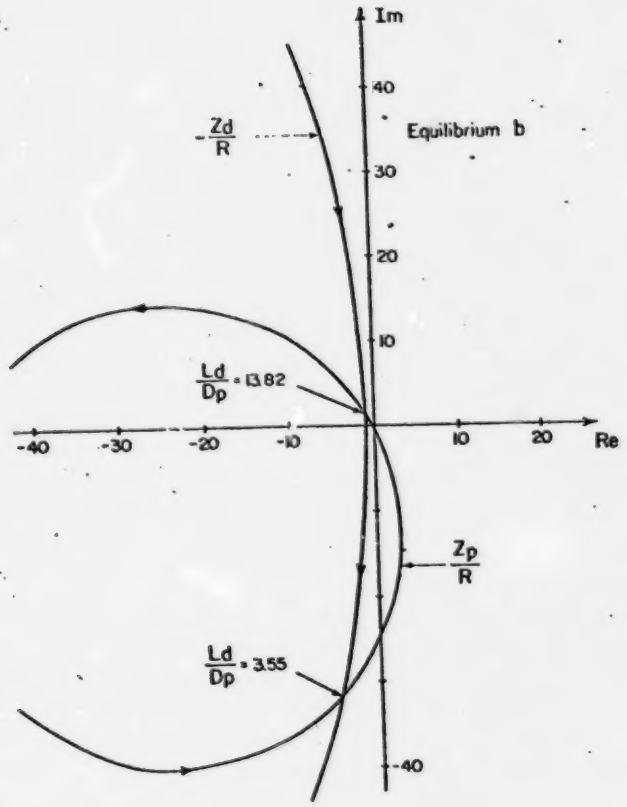

MIT TRANSMISSION LINE RESULTS FOR CASE 6

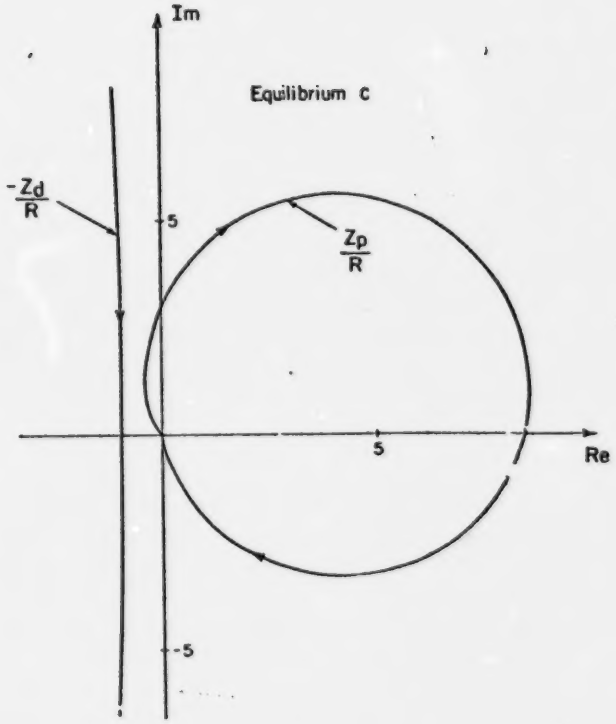

FIG. 2.8 TRANSMISSION LINE RESULTS FOR CASE 6.

should include both inertance and capacitance, as recommended in [Refs. 2.5, 2.18]. For some operating conditions, the system behaved like a Helmholtz resonator. The nonlinear calculations showed that the linear analysis could be used for practical stability calculations. It is worth noting that the lumped parameter models provide the basis for various insights not explicitly obvious in the finite element procedure used here or even the classic wave equation analysis used in [2.5, 2.18]. The Helmholtz resonator effect is an example of this. Also, examination of the Routh-Hurwitz criteria for the lumped capacitance model indicates that the value of p_{ce} for critical stability for geometrically similar cushion systems operating at the same value of C_{QC} or h_e/D_p should be the same for both model and full scale system. This argument does not hold for the lumped inertance model of duct behaviour, but since the lumped capacitance models with constant pressure and constant volume flow sources have been shown to be limiting cases of the lumped inertance model, one would expect the curves showing duct effects to scale approximately. Computation of stability boundaries for a cushion which was half the size of the one used here showed that the boundaries moved by a few percent at most. Finally, the duct effects are strongly dependent on h_e/D_p and usually tend to disappear as h_e/D_p increases. It is important to note that the results presented here are for a practical range of h_e/D_p.

3 EFFECT OF DUCTING ON THE DYNAMIC FAN CHARACTERISTICS OF AIR CUSHIONS

3.1 Introduction

Experimental results have recently been reported [Ref. 3.1] which show that the dynamic characteristics of an air cushion fan can deviate appreciably from its static characteristic, where, by definition, the characteristic of a fan is its pressure-volume flow relationship. These results are qualitatively in agreement with earlier results obtained by Durkin and Langhi [Ref. 3.2]. Typically, the results show that for low disturbance frequencies the deviations from the static characteristic are small, whereas for intermediate frequencies the deviations can be very large. Deviations from the static characteristic associated with the dynamics of a vehicle supported by the cushion can arise from at least three sources: unsteady aerodynamics of the flow through the fan blades, one dimensional air slug flow in the fan volute-duct system and, ultimately at high enough frequencies, wave propagation phenomena in the ducting.

It is the purpose of this section to observe that, for the frequencies and duct lengths typically involved in the dynamic operation of air cushion vehicles over land and water, the inertance of the air flow in the fan volute-duct or annulus-duct system appears to be the dominant factor in generating the effective unsteady characteristics. This conclusion was drawn from results obtained by analysis based on well-established models and numerical procedures for treating one-dimensional unsteady flows. [Ref. 3.3], together with an application of a criterion available for determining the importance of unsteady aerodynamic effects in fan blades [Ref. 3.4]. The analysis is reported in greater detail in Ref. [3.5].

3.2 Analytical Model

The system examined consisted of one cell of a Canadian multicell amphibious ACV raft known as the HJ-15 together with its duct-volute work. The cell, which was 1.83 m in diameter and 0.915 m deep, was modelled as a lumped capacitance. The duct flow was modelled in two ways, first as a one dimensional unsteady flow with friction, and second as a lumped inertance. It should be noted that the first model included the possibility of wave propagation effects. For this analysis, following the methods outlined for hydraulic transients [Ref. 3.3], the partial differential equations describing unsteady duct flow, namely, continuity and momentum, were reduced to ordinary differential equations by the method characteristics [Ref. 3.3]. For the lumped inertance analysis, Newton's second law for the motion of the slug of air in the duct was used. The nonlinear quasi-steady inviscid incompressible orifice law was used to describe the flow from the duct into the cell and from the cell to atmosphere. The cell inlet orifice diameter was 0.305 m. The ordinary differential equations for each model were integrated numerically.

3.3 Results

Typical computed dynamic characteristics are shown in Figure 3.1 where the standard fan pressure and volume flow coefficients [Ref. 3.6] are used to present the results nondimensionally. That is, $C_p = p/\rho N^2 D^2$, where p is the pressure at the end of the supply duct adjacent to the cushion, ρ is the atmospheric air density, N is the fan rotational speed and D is the wheel

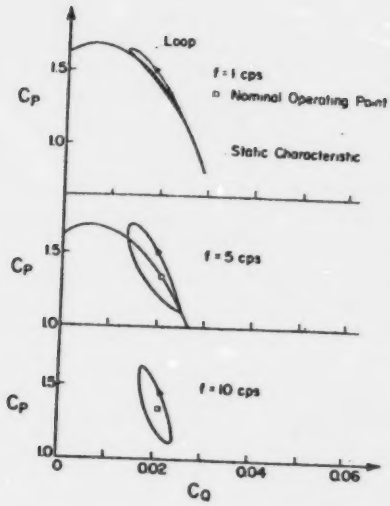

FIG. 3.1 DYNAMIC FAN CHARACTERISTICS FOR A DUCT LENGTH OF 3.03 METRES

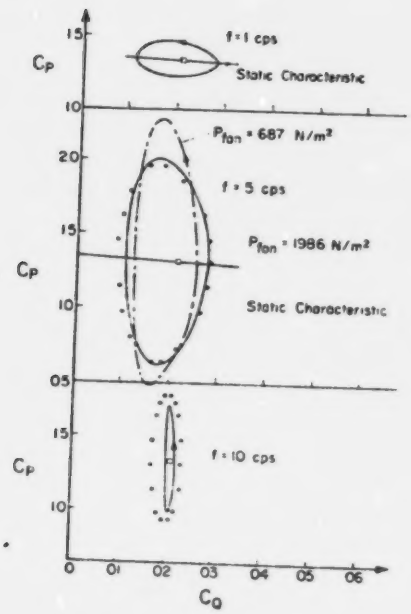

FIG. 3.2 DYNAMIC FAN CHARACTERISTICS FOR A DUCT LENGTH OF 7.62 METRES

diameter. Also $C_Q = Q/ND^3$ where Q is the instantaneous volume flow rate at the entrance to the cushion. The results show the dynamic pressure-flow characteristics which occur at the downstream end of the duct when the hover-gap is oscillating sinusoidally, and thus the effect of ducting on the fan characteristic as seen at the cushion. For these results, the duct, which has the proportions typically occurring on a practical vehicle, is 3.04 m in length and 0.457 m in diameter. A typical static fan characteristic is imposed at the upstream end of the duct, and the effective static characteristic as seen at the duct end is given for reference in Figure 3.1. The mean hover-gap is 0.64 cm while the amplitude of the sinusoidal variation is 50% of this gap. The cell volume variation associated with the hover-gap variation has not been included. The arrowhead on the loops shows the direction in which the operating point is moving in time. The results are qualitatively in agreement with those presented in [Refs. 3.1 and 3.2]. For the three frequencies f given, which span the range typically occurring in the dynamics of the vehicle modelled, and which are 1, 5 and 10 cps respectively, the lumped inertance and the full one dimensional unsteady results are in very close agreement. In fact, the difference is too small to be plotted. This implies that wave propagation effects are not significant. When one considers the duct length and frequencies involved, this is not surprising. As is discussed in Section 2 of this report, the system is behaving something like a Helmholtz resonator, and the air in the volute and duct is oscillating as a single mass on the spring associated with the plenum air capacitance.

Some results for a case in which the duct length has been increased to 7.62 m and the static fan characteristic is replaced by a constant pressure source are given in Figure 3.2. The use of a constant pressure source facilitates the demonstration of a scale effect to be discussed below. All results in Figure 3.2, except for the chain-dotted line marked "P_{fan} = 687 N/m^2", correspond to a nominal equilibrium operating fan pressure of 1986 N/m^2. The latter fan pressure is representative of that obtained on the prototype vehicle at full load. For the latter fan pressure, the continuous lines give the results of the one-dimensional unsteady analysis, and the dots are the results given by the lumped inertance model. The slight negative slope of the static characteristic is caused by friction losses in the duct. The peak in pressure fluctuations at about f = 5 cps is believed to be a Helmholtz resonator effect because for this geometry the Helmholtz resonator frequency is f_h = 5.2 cps [Ref. 3.7]. A minimum in flow fluctuations, which occurs about f = 10 cps, is believed to be a wave propagation effect because the natural frequency of the ducting f_d based on its wave propagation time is f_d = 11.3 cps [Ref. 3.3]. Thus it appears that for this case both Helmoltz resonator and wave effects are important. For frequencies greater than 10 cps, the direction of the loop often reverses, but the amplitude of both pressure and flow fluctuations remain small. As expected, the agreement between lumped inertance and full unsteady results becomes increasingly poorer as f increases.

The chain dotted line for the results at 5 cps in Figure 3.2 illustrate that, as might be expected, these effects do not scale according to the basic steady fan laws. It corresponds to a reduction of vehicle weight by a factor of about 2.90, but with the vehicle geometry unchanged and the equilibrium volume flow adjusted so that the same mean hover-gap, namely 0.64 cm, is obtained. In the analysis the effective fan speed N was reduced to keep Cp the same as for the earlier results. It follows from the definitions of C_Q and the one dimensional Bernoulli law for the air escaping from the cushion that if the hover-gap is the same for both cases then C_Q is also the same.

Using unsteady airfoil and cascade theory, Ohashi [Ref. 3.4] has analysed the unsteady aerodynamic problem for the flow past the fan blades. He defines a critical frequency which characterizes the frequencies required for significant unsteady blade aerodynamics to occur. It was found that for the present system this critical frequency is well above the typical frequencies expected to be encountered, so that unsteady blade aerodynamic effects are not significant.

3.4 Conclusions

In those ACV's which have ducting between the air supply fan and the cushion, the effective or equivalent fan characteristic at the end of the duct nearest the cushion differs little from the basic fan characteristic only when the cushion is hovering at equilibrium. During dynamic motion, even moderately short ducts will cause the equivalent characteristic to exhibit large deviations from the equilibrium behaviour. Even at moderate frequencies, the "unsteady" characteristic may be quite unrelated to the equilibrium behaviour. For the duct lengths typically used on ACV's, this phenomenon seems to be almost entirely due to the inertia of the air in the duct; this is consistent with the effects on stability discussed in Section 2. Acoustic wave propagation phenomena are significant only for ducts which are much longer than those likely to be used on air cushions.

4. LIMIT CYCLE OSCILLATIONS OF AIR CUSHIONS

4.1 Introduction

A problem that has been encountered during the development of various types of air cushion vehicle (ACV) is the sporadic occurrence of self-excited oscillations. Frequently these oscillations are simply a translation in the vertical direction, that is, a pure heave, but other motions have been observed. They may only be of nuisance value, and a nominal change in operating conditions, such as changing from stationary hover over a smooth surface to forward motion over a slightly roughened one, is often sufficient to suppress them. However, they can cause operational difficulties [Ref. 4.1] and, in extreme cases, lead to destruction of the vehicle. Evidently, progress in this technology would be aided by the development of analytical models of cushion dynamics which could allow design to avoid such oscillations or to investigate possible methods of suppression. However, it is to be noted that the limited amount of evidence available from industrial practice indicates that their onset may be governed by many factors, two recently documented examples of which are: the cushion as a wave generator or pump when hovering over water at zero forward speed [Ref. 4.2], and the inherent nonlinear characteristics of the material used in the flexible inflated structure of "skirt" characteristic of the modern ACV [Refs. 4.2, 4.3]. It is apparent that a systematic investigation starting from relatively simple configurations is required.

Significant progress in understanding ACV dynamics has been made by many authors using linear analysis techniques. Prominent among these are the contributions made by Richardson and others at the Massachusetts Institute of Technology [Refs. 4.4, 4.5]. They pointed out that, for a cushion operating at low pressure, although the air escape process can be assumed to be incompressible, the air in the cushion volume has to be considered compressible. For a linear analysis, the cushion volumes are therefore modelled as lumped pneumatic capacitances. The present authors analysed the structure of stability boundaries for a family of duct-plenum systems in terms of the two parameters of basic design interest: cushion pressure and cushion volume flow. This analysis indicated that even relatively short ducts could have a major destabilizing effect, and that the primary source of the effect was the inertia of the air in the duct. Numerical simulation of the nonlinear dynamics for selected cases generally confirmed the predictions made by the linear analysis [Ref. 4.6]. More recently, Hinchey [Ref. 4.7] has shown that, under suitably controlled experimental conditions, these boundaries can be accurately reproduced. These and other experiments [Ref. 4.5] therefore generally confirm the validity of the assumptions used in the linear analytical models of cushion dynamics described above. They also suggest that linear analysis may be useful for the design of cushion systems.

Very little work on nonlinear ACV dynamics is available in the open literature. However, nonlinear effects may have practical significance. For example, Leatherwood [Ref. 4.8], using an analog computer simulation, showed that small transient disturbances superimposed on a sinusoidal input could generate large subharmonic responses. Also, nonlinear stability problems can occur in practice. The authors have observed such instabilities for two radically different cushion geometries constrained to move in two degrees of freedom, that is, heave and a rotation which is equivalent to

pitch or roll. These systems were found to be stable for small initial pitch angles but clearly unstable beyond a certain critical angle [Ref. 4.3].

A fundamental limitation of a linear analysis is that, although it may predict a divergent oscillation at the onset of instability, it cannot predict the ultimate nature of the motion. Observations of laboratory experiments suggest that the motion is frequently a stable finite amplitude oscillation which, presumably, is a limit cycle, since the fluid flow processes involve turbulent and viscous decay phenomena [Ref. 4.9]. The purpose of the present work is to ascertain if the nonlinearities that are characteristic of air cushion dynamics can cause such oscillations near stability boundaries. An approximate analytical technique is used to ascertain their existence, and the results are compared with those from direct numerical simulations. Only a very simple case is considered; this is a single cell flexible skirted plenum chamber constrained to move in pure heave. The cushion air supply system is modelled in two ways thought to be representative of those that occur in practice: a plenum box and a duct. The basic geometries are shown in Figure 4.1.

A practical motivation for the present work is that these oscillations might be used to generate pressure oscillations on the ground for geological and other purposes. However, in relation to the present contract, the work is motivated mainly by the fact that experimental measurements of amplitudes and frequencies of limit cycles are very straightforward and might be used as a sensitive test of the validity of the mathematical models for nonlinear dynamics.

4.2 Nonlinearities in Air Cushion Dynamics

The mathematical models of cushion dynamics described in References [4.4 to 4.7] include several nonlinear features. The source of cushion air – usually a fan or blower – often has a nonlinear static pressure-volume flow relationship or "characteristic". For sufficiently high cushion oscillation frequencies or for very low cushion flow rates the aerodynamics of unsteady flow through the fan blades will be significant, and at sufficiently large amplitudes, nonlinear effects will be present. The compression-expansion process in the cushion volume itself is usually modelled by a polytropic equation of state P_c/ρ^n = constant, where P_c is the absolute cushion pressure, ρ is the cushion air density, and n is assumed to be equal to the specific heat ratio $\gamma = C_p/C_v$ Refs.[4.3, 4.4]. This may contribute significant nonlinear effects if the pressure oscillations are large compared to atmospheric pressure.

The air escape process from the cushion to atmosphere is usually assumed to be quasisteady, and is consequently modelled by the one-dimensional orifice flow law based on Bernoulli's law and a suitable discharge coefficient [Refs. 4.3, 4.4]. The frequency of oscillation is usually low enough to make this approximation acceptable [Ref. 4.6], but it has two associated nonlinearities. One is the square-root dependence of the volume flux of air escaping from the cushion coupled to the varying air escape area. In the simplified model of Figure 4.1, this area is directly proportional to the hovergap h. The second is characteristic of vehicles equipped with flexible skirts. For sufficiently large amplitude oscillations, skirt-ground contact occurs, and there is an abrupt change in the

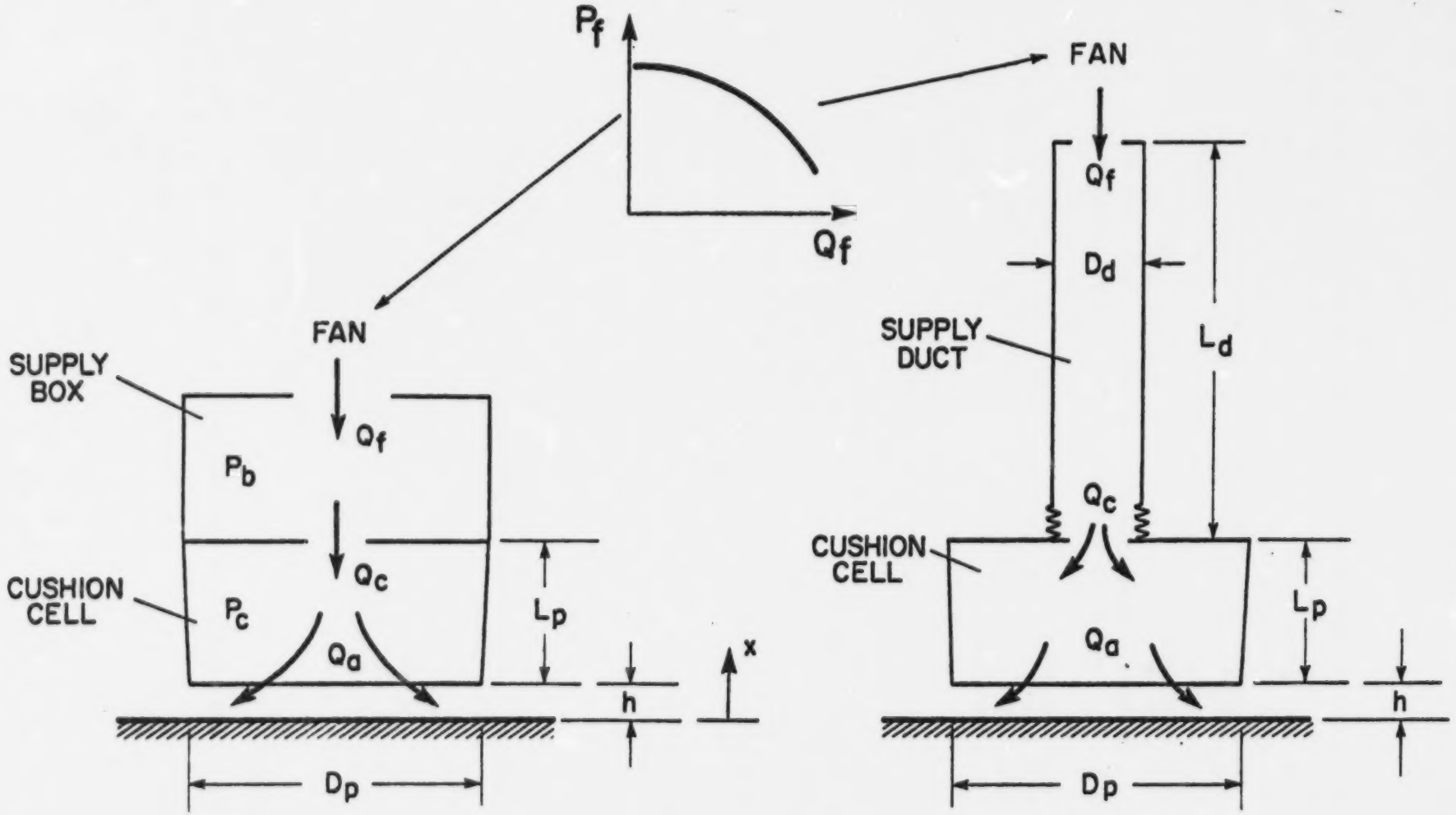

FIG. 4.1 BASIC AIR CUSHION GEOMETRIES STUDIED

functional relationship between the cushion air escape area and vehicle heave height. In the case depicted in Figure 4.1, as soon as skirt-ground contact occurs, the cushion air flow is, for all practical purposes, completely shut off [Ref. 4.10]. For more complex skirt geometries and for hover over irregular surfaces, the transition to shut-off is not so abrupt, but it is clear that this "valving" – as it has been called [Ref. 4.1] – can have a major effect on the system dynamics. The observed amplitudes of the oscillations are frequently such as to cause shut-off or valving.

Finally, it is now known that under certain circumstances the static heave pitch and roll stiffness characteristics of flexible skirted cushions can display significant hysteretic behaviour. This on its own can cause a system to enter a limit cycle [Ref. 4.9, p. 196]. For a cushion system, at least three possible sources have been identified [Refs. 4.3, 4.10, 4.11]. One is a structural instability; that is, flexible skirts are pressure-stabilized membrane structures, and for certain skirt geometries and under certain load conditions, they can buckle in such a way as to cause loss of the cushion seal. This in turn causes cushion venting and large reductions in cushion pressure. A second possible source is sliding friction forces generated by those parts of the skirt which are in contact with the ground and which move relative to it when the vehicle rolls or pitches [Ref. 4.3]. A third is related to the ability of the skirt system to transmit the small membrane compression forces generated during the loading portion of a skirt contact cycle when the skirt is pushed down onto the ground [Ref. 4.11]. These forces are not present during the unloading portion owing, apparently, to stress relaxation phenomena characteristic of certain elastomers. Although all three phenomena have been observed during laboratory model tests, their practical significance remains to be determined. For example, the first mechanism has been observed at full scale [Ref. 4.1], but only for particular geometries [Refs. 4.10, 4.11]. The third can have very large effects on vehicle dynamics at model scale [Ref. 4.3], but it occurs only for certain types of skirt material, and it is currently not clear if it is significant at full scale or on adequately modelled skirts.

The numerical simulations used to check the linear heave stability analysis described in Ref. [4.6] suggest that not all of the nonlinearities need to be included in a first analysis of the problem. For example, whereas the perturbations in cushion pressure may well be large when compared to the equilibrium gauge value, the deviation from a linearized approximation to the isentrope law is usually very small. Also, in view of the uncertainty about the practical significance of the hysteresis phenomena it seems appropriate to omit them from the analysis. Therefore attention is here restricted to twononlinearities: the Bernoulli law for orifice flows, and shut off.

4.3 Air Cushion Model and Equations

The basic models are shown in Figure 4.1. A fan or other source with a known static pressure-volume flow characteristic for gauge pressure p_f as a function of volume flow Q_f pumps air through an orifice of diameter D_f into either a supply box having a volume V_b or a circular supply duct of diameter D_d and length L_d. The supply system in turn feeds a single cell plenum chamber cushion through an orifice having diameter D_c.

The fan, supply system, and cushion are free to move as a single rigid unit, so the system has one degree of freedom, the distance x of a point on the base above an inertial datum line. The cushion cell wall or skirt is, for simplicity, depicted as a slightly tapered truncated cone having a base diameter D_p and height L_p. It is made of a very flexible but inextensible membrane, and the slight taper introduces a longitudinal tension into the membrane in order to keep it deployed. When the system is hovering at a stable equilibrium, the skirt forms a uniform hovergap of height h_e relative to the ground plane. When it is moving with the skirt not in contact with the ground, the hovergap remains uniform around the periphery of the cone, since the motion is constrained to be pure heave. The inertial datum is chosen such that $x = h$ for $x \geq 0$.

When $x \leq 0$, skirt-ground contact occurs, and the bottom part of the skirt is forced to collapse. Observations of this type of skirt in motion indicate that the typical skirt material is so thin and flexible that collapse occurs only in a very small region close to the ground-plane and that the deployed portion remains conical as shown in Figure 4.2. Furthermore, the geometry in the neighbourhood of the region of skirt-ground contact is such as to form a good seal; it is effectively shut-off as discussed previously. It is now assumed that the vertical force generated by the cell may be calculated by assuming that the cell hydrostatic pressure is uniform and acts over the area defined by the intersection of the fully deployed cell and the ground plane. This assumption was made for the development of a simple theory for the static roll stiffness of a cushion system using these cells as the basic element, and it was found to be adequate [Ref. 4.10]. The skirt material is also assumed to be so light that it adjusts quasistatically to the motion of the cushion.

The equations governing the motion may now be formulated. First, Newton's law for the forces on the cushion system is

$$m \frac{d^2x}{dt^2} = S_a(x)p_c - mg \qquad (1)$$

In Equation (1), m is the mass of the system, t is time, $S_a(x)$ is the pressurized support or cushion "foot-print" area, p_c is the cushion gauge pressure and g is the acceleration due to gravity. The foot-print area is a nonlinear function of x, that is

$$S_a(x) = \pi/4(D_p - 2x \tan\Phi)^2, \qquad x < 0 \qquad (2a)$$

$$S_a(x) = S_{ao} = \pi/4 D_p^2, \qquad x \geq 0 \qquad (2b)$$

Usually $x/D_p \ll 1$ so that Equation (2a) is accurately approximated by

$$S_a(x) = S_{ao} - L_c x \tan\Phi \qquad (2c)$$

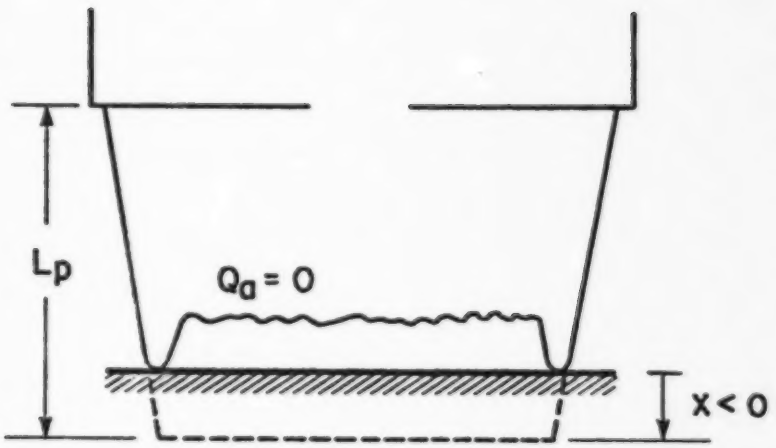

FIG. 4.2 ASSUMED BEHAVIOUR OF SKIRT FOR x<o

where L_c is the length of the perimeter of the skirt bottom, which is here πD_p. For the model depicted in Figure 4.1, $\Phi \ll 1$ so that S_a is approximated accurately by S_{ao} for values of x of interest.

The second equation is the mass conservation statement for the cushion volume:

$$\frac{d}{dt}(\rho_c V_c) = \dot{m}_c - \dot{m}_a \tag{3}$$

Here ρ_c is the density of the air in the cushion volume V_c, $\dot{m}_c$ is the mass flux from the supply system and $\dot{m}_a$ is the mass flux from cushion to atmosphere. The isentropic compression-expansion process in V_c is modelled by

$$\frac{P_c}{\rho_c^{\gamma}} = \text{constant} \tag{4}$$

where P_c is the absolute cushion pressure, that is $P_c = P_a + p_c$, and γ is the isentropic exponent. As noted above, it is expected that the $p_c/P_a \ll 1$; consequently the nonlinear effects associated with the air compressibility are omitted, and Equations (3) and (4) are replaced by their linearized equivalent. This is

$$C_c \dot{p}_c + S_a \dot{x} = Q_c - Q_a \tag{5}$$

where Q = the volume flux of air, and

$$C_c = \frac{V_c}{\rho a^2} \tag{6}$$

C_c is the pneumatic capacitance of the cushion volume. The quantity a is the atmospheric sound speed.

Two cushion air supply systems are being considered. One is a plenum supply box, which is modelled by a pneumatic capacitance:

$$C_b \dot{p}_b = Q_p - Q_c; \qquad C_b = \frac{V_b}{\rho a^2} \tag{7}$$

The other is a moderately long duct, which is modelled by a lumped inertance [Refs. 4.5, 4.6]:

$$\frac{\rho_a L_d}{A_d} \dot{Q}_d = p_{df} - p_{dc} \tag{8}$$

Here L_d and A_d are the length and the cross-sectional area of the duct respectively, and p_{df} and p_{dc} are the pressures in the duct at the fan

end and cushion end respectively. Losses at the duct inlet make $p_{df} < p_f$; also p_{dc} is not the same as p_c since a stabilizing orifice is included at the cushion inlet.

The flow orifices and the cushion air escape process is assumed to be inviscid, incompressible and quasisteady. Thus

$$Q_a = \pm C_m L_c h \sqrt{\left|\frac{2p_c}{\rho}\right|} \tag{9}$$

This form of the equation allows for the possibility of flow reversal; C_m is the usual discharge coefficient, which is assumed to be 0.61. The flow from the cushion supply system into the cushion is governed by

$$Q_c = \pm C_m A_c \sqrt{\left|\frac{2(p_i - p_c)}{\rho}\right|} \tag{10}$$

where A_c is the stabilizing orifice area, $i = b$ for the box case, and $i = dc$ for the duct case. For both cases it is assumed that a feed orifice separates the fan from the supply in which case one has

$$Q_f = \pm C_m A_f \sqrt{\left|\frac{2(p_f - p_i)}{\rho}\right|} \tag{11}$$

where $i = b$ for the box case and $i = df$ for the duct case.

It must be noted that the use of Equations (9) to (11) to describe flow shut-off and reversal implies making an assumption which is not tested by the available experimental confirmations of the linear analysis mentioned above. The quasisteady flow assumption for unsteady flows requires that the contribution of the local or unsteady inertia terms in Euler's equations must be small compared to the convective inertia terms. For typical ACV processes which are perturbations about a nonzero mean flow, this requirement is usually satisfied. If shut-off or reversal occurs, then for at least part of the time, the unsteady inertia terms will be important or dominant. Indeed, for small enough amplitude of the oscillatory flow, it could be argued that the correct model of the motion is that used to describe the processes in a Helmholtz orifice-cavity resonator [Ref. 4.12, p. 186]. However, in an investigation of the frequency response characteristics of an air cushion suspension subject to heaving ground-board inputs and described in Ref. [4.13], the effect of orifice-cavity systems intended to act as dampers were evaluated. Good agreement between the results obtained from a nonlinear theory – based essentially on the assumptions employed for the present analysis – and the experimental data for a wide range of frequencies, including the resonance peak for the system, strongly suggest that the Bernoulli model of the orifice flow is a useful approximation for most of the oscillatory cycle. Hence its use here is believed to be appropriate.

Two additional equations are required to form a closed system. The first is the given fan law, which is here assumed to be linear. That is,

$$p_f = p_{fo} + C_s Q_f \tag{12}$$

where p_{fo} is the fan supply pressure corresponding to zero Q_f, and C_s is a given constant. The second is the relationship between h and x, which is

$$h = x, \quad x > 0; \qquad h = 0; \quad x < 0 \tag{13}$$

It should be observed that, although the particular cushion geometry used here was chosen for its simplicity, it is a straightforward exercise to extend the analysis to include the more complicated geometries which are representative of those used in current practice. For many practical geometries, the footprint is not circular, and Φ is not small, but Equations (2) with an appropriate calculation of L_c describes these cases.

4.4 Approximate Methods

The number of approximate methods which are available for the analysis of steady state oscillations in nonlinear systems, and which do not assume that the nonlinearities are small in some sense, is very restricted. One method which is widely considered to be applicable to systems involving relatively large nonlinearities, and which provided a motivation for some of the ideas explored in this paper, is an extension of the block diagram concepts developed for the treatment of linear automatic control systems. It is generally known as the describing function technique, and a detailed account of its application to a variety of phenomena is given in the book by Gelb and Vander Velde [Ref. 4.9].

The simplest case considers only a single input, single output system containing one nonlinear element. This is cast into the form of the unity feedback canonical block diagram shown in Figure 4.3. The limitations of the method, and its relationship to the method finally chosen for the present problem may be most simply illustrated by consideration of a specific example, namely van der Pol's equation:

$$\ddot{y} - \alpha(1 - \beta y^2)\dot{y} + y = f(t) \tag{14}$$

Here f(t) is the input or forcing function, which is zero in the case of a limit cycle oscillation. This can be cast into the block diagram form by noting that:

$$(1 - \beta y^2)\dot{y} = \frac{d}{dt}\left[y - \frac{\beta y^3}{3} \right] \tag{15}$$

By using the rules of block diagram algebra, one then obtains after some simplification the system shown in Figure 4.4.

The calculation proceeds by assuming that, for a steady state oscillation, the output of the linear part of the system can be approximated by a sinusoid of the form $x(t) = A \sin\Psi$, with $\Psi = \omega t + \phi$. The single sinusoidal input describing function (DF), denoted by $N_s(A, \omega)$, is the complex fundamental-harmonic gain of the nonlinear element in response to the

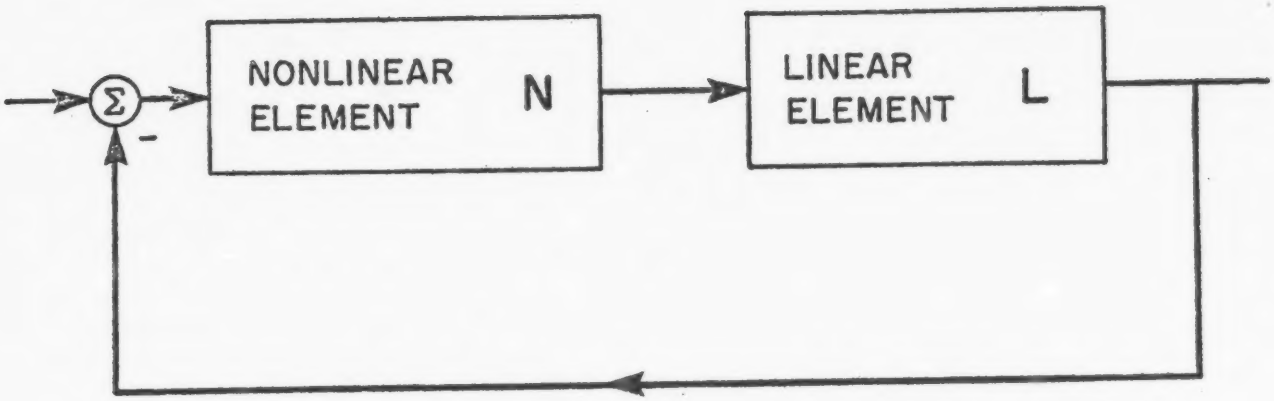

FIG. 4.3 CANONICAL BLOCK DIAGRAM WITH ONE NONLINEAR ELEMENT.

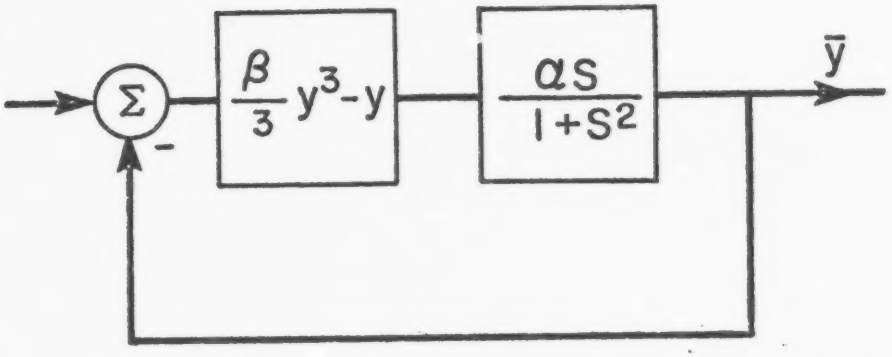

FIG. 4.4 A BLOCK DIAGRAM FOR THE VANDER POL OSCILLATOR.

sinusoid. Now, in general, the output response to a single sinusoid also contains a steady state term or "bias" and higher order harmonics; but in many practical cases, the combined linear parts of the system act as a suitable band-pass filter, and thereby attenuate the bias and the higher order harmonics sufficiently to allow them to be ignored. The assumption that this occurs is called the "filter hypothesis" [Ref. 4.9, p. 110].

The next step is to argue that, for a limit cycle to exist in the absence of any input, system connections require

$$1 + N_s(A, \omega)\, L(j\omega) = 0 \qquad (16)$$

Here the Laplace variable $s = \sigma + j\omega$ and the above equation provides two real equations for A and ω. For the Van der Pol equation, $N_s(A, \omega) = 1/4\ \beta A^2$, which gives $\omega = 1$ and $A = 2/\sqrt{\beta}$ for all α.

It is to be noted that, because the method is based on a Fourier analysis of the periodic output of the nonlinear element, it approximates the nonlinearity in a mean square sense [Ref. 4.9, p. 51]. This means that, if $e(t) = N(A, \Psi) - N_s(A, \Psi)$ is the error incurred at any instant of time, then N_s is chosen such that

$$\overline{e^2} = \frac{\omega}{2\pi} \int_0^{2\pi/\omega} e^2(t)\,dt \qquad (17)$$

is a minimum.

A number of extensions and modifications of the concept have been defined. For example, the DF is defined for nonlinearities which are explicit functions of the input $y(t)$ and its derivative $\dot{y}(t)$ [Ref. 4.9, p. 49]. In the event that the linear parts of the system act only as a low pass filter, so that significant bias propagates around the loop, one may use the so-called dual input describing function (DIDF). This is the sum of the constant gain and the fundamental harmonic gain obtained from a Fourier analysis of the output of the nonlinear element that occurs in response to an input $x(t)$ having the form $x = A_0 + A_1 \sin\Psi$. Similarly a two-sinusoidal input describing function (TSIDF) is defined for systems in which the second harmonic cannot be omitted at the input. The method can also treat systems with more than one nonlinear element and with more than one variable provided that the linear parts of the system act as suitable filters [Ref. 4.9, p. 15-].

There are, however, attendant disadvantages. Firstly, although intuitively based guidelines are available for suggesting conditions under which the filter hypothesis holds [Ref. 4.9, p. 172], for anything but relatively simple systems, it may be difficult to make the required judgements. Considerable physical insight may be required to achieve this end. Typically, even for simple systems it is known that, unless the nonlinearities have odd symmetry, which for a static nonlinearity of the

form $y = y(x)$ implies $y(-x) = -y(s)$, one must use at least the DIDF. Furthermore, many nonlinear problems are originally posed as differential equations and it may be cumbersome or even impossible to formulate them in terms of block diagrams. Gelb and Vander Velde [Ref. 4.9, p. 83] distinguish between explicit and implicit nonlinearites in this respect. In the former case, the nonlinear relation is described in an input-output form, whereas the latter requires solution of an algebraic or differential equation. The above authors note that conversion of implicit nonlinearities to explicit form may amount to solution of the differential equation, and in some cases this has been done. They also suggest that one way to circumvent this is to assume a form of the output, and then solve approximately for the input by the method of harmonic balance [Ref. 4.9, p. 83]. Very recently it has been observed that this method is essentially an ad hoc procedure which can introduce inconsistencies [Ref. 4.14, pp. 59-63].

The describing function technique itself has also been criticised as an ad hoc approximation. However this is not the case. For example, the accuracy of the DIDF can be examined by defining a "bias plus two-sinusoidal input" describing function. It is suggested here that this may be more elegantly achieved by considering the concept to be equivalent to the application of a particular Galerkin procedure to the differential equations for the problem. This is a point that seems to have been hinted at many years ago, but not appreciated in the recent literature. Typically, in 1956 Klotter introduced a "Hamilton harmonic" concept to aid analysis of implicit dynamic nonlinearities [Refs. 4.15, 4.16] yet even relatively recent literature seems not to appreciate the relationship [Refs. 4.17, 4.18, 4.19]. For example, Bergen and Franks [Ref. 4.18], in developing a rigorous justification of the describing function method, make only an oblique reference to the work by Cesari [Ref. 4.19] on the application of the Galerkin method to the same class of problem. The equivalence may be demonstrated by working selected classes of problem.

The Galerkin technique is that particular case of the method of weighted residuals which used the selected trial functions as weight or test functions [Ref. 4.20]. It is described here by consideration of the van der Pol oscillator. To ascertain the existence of a limit cycle, one chooses trial functions which are periodic. It is natural, though not necessary, to choose the set of sinusoids ($\sin n\omega t$, $\cos n\omega t$; $n = 0$, 1 to N) as trial functions, and thereby seek an approximate solution $Y_a(t)$ in the form of the linear combination:

$$Y_a(t) = A_o + \sum_{n=1}^{N} \{A_n \sin n\omega t + B_n \cos n\omega t\} \qquad (18)$$

Substitution of Equation (18) into a differential equation $N[y(t)] = 0$ then gives a residual $\epsilon(t)$, that is $N[Y_a(t)] = \epsilon(t)$, and the Galerkin procedure generates equations for the unknown coefficients in (18) by requiring $\epsilon(t)$ to be orthogonal to the basis functions. For a steady state oscillation having a circular frequency ω, one puts

$$\int_o^{2\pi/\omega} \epsilon(t)\,dt = \int_o^{2\pi/\omega} \epsilon \sin\omega t\,dt = \int_o^{2\pi/\omega} \epsilon \cos\omega t\,dt = 0, \text{ etc.} \qquad (19)$$

The advantage of the Galerkin technique is that it minimizes the residual in a least squares sense, so that if the trial functions are complete, convergence to the exact solution is assured [Ref. 4.20].

The use of this procedure to determine possible existence of a limit cycle leads in general to a nonlinear eigenvalue problem for the A_n, B_n. For the van der Pol oscillator, one seeks a first approximation in the form

$$Y_a(t) = A_o + A_1 \sin\omega t + B_1 \cos\omega t \tag{20}$$

The equation generated using the unity test function is

$$\int_o^{2\pi/\omega} \epsilon dt = 0: \quad A_o = 0 \tag{21}$$

The equations for A_1 and B_1 are:

$$\int_o^{2\pi/\omega} \epsilon \sin\omega t\, dt = 0: \quad (1 - \omega^2)A_1 + \alpha\omega B_1 - \frac{1}{4}\alpha\beta\omega B_1(A_1^2 + B_1^2) = 0 \tag{22}$$

$$\int_o^{2\pi/\omega} \epsilon \cos\omega t\, dt = 0: \quad (1 - \omega^2)B_1 - \alpha\omega A_1 + \frac{1}{4}\alpha\beta\omega A_1(A_1^2 + B_1^2) = 0 \tag{23}$$

By multiplying (22) by B_1 and (23) by A_1, and then subtracting the resulting equations, one obtains,

$$A_1^2 + B_1^2 = \frac{4}{\beta} \tag{24}$$

Substitution of (24) into (22) and (23) gives

$$(1 - \omega^2)A_1 = (1 - \omega^2)B_1 = 0 \tag{25}$$

It follows that non-zero solutions exist only if $\omega = 1$, in which case Equation (24) gives the amplitude of the oscillation. This result is identical to that obtained by the DF procedure. Note that, as must be expected, the solution exists for arbitrary phase, that is only $(A_1^2 + B_1^2)$ is specified.

4.5 Illustration of Galerkin Procedure Applied to ACV Problem: The Box Supply Case

When there is neither flow reversal nor shut-off, and the air source has constant $p_T = p_{To}$, the differential equations are:

$$m\ddot{x} = S_a P_c - mg \tag{26}$$

$$S_a\dot{x} + C_c\dot{P}_c = C_m A_c \sqrt{\frac{2(P_b - P_c)}{\rho}} - C_m I x \sqrt{\frac{2P_c}{\rho}} \tag{27}$$

$$C_b\dot{P}_b = C_m A_f \sqrt{\frac{2(P_{fo} - P_b)}{\rho}} - C_m A_c \sqrt{\frac{2(P_b - P_c)}{\rho}} \tag{28}$$

To obtain a first order solution one puts $\tau = \omega t$, and

$$x_a = x_o + x_1 \sin\tau \tag{29}$$

$$P_{ca} = P_{co} + P_{c1} \sin(\tau + \phi_{c1}) \tag{30}$$

$$P_{ba} = P_{bo} + P_{b1} \sin(\tau + \phi_{b1}) \tag{31}$$

Note that, if the phase of one of the variables, say x, is chosen to simplify manipulation, the phases of other variables are determined by the analysis relative to that of x.

The residual for Equation (26) is ϵ_N, where

$$\epsilon_N = \omega^2 m x_1 \sin\tau + S_a[P_{co} + P_{c1}\sin(\tau + \phi_{c1})] - mg \tag{32}$$

and the integrals

$$\int_0^{2\pi} \epsilon_N d\tau = \int_0^{2\pi} \epsilon_N \sin\tau \, d\tau = \int_0^{2\pi} \epsilon_N \cos\tau \, d\tau = 0$$

give, respectively,

$$S_a P_{co} = mg \tag{33}$$

$$\omega^2 m x_1 + S_a P_{c1} \cos\phi_{c1} = 0 \tag{34}$$

$$S_a p_{c1} \sin\phi_{c1} = 0 \tag{35}$$

from which we have

$$p_{co} = \frac{mg}{S_a} = p_{ce}, \qquad \phi_{c1} = 180°, \qquad \omega^2 m x_1 - S_a p_{c1} = 0 \tag{36}$$

However, application of the procedure to the other equations is not so straightforward. The residual ϵ_c for the cushion capacitance equation is

$$\begin{aligned}\epsilon_c = {} & \omega[S_a x_1 - C_c p_{c1}]\cos\tau \\ & + \left(\frac{2}{\rho_a}\right)^{1/2} C_m L_c[(x_o + x_1 \sin\tau)(p_{ce} - p_{c1}\sin\tau)^{1/2}] \\ & - \left(\frac{2}{\rho_a}\right)^{1/2} C_r A_c[p_{bo} - p_{ce} + p_{b1}\sin(\tau + \phi_{b1}) + p_{c1}\sin\tau]^{1/2}\end{aligned} \tag{37}$$

The integral $\int_o^{2\pi} \epsilon_c d\tau = 0$ becomes

$$\begin{aligned}L_c \Big[x_o \int_o^{2\pi} (p_{ce} - p_{c1}\sin\tau)^{1/2} d\tau + x_1 \int_o^{2\pi} \sin\tau (p_{ce} - p_{c1}\sin\tau)^{1/2} d\tau \Big] \\ - A_c \Big[\int_o^{2\pi} (p_{bo} - p_{ce} + p_{b1}\sin(\tau + \phi_{b1}) + p_{c1}\sin\tau)^{1/2} d\tau \Big] = 0\end{aligned} \tag{38}$$

Most of the integrals in Equation (38) and others that are formed by the Galerkin procedure are elliptic. Many of these forms have been tabulated [Ref. -.21]. However, the standard forms required depend on the relative magnitude of the unknown coefficients, which are parameters in the integrals.

The task of reducing the integrals to standard forms becomes particularly onerous when shut-off and flow reversal are included. Consequently, the analysis proceeded by direct application of numerical methods to the equations of which (38) is representative. A combination of numerical integration and Newton-Raphson techniques was employed as follows. Equation (38) and its companions comprise a set of nonlinear algebraic equations $f_i(\underset{\sim}{x}) = 0$, i = 1, 2...N, for the vector of unknowns $\underset{\sim}{x} = (x_o, x_1, p_{c1}, \cdots \phi_{b1})^T$. Given $\underset{\sim}{x}^{(k)}$, the k-th approximation to $\underset{\sim}{x}$, the integrations in equations such as (38) were computed using Simpson's rule (100 points). This gave $f_i^{(k)}(\underset{\sim}{x})$. The Newton-Raphson technique was then applied to generate $\underset{\sim}{x}^{(k+1)}$:

$$\underset{\sim}{x}^{(k+1)} = \underset{\sim}{x}^{(k)} - \lambda \left(\frac{\partial f_i}{\partial x} \right)^{-1} f_i[\underset{\sim}{x}^{(k)}]$$

The square matrix of derivatives $\partial f_i / \partial \underset{\sim}{x}$ at each $\underset{\sim}{x}^{(k)}$ was determined by a finite difference procedure, and the factor $\lambda < 1$ was included to ensure convergence. It is noted that, for an inappropriate initial estimate of the unknowns, the process would either diverge or converge to the unstable trivial solution $x_1 = 0$, $p_{c1} = 0$, $p_{b1} = 0$.

4.6 Typical Results

4.6.1 Box Plenum Model

Numerical results are given for a system in which the cushion base diameter $D_p = 1.83$ m and height $L_b = 0.914$ m. The box volume $V_b = 1.415$ m^3, and the feed areas $A_c = A_e = 0.073$ m^3. The fan slope coefficient C_s is set equal to zero. This geometry is representative of that used on a multicell system developed for a towed raft application.

The linear heave stability boundary for this system in terms of cushion pressure p_{ce} and hovergap h_e is obtained from Equations (1) to (13) in the usual way [Refs. 4.4, 4.5, 4.6]. The results are given in Figure 4.5; the hatched side of the curve indicates the unstable region. Points "a", "b" and "c", corresponding to $h_e = 4.58$ mm, are examined for limit cycle behaviour. Typical first order Galerkin results are given in Table 4.1. For these the initial estimates given in Table 4.2 were used. The results indicate that a limit cycle does exist in the unstable region close to the boundary and that, as might be expected, the amplitude of the oscillation increases with increase in distance from the boundary.

Numerical results obtained from a Runge-Kutta integration of the governing nonlinear equations are shown in Figure 4.6. Fourier decompositions of the signals are given in Table 4.3. On comparing Tables 4.1 and 4.3, one can see that for point "b" the agreement is quite good, whereas for point "a" it is not. Table 4.4 gives Galerkin results for point "a" obtained with second order harmonics retained. On comparing these results with those in Table 4.3, one can see that the agreement with the harmonics included is much improved. Figure 4.6 suggests that the higher harmonics are associated primarily with shut-off.

4.6.2 Duct-Plenum Model

Numerical results are given for a system with feed areas having the same dimensions as in the plenum-box model. The duct has the same volume as the box; it is 6.1 m long and 0.914 m in diameter. This is typical of the multicell mentioned previously as modified for overwater operation. As for the previous results C_s is set equal to zero.

The linear heave stability boundary for this system in terms of p_{ce} and h_e is shown in Figure 4.7, where again the hatched side of the curve indicates the unstable region. An important point to note in Figure 4.7 is

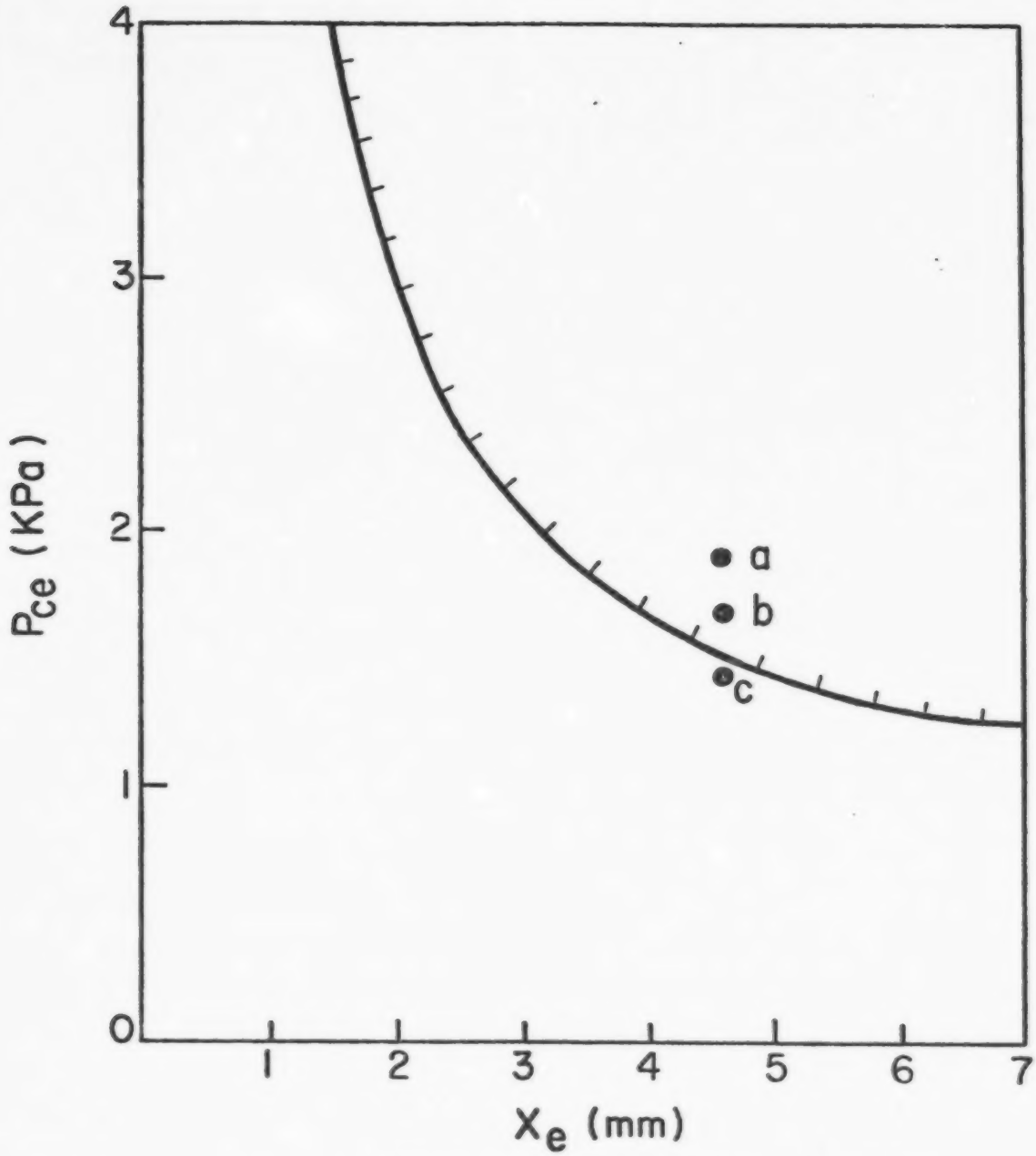

FIG. 4.5 LINEAR HEAVE STABILITY BOUNDARY FOR BOX-PLENUM SYSTEM

Table 4.1

Typical Galerkin Results for Plenum-Box Model

with First Order Harmonics Only

Hovergap h_e = 4.58 mm. Lengths in mm, pressures in kPa

Operating Point	Variable	ω	Coefficients in Expansion		
				First Harmonic	
			Constant	Amplitude	Phase
a	x	26.04	4.12	4.17	0
p_{ce}=1.914	p_c		1.9147	0.552	+180°
	p_b		2.1613	0.275	+177.0°
b	x	27.84	4.38	3.21	0
p_{ce}=1.675	p_c		1.6754	0.425	+180°
	p_b		1.8928	0.212	+176.5°
c	x	30.07	4.57	0	
p_{ce}=1.436	p_c		1.4360	0	
	p_b		1.6221	0	

Table 4.2

Initial Estimates for Iteration: Box Supply Case

Variable	Coefficients in Expansion				
	Constant	First Harmonic		Second Harmonic	
		Amplitude	Phase	Amplitude	Phase
x	x_e	$\frac{S_a(p_f-p_{ce})}{m\omega_{lin}^2}$	0	0	0
p_c	p_{ce}	p_f-p_{ce}	180°	0	0
p_b	p_{be}	p_f-p_{be}	180°	0	0
ω	linear eigenvalue analysis				

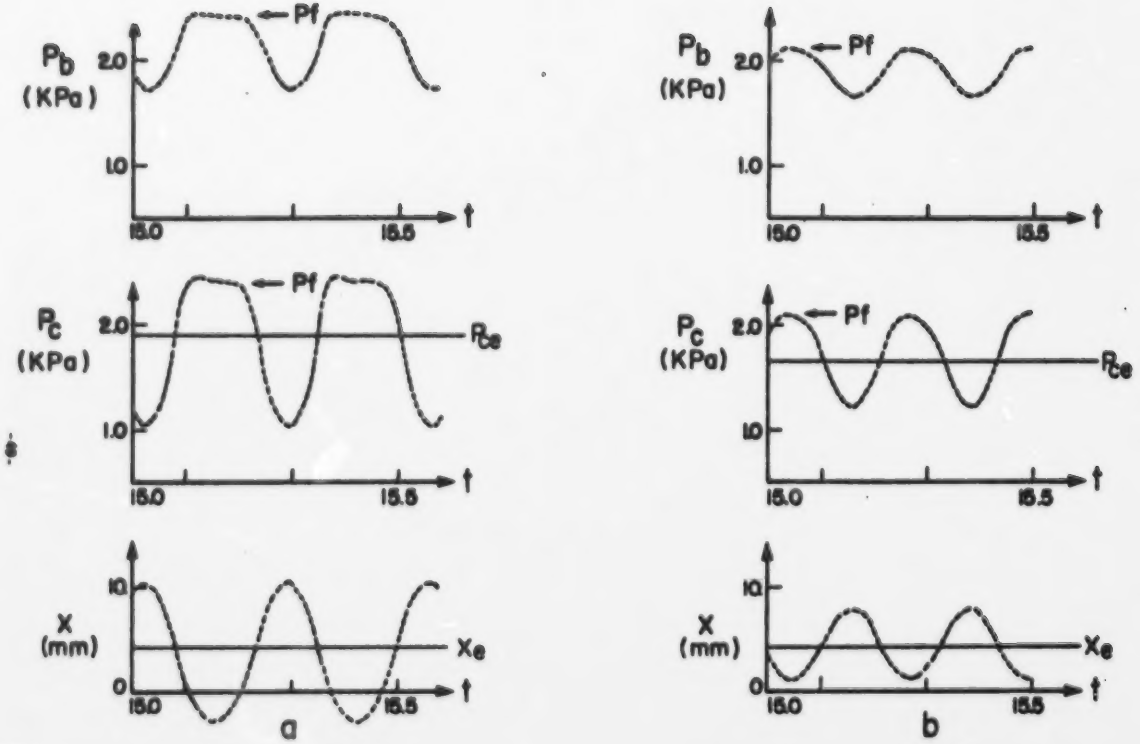

FIG. 4.6 RUNGE-KUTTA NUMERICAL INTEGRATION RESULTS FOR BOX-PLENUM SYSTEM.

Table 4.3

Fourier Decomposition of Numerical Simulation for Plenum-Box Model

Hovergap h_e = 4.58 mm

Operating Point	Variable	Frequency ω	Coefficients in Expansion				
			Constant	First Harmonic		Second Harmonic	
				Amplitude	Phase	Amplitude	Phase
a	x	23.3	3.26	6.65	0	0.46	+106°
	p_c		1.916	0.715	180°	0.211	-94°
	p_b		2.162	0.354	+177°	0.107	-105°
b	x	27.9	4.39	3.37	0	0.05	+79°
	p_c		1.675	0.451	180°	0.03	-116°
	p_b		1.893	0.224	+176°	0.0179	-138°

Table 4.4

Galerkin Results for Point "a" with Second Harmonics Included

Variable	Frequency ω	Constant	First Harmonic		Second Harmonic	
			Amplitude	Phase	Amplitude	Phase
x	23.16	3.21	7.06	0	0.600	+79°
p_c		1.915	0.739	180°	0.251	-101°
p_b		2.164	0.368	+176°	0.135	-109°

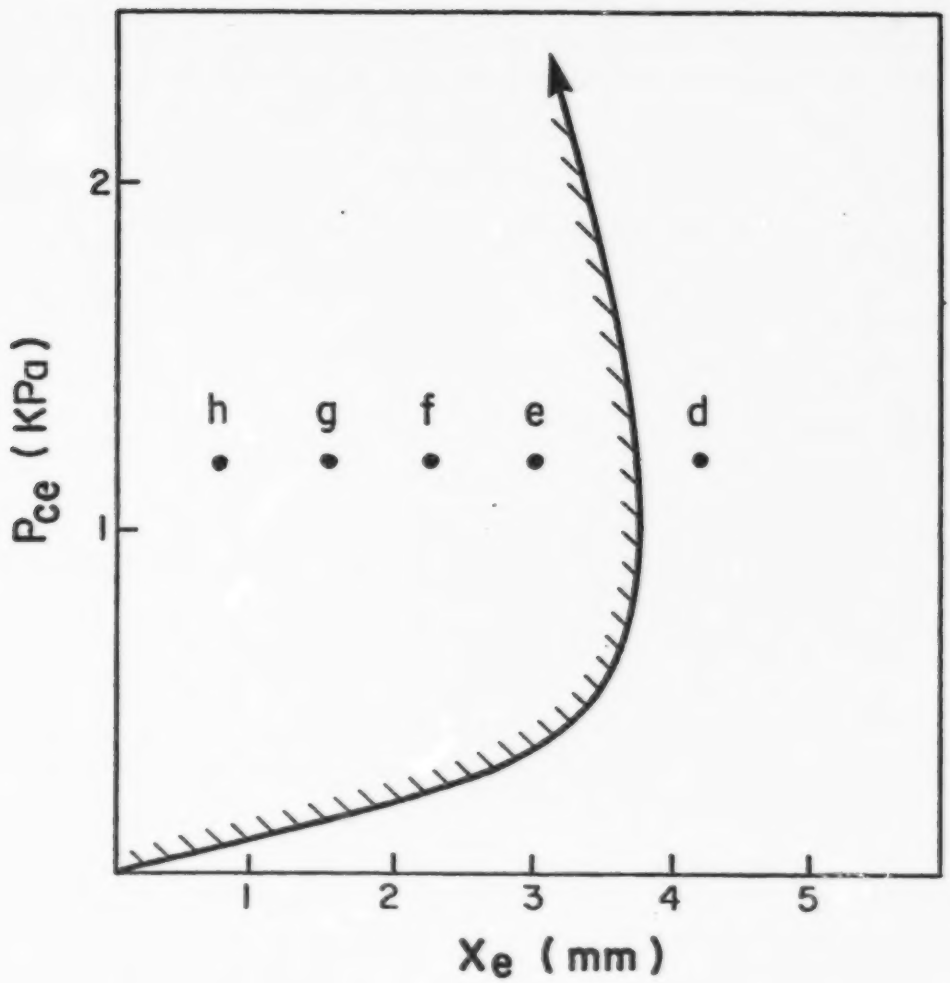

FIG. 4.7 Linear Heave Stability Boundary for Duct-Plenum System

that, whereas the plenum-box model was very stable at low flows or hovergaps, the plenum duct model is unstable. This instability is dealt with in detail in [Refs. 4.6, 4.7], where it is shown to be a Helmholtz resonator effect associated with the inertance of the air in the duct and the compressibility of the air in the cushion. Here, points "d" to "h" are examined for limit cycle behaviour.

Typical first order Galerkin results are given in Table 4.5. For these, the initial estimates given in Table 4.6 were used. The amplitude of the signals for x in Table 4.5 is plotted in Figure 4.8. This plot shows how the amplitude first increases rapidly with distance from the stability boundary and then decreases as h_e approaches zero.

Table 4.5

Typical Galerkin Results for Duct-Plenum Model

with First Order Harmonics Only

P_{ce} = 1.197 kPa

Operating Point	Variable	Frequency ω	Coefficients in Expansion		
				First Harmonic	
			Constant	Amplitude	Phase
e	x	54.0	2.77	3.32	0
	P_c		1.197	1.178	180°
h_e=3.03	Q_d		0.2595	0.6797	-75.9
f	x	54.3	1.44	3.29	0
	P_c		1.197	1.183	180°
h_e=2.29	Q_d		0.1480	0.6810	-77.5
g	x	54.5	-.05	2.86	0
	P_c		1.197	1.039	180°
h_e=1.52	Q_d		0.0750	0.6014	-79.5
h	x	54.9	-.81	1.90	0
	P_c		1.197	.694	180°
h_e=0.76	Q_d		0.0279	0.4048	-83.1

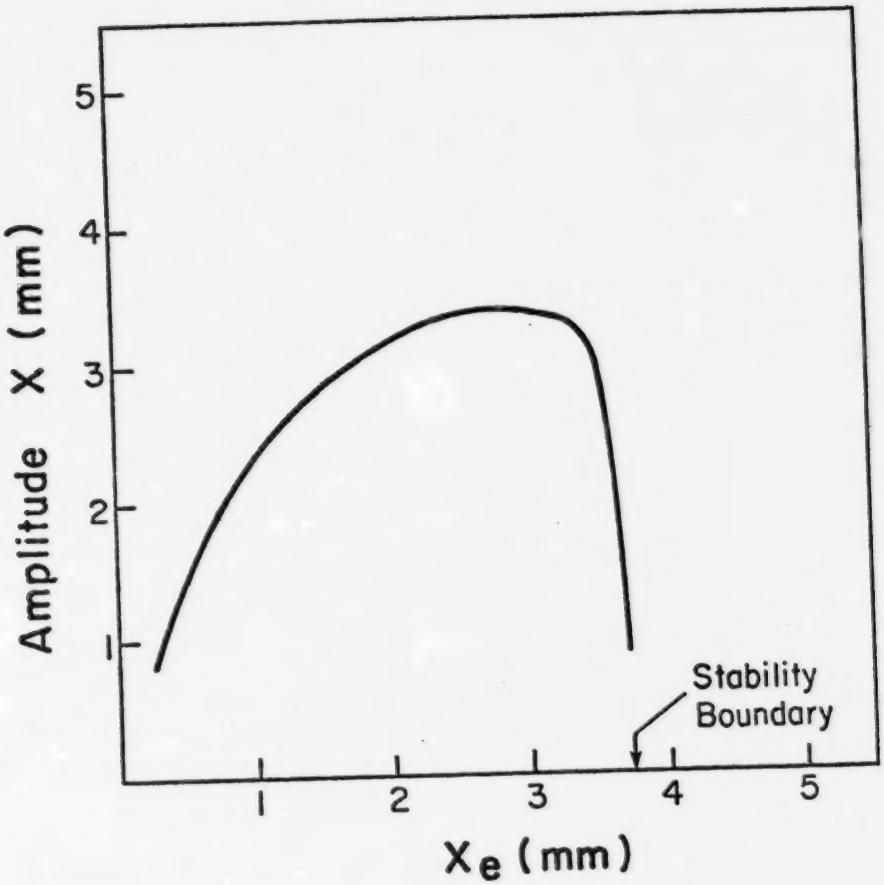

FIG. 4.8 Amplitude of Limit Cycle for Duct-Plenum System

Table 4.6

Initial Estimates for Iteration: Duct Supply Case

Variable	Coefficients in Expansion		
	Constant	First Harmonic	
		Amplitude	Phase
x	x_e	$\frac{S_a p_{ce}}{m\omega_{lin}^2}$	0
p_c	p_{ce}	p_{ce}	180
q_d	Q_{de}	$\frac{A_d}{L_d \rho} \frac{p_{ce}}{\omega}$	-90
ω	linear eigenvalue analysis		

Numerical results for x obtained from a Runge-Kutta integration of the governing equations are shown in Figure 4.9. Fourier decompositions of these signals together with those for p_c and Q_d for points "e" and "g" are given in Table 4.7. Comparison with the Galerkin results shows that the agreement is reasonable.

4.7 Limit Cycle Suppression

In a series of papers published in the late fifties and early sixties, Oldenburger and his colleagues [Refs. 4.22-4.25] demonstrated experimentally and confirmed theoretically that a high frequency signal at the input to the nonlinearity of a simple limit cycling control system could quench or suppress the limit cycle. Using describing function theory, they showed how this 'dither' signal modified the input-output characteristics of the nonlinearity; for example very often it had the effect of linearizing in a particular way the input-output relationship of the nonlinearity about the origin.

It is shown here that a similar procedure can be used to suppress ACV limit cycle oscillations. For the present problem, a high frequency pressure signal is introduced by adding to the mass conservation equation for the cushion a term which gives a periodic volume variation; that is one puts

$$C_c \dot{p}_c = (Q_c - Q_a) - S_a \dot{x} + \frac{d}{dt}(\Delta V_o) \tag{39}$$

where

$$\Delta V_o = C_d \sin(\omega_d t) \tag{40}$$

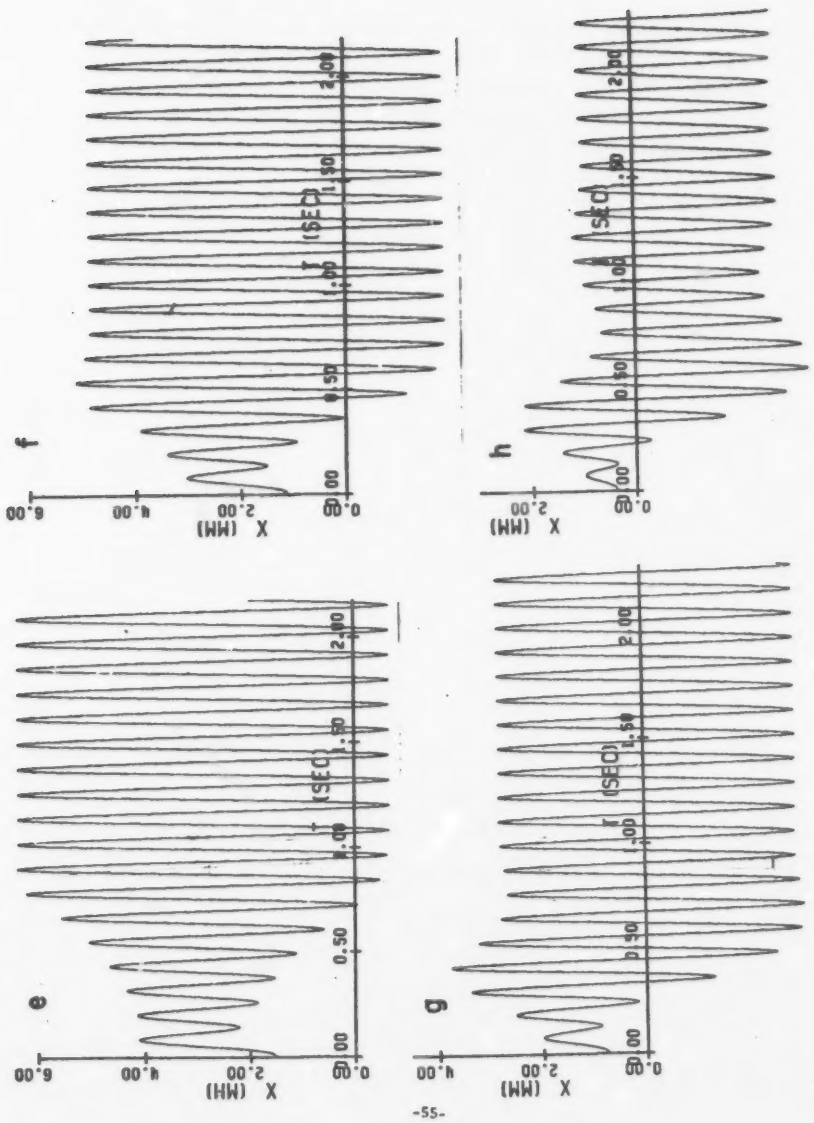

FIG. 4.9 RUNGE-KUTTA RESULTS FOR DUCT-PLENUM SYSTEM.

-55-

Here, following Oldenburger, ω_d is set equal to ten times the limit cycle frequency ω. This volume variation, which may be obtained by using a piston, induces a high frequency pressure variation which serves as an extra input into the nonlinearities.

Typical Galerkin results for the box-plenum system with $C_d = 0.012$ which, for the present geometry gives a cushion volume variation from equilibrium of only 0.5% of the basic cushion volume, are given in Table 4.8, where the subscript "d" indicates a component associated with the dither signal. These results show that the limit cycles at "a" and "b" have been effectively quenched. They are in close agreement with results obtained from a Runge-Kutta numerical integration. It is interesting to note that the volume variation creates bias values of p_c and x, namely, p_{co} and x_o, which when plotted in Figure 4.5 lie in or close to the stable region. The quenching effect is probably associated with this shift. With $C_d = .006$, the limit cycles are not quenched. However, they are reduced in amplitude and again this is believed to be associated with a shift in bias values. A typical result for the unquenched case is given in Table 4.9.

It is to be noted that, because the dither signal frequencies used here are of the order of 50 cps, the use of a quasi-steady orifice flow law is questionable. In fact, an order of magnitude analysis presented in [Ref. 4.7] indicates that for the box and cushion inlet orifices the local term in Euler's equation could be of the order of the convective term. Thus, for these flows a combined resistance-reactance model is more appropriate [Ref. 4.12].

Table 4.7

Fourier Decomposition of Numerical Simulation for Duct-Plenum Model

$p_{ce} = 1.197$ kPa

Operating Point	Variable	Frequency ω	Coefficients in Expansion				
			Constant	First Harmonic		Second Harmonic	
				Amplitude	Phase	Amplitude	Phase
e	x	52.8	2.84	3.51	0	.1275	-165
	p_c		1.197	1.190	180	0.153	16
h_e=3.05	Q_d		0.2663	0.7023	-75.8	0.0586	91.9
g	x	54.6	-.07	2.85	0.0	0.0036	47.8
	p_c		1.197	1.030	180	0.013	-160
h_e=1.52	Q_d		0.0747	0.6003	-79.7	0.0070	-4.6

Table 4.8

Galerkin Limit Cycle Quenching Results for Box-Plenum System

Hovergap h_e = 4.58 mm

Operating Point	Variable	Coefficients in Expansion				
		Constant	First Harmonic		Dither Content	
			Amplitude	Phase	Amplitude	Phase
a	x	3.51	0.0		0.045	20
	p_c	1.9147	0.0		.5940	-160
	p_b	2.1881	0.0		.2591	173.0
b	x	3.26	0.0		0.045	20
	p_c	1.6754	0.0		.5966	-160
	p_b	1.9161	0.0		.2548	174

Table 4.9

Galerkin Limit Cycle Suppression Results for Box Plenum System

Hovergap h_e = 4.58 mm, Point "a"

Variable	Coefficients in Expansion				
	Constant	First Harmonic		Dither Content	
		Amplitude	Phase	Amplitude	Phase
x	4.05	3.51	0	0.022	20
p_c	1.9147	.4660	180	.2958	-160
p_b	2.1687	.2338	176.6	.1286	175

4.8 Conclusions

Application of a Galerkin-describing function technique suitable for the analysis of oscillations of nonlinear systems to the equations describing the motion of two simple air cushion systems confirms inferences made from detailed numerical simulations, namely that the motion near linear stability boundaries is usually a limit cycle. The limit cycle is associated with the nonlinearities that seem to be universally characteristic of an air cushion: the Bernoulli law governing the quasisteady air flow escape process from the cushion coupled to the varying hovergap, and the phenomenon of shut-off. Even for operating points which are relatively close to stability boundaries the oscillations may be large, in the sense that the amplitudes of both the cushion pressure and vehicle motion may be larger than their respective equilibrium or mean values. Comparison of the results of a Galerkin-describing function analysis with those obtained from Fourier analysis of detailed numerical simulations show that, when shut-off occurs, significant second order harmonics may be present.

The approximate technique used in the present work is well suited to the analysis of large nonlinearities, but it has two associated difficulties. One is the computational burden, and the other is that, at a given level of approximation, no indication is given as to the significance of omitted higher order harmonics. Unlike the results that might be obtained from perturbation techniques used to study small amplitude oscillations, investigation of the higher order harmonics requires a complete reformulation of the lower order analysis. In view of the computational burden, such a procedure is tedious. For the present work, which is limited to comparisons of the results with those obtained from numerical simulations, this is not a problem. However, for the exploration of new situations it poses a major difficulty. It is to be noted that a complete investigation should, ideally, include a stability analysis similar to that described by Gelb and Vander Velde [Ref. -.9].

Finally it is shown that an equivalent of the "artificial dither" technique used in the describing function literature for suppression of limit cycles may also be used to suppress air cushion oscillations. This is achieved by introducing a very small high frequency oscillation to the cushion volume. Its practical implementation seems to be straightforward, but the idea needs to be confirmed experimentally.

5. USE OF ORIFICE-CAVITY COMBINATIONS TO CONTROL STABILITY AND DAMPING

5.1 Introduction

Interest in the application of orifice-cavity combinations to cushion dynamics originated partly in work done under contract to TDC (File D500-210) by Parravano and Sullivan and completed in March 1977 [Ref. 5.1]. This showed that such devices could add significant damping to the system. They have also been successfully used to suppress self-excited oscillations [Refs. 5.2, 5.3], and it is in this context that they are relevant to the present contract. The basic aim of the work described here is to develop a satisfactory theoretical understanding of the way in which they influence cushion dynamics.

The theoretical problem associated with the use of orifice-cavity combinations is best appreciated by consideration of the earlier work undertaken by UTIAS for TDC. The contract report [Ref. 5.1] described an investigation of the heave response of a plenum chamber equipped with a secondary suspension consisting of hinged lips supported by air-bag damper-springs. The geometry is shown in Figure 5.1. In the diffusion chamber, the cushion air is dispersed by a deflector plate and then passed through a series of orifices into the damper bag to inflate the secondary suspension, and into the cushion to create lift. A theoretical model for this cushion was developed using the ideas employed in the analysis of the duct problem as described in Sections 2 and 4 of this report. A basic feature was the use of a quasi-steady Bernoulli type orifice law for all cushion flow processes, including that between the diffusion chamber and the damper-spring. The full nonlinear equations were solved numerically on a digital computer, and theoretical results for the response to a ground oscillating sinusoidally in heave were obtained. Experimentally measured responses were obtained by using the UTIAS servohydraulically driven heave table. Two cases were studied in detail:

(i) K_D the ratio of feed area into the damper bag to feed area into the cushion = 3

(ii) $K_D = 0.1$.

Figure 5.2 compares the amplitude of the experimentally measured frequency response for the two values of K_D. It is clear that changing K_D from 3 to 0.1 significantly increases the damping. Figures 5.3 and 5.4 compare the experimentally measured amplitude response with the theoretical predictions. The good agreement indicates that the analytical model provides a useful description of the dynamics.

5.2 Basic Problem

The equation describing the damper-orifice flow used in Ref. 5.1 is based on the Bernoulli law with the implicit assumption that the flow is quasi-steady. This model is clearly invalid for sufficiently high frequencies, since the latter assumption no longer holds. Furthermore, in the limit of

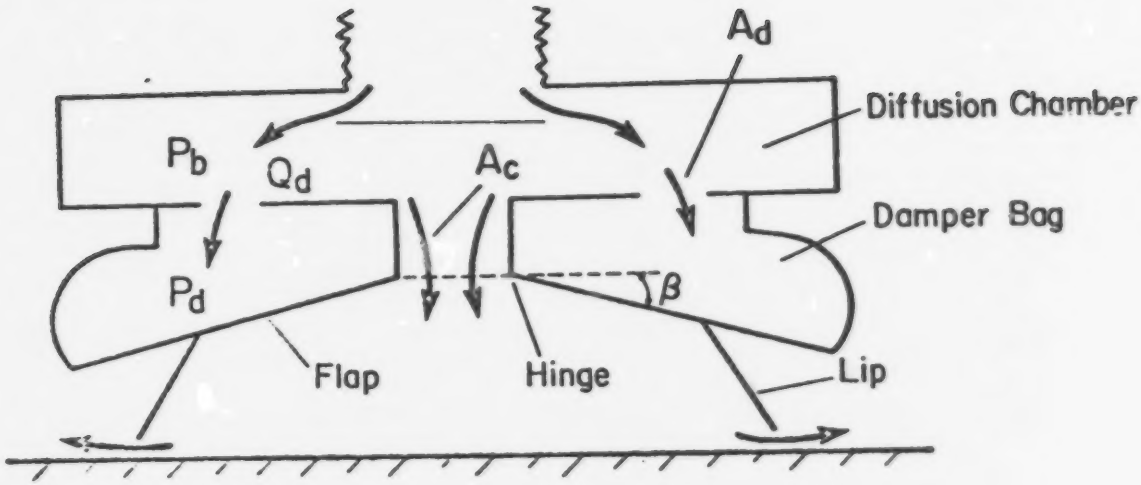

FIG. 5.1 GEOMETRY OF HINGED LIP TACV CUSHION TESTED AT UTIAS

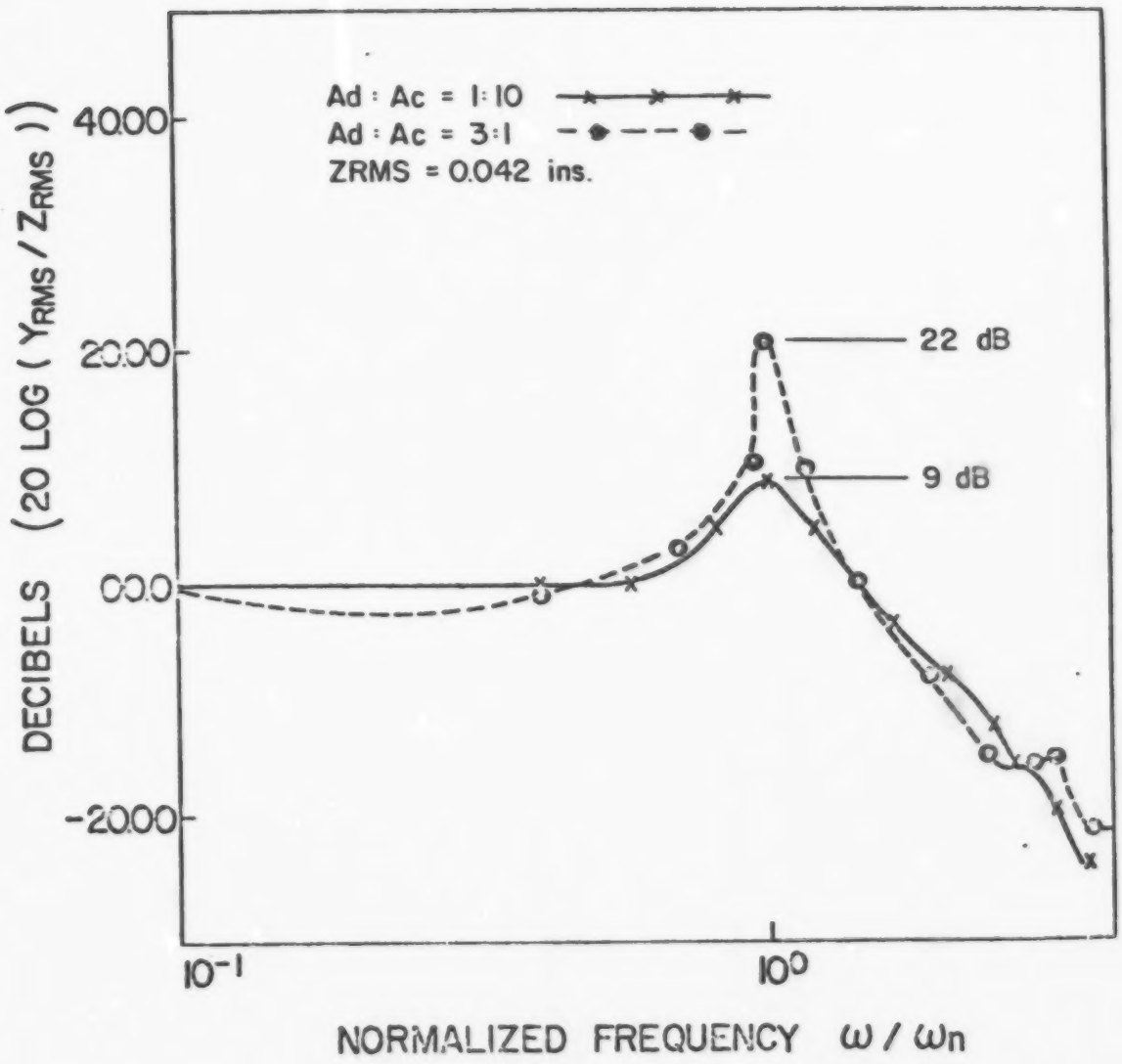

FIG. 5.2 TYPICAL MEASURED AMPLITUDE RESPONSE OF HINGED-LIP CUSHION AT TWO DAMPER INLET AREAS. THE HEAVE TABLE GROUND INPUT IS Z AND THE VEHICLE RESPONSE IS Y

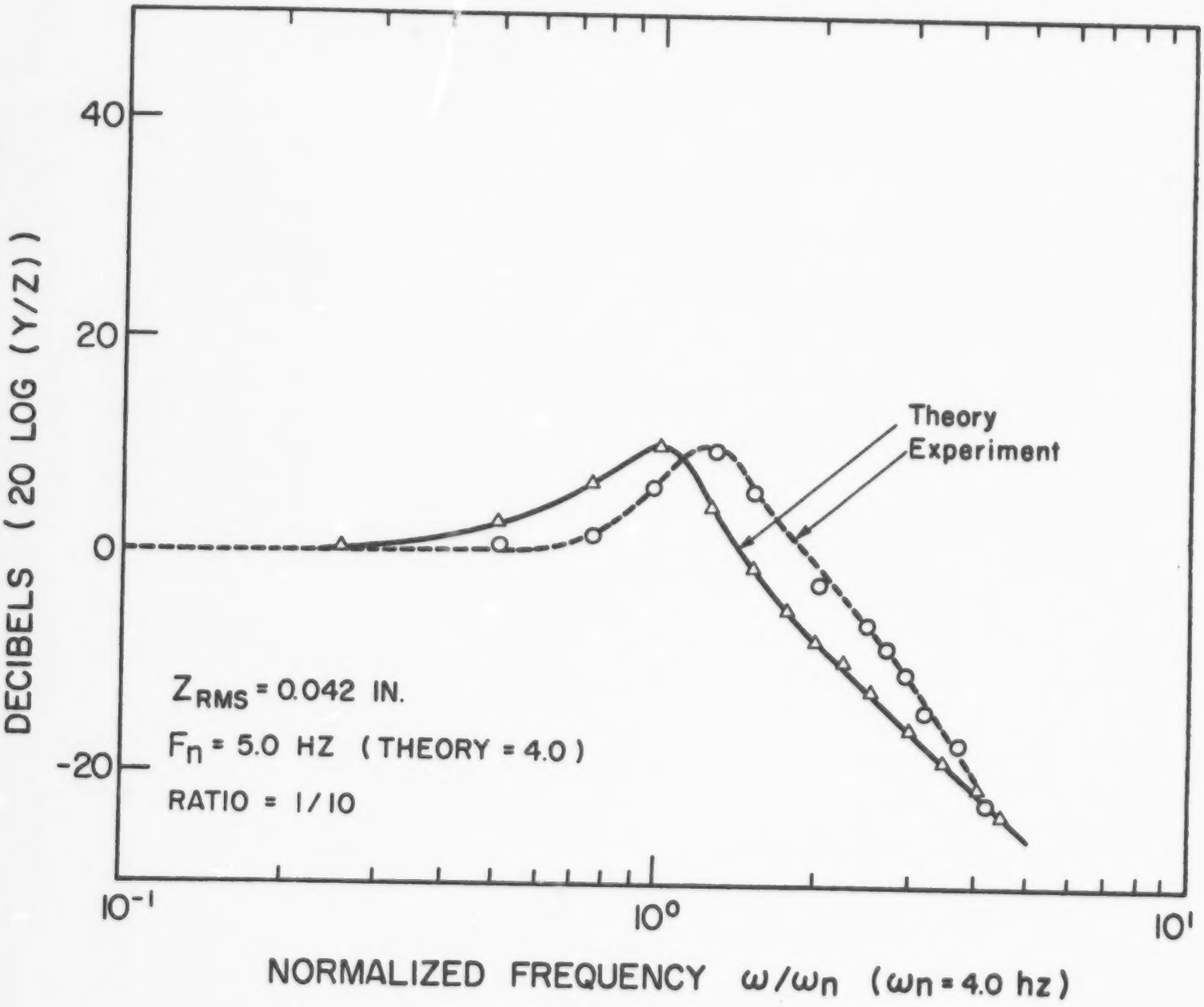

FIG. 5.5 COMPARISON OF THEORY AND EXPERIMENT FOR HINGED FLAP CASE
RATIO = 1/10

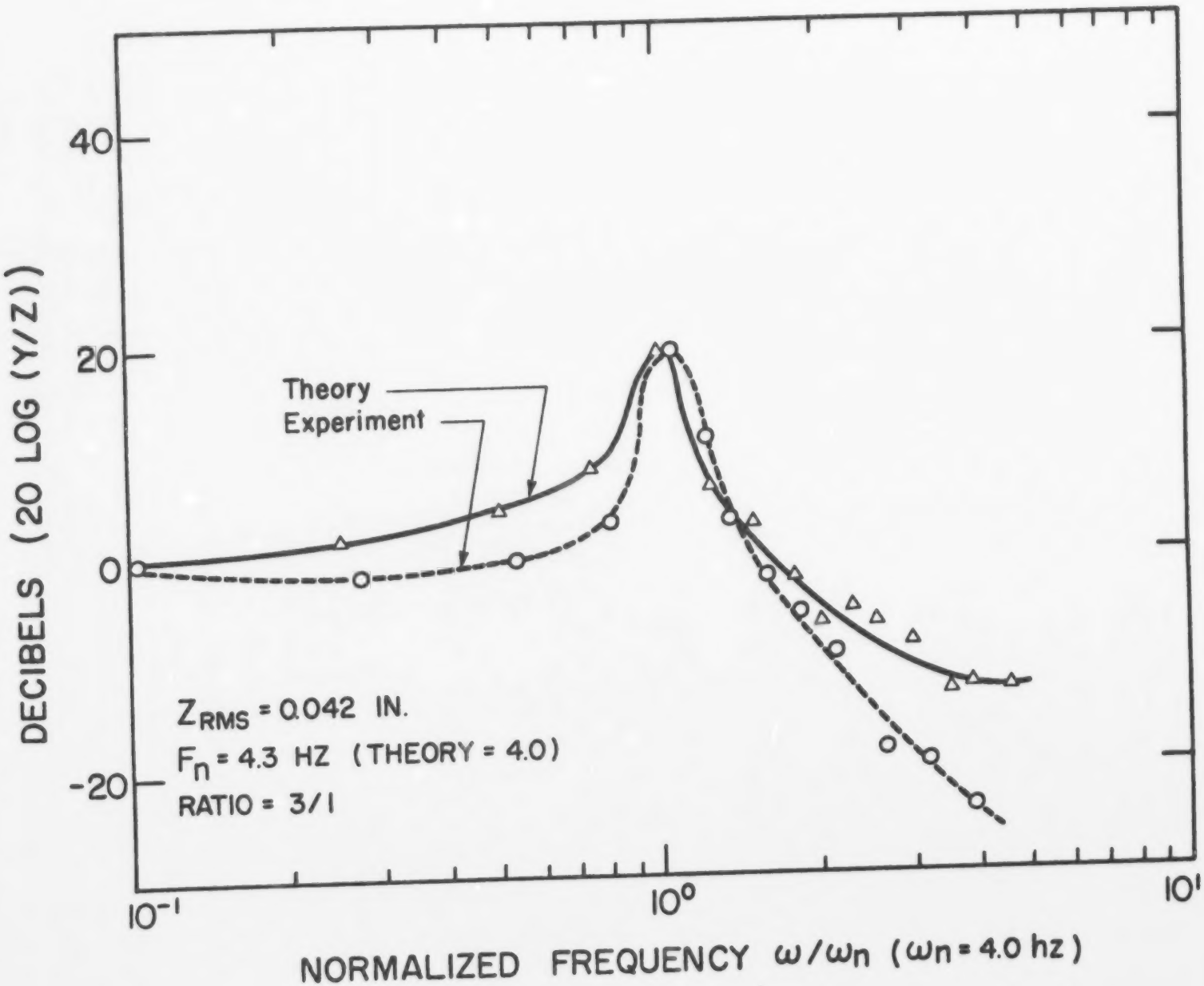

FIG. 5.4 COMPARISON OF THEORY AND EXPERIMENT FOR HINGED LIP CUSHION WITH A_D/A_C = 3

zero mean flow, owing to the square root dependence of flow on pressure difference, it is not possible to linearize the expression about the equilibrium condition corresponding to zero mean pressure differential across the orifice. That is, the model is inherently nonlinear.

In the limit of zero mean flow and for small enough flow oscillation amplitudes, it seems reasonable to suggest that the orifice-cavity behaviour approaches the model used in acoustics [Ref. 5.4, p. 186]. This is usually termed a Helmholtz resonator. In the language used in acoustics, it is a linear lossless reactive model, in contrast to the Bernoulli model, which is resistive, in addition to being inherently nonlinear. All of the fluid particles oscillate in phase, so that one can model the process by a single lumped mass as shown in Figure 5.5. As for the Bernoulli model, the cavity acts like an air spring.

The equivalent mass for the lumped mass model of the process consists of two parts:

(a) the core mass in the orifice or tube, which is equal to $\rho A_d \ell$, where A_d is the orifice area and ℓ is the tube length;

(b) the "attached" mass associated with the motion of the air outside the core = $\rho 2 A_d \Delta\ell$.

For low enough frequencies, and circular orifices which are sufficiently small to be approximated by a hole in an infinite baffle, it has been shown that [Ref. 5.-]

$$\Delta\ell = \frac{4d}{3\pi}$$

where d is the diameter of the orifice. The total equivalent slug length is then $\ell' = \ell + 8d/3\pi$.

It seems plausible to suggest that, for a linear stability analysis, the Helmholtz resonator model provides the resolution of the ACV problem. Apart from the fact that it is linear, it seems likely that, since linear analyses consider infinitesimal perturbations from an equilibrium state, it is a correct first order model of the physics.

5.3 Application to Air Cushion Stability Analysis

5.3.1 Formulation

Consider the simple box-plenum system depicted in Figure 5.6. It is fed through a flexible duct and stabilizing orifice of area A_f by a fan. It hovers at height "h" above a smooth flat ground. A "Helmholtz resonator" cavity is fixed rigidly to the cushion and the volume of this cavity, V_d, is connected to the cushion by a single circular orifice having an area A_d.

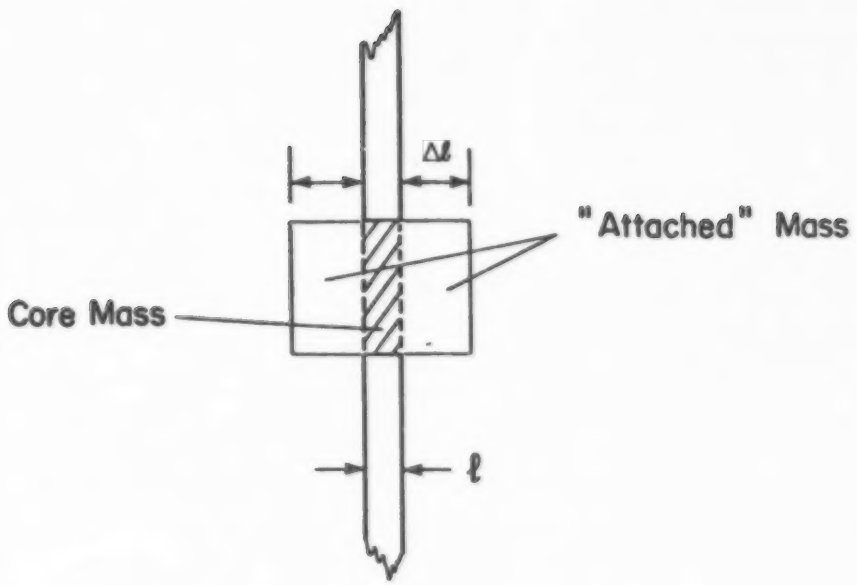

FIG. 5.5 ILLUSTRATING THE HELMHOLTZ RESONATOR MODEL

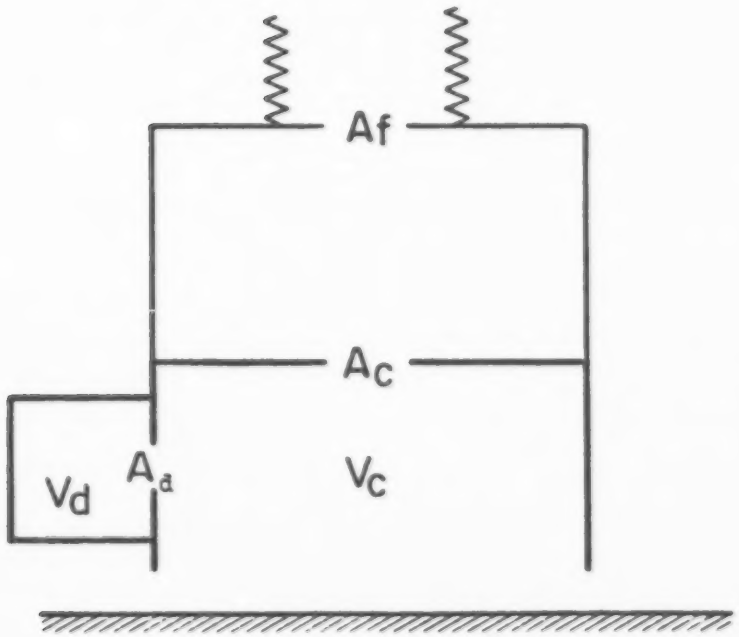

FIG. 5.6 BASIC CUSHION WITH ORIFICE-CAVITY ATTACHED

To apply the Helmholtz resonator model to this configuration, let v_d be the velocity of the equivalent lumped mass at the orifice, with v_d positive corresponding to motion into the resonator. According to this concept, the pressure differences between cushion and cavity act directly on the lumped mass to accelerate and decelerate it as it oscillates back and forth. Newton's law applied to the lumped mass or "slug" gives

$$m_{slug} \frac{dv_d}{dt} = (p_c - p_d)A_d \tag{1}$$

where $m_{slug} = \rho_a A_d \ell'$ and ρ_a is the atmospheric air density. Equation (1) may be written in terms of the equivalent volume flux Q_d through the orifice, that is $Q_d = v_d A_d$, so

$$m_{slug} \frac{dQ_d}{dt} = (p_c - p_d)A_d^2 \tag{2}$$

It is noted here that this equation is the limiting case for zero mean flow proposed by Bellegrin and Bajura in their treatment of pulsating flow through orifice-meters [Ref. 5.5]. Equation (2) may be rewritten in the form

$$C_A \frac{dQ_d}{dt} = (p_c - p_d), \quad C_A = \frac{\rho_a \ell'}{A_d} \tag{3}$$

To complete the description of the Helmholtz resonator, the spring effect of the cavity has to be modelled. It is assumed that the air in the cavity is compressed and expanded isentropically by the action of the slug of air at the orifice. Following the usual acoustic approximation, for pressure oscillations with amplitudes which are small compared to atmospheric pressure, the linearized equivalent of the isentrope law is a pneumatic capacitance:

$$C_d \frac{dp_d}{dt} = Q_d; \qquad C_d \triangleq \frac{V_d}{\rho_a a^2} \tag{4}$$

Here, a is the atmospheric sound speed.

The remaining equations for the cushion heave dynamics are now formulated. They are the same as those used in the analyses given in Sections 2 and 4, except that the cushion capacitance equation is modified to account for the compression and expansion of the cushion air by the slug. We have:

(i) flow from box to cushion:

$$Q_c = C_m A_c \sqrt{\frac{2}{\rho_a}(p_b - p_c)} \tag{5}$$

(ii) flow from fan to box

$$Q_f = C_m A_f \sqrt{\frac{2}{\rho_a}(p_f - p_b)} \tag{6}$$

(iii) fan law, which for simplicity is taken here to be:

$$p_f = \text{constant} \tag{7}$$

(iv) cushion air escape law:

$$Q_a = C_m L_p h \sqrt{\frac{2p_c}{\rho_a}}, \tag{8}$$

(v) Newton's law for the heaving motion of the cushion:

$$M \frac{d^2h}{dt^2} = S_a p_c - Mg, \tag{9}$$

(vi) modified cushion capacitance law

$$\frac{dp_c}{dt} = \frac{1}{C_c} \left\{ (Q_c - Q_a - Q_d) - S_a \frac{dh}{dt} \right\} \tag{10}$$

where

$$C_c = \text{cushion capacitance} = \frac{V_c}{\rho_a a^2} \tag{11}$$

and V_c is the total volume enclosed by the cushion.

(vii) box capacitance law

$$\frac{dp_b}{dt} = \frac{1}{C_b}(Q_f - Q_c) \tag{12}$$

5.3.2 Linear Stability Analysis

The equations are linearized and the Laplace transform technique is applied in the usual way. Perturbations of a variable ψ from its equilibrium value ψ_e are denoted by $\Delta\psi$, thus $\Delta\psi = \psi(t) - \psi_e$. Also Laplace transformed variables are denoted by a bar, that is

$$\int_0^\infty e^{-st} \psi(t) dt = \bar{\psi}(s)$$

The law for the flow from box to cushion (5) becomes

$$\bar{Q}_c = \frac{1}{R_c}\left(\overline{\Delta p_b} - \overline{\Delta p_c}\right) \tag{13}$$

where the feed orifice resistance R_c is defined as

$$R_c = \frac{2(p_{be} - p_{ce})}{Q_{ce}}$$

The orifice law (6) becomes

$$\Delta\bar{Q}_f = \frac{-1}{R_f}\Delta\bar{p}_b \qquad R_f = \frac{2(p_f - p_{be})}{Q_{ce}}$$

where the cushion air discharge law (8) becomes

$$\Delta\bar{Q}_a = \frac{1}{\alpha_A}\Delta\bar{h} + \frac{1}{R_A}\Delta\bar{p}_c \tag{14}$$

where

$$\alpha_a = \frac{h_e}{Q_{ae}}, \qquad R_A = \frac{2p_{ce}}{Q_{ae}}$$

Newton's law for the slug in the orifice cavity becomes

$$C_A s\Delta\bar{Q}_d = \Delta\bar{p}_c - \Delta\bar{p}_d \tag{15}$$

The capacitance law for the cavity is

$$C_d s\Delta\bar{p}_d = \Delta\bar{Q}_d \tag{16}$$

and for the cushion, the capacitance law is

$$C_c s\Delta\bar{p}_c + S_a\Delta s\,\bar{h} = \Delta\bar{Q}_c - \Delta\bar{Q}_a - \Delta\bar{Q}_d \tag{17}$$

while for the box the capacitance law is

$$C_b s\Delta\bar{p}_b = \Delta\bar{Q}_e - \Delta\bar{Q}_c \tag{18}$$

Finally Newton's law for the heaving motion(s) becomes

$$Ms^2\Delta\bar{h} = S_a\Delta\bar{p}_c \tag{19}$$

Note that if the cushion is fed directly the following characteristic equation is obtained for the system:

$$C_5s^5 + C_4s^4 + C_3s^3 + C_2s^2 + C_1s + C_o = 0 \tag{20}$$

with

$$C_5 = C_AC_cC_d; \qquad C_4 = C_AC_d\left(\frac{1}{R_c} + \frac{1}{R_A}\right)$$

$$C_3 = \left(C_c + C_d + \frac{C_AC_d}{M}S_a^2\right); \qquad C_2 = \left(\frac{1}{R_c} + \frac{1}{R_a} + \frac{C_AC_dS_a}{\alpha_AM}\right)$$

$$C_1 = \frac{S_a^2}{M}; \qquad C_o = \frac{S_a}{\alpha_AM} \tag{21}$$

A useful consistency check can be made by noting that, as A_d becomes large, one would expect the system to revert to a simple cushion, but with total cushion volume equal to the sum of the cushion and damper volumes. The characteristic equation for a simple cushion is third order in the Laplace variable s. Now equation (3) shows that, as A_d becomes large, $C_A \to 0$. Since in equation (20), C_5 and $C_4 \to 0$ in this limit, the equation reduces to

$$(C_c + C_d)s^3 + \left(\frac{1}{R_c} + \frac{1}{R_a}\right)s^2 + \frac{S_a^2}{M}s + \frac{S_a}{\alpha_aM} = 0 \tag{22}$$

which is the characteristic equation for a simple cushion with total cushion volume equal to the sum of the cushion and damper volumes.

One should also note that as A_d becomes small, $C_A \to \infty$ and the characteristic equation reduces to

$$C_cs^5 + \left(\frac{1}{R_c} + \frac{1}{R_A}\right)s^4 + \frac{S_a^2}{M}s^3 + \frac{S_a}{\alpha_aM}s^2 = 0$$

The Routh-Hurwitz criteria for this shows that the resulting system can never be asymptotically stable. The significance of this result remains to be established.

5.3.3 Typical Results

Typical results are shown in Figure 5.7. For these, the basic cushion system has the dimensions of the HJ-15 box-cell mentioned earlier, A_d is equal to A_f and A_c, and V_d is equal to V_b. The results suggest that the orifice-cavity actually has a destabilizing effect, in contrast to the suggestions made in the Introduction. A reason for this is not hard to find. The value of C_A for these results is such that the slug mass responds almost quasi-statically to the heave motion. Thus, the system is effectively a simple box-cushion with total cushion volume equal to the sum of the cushion and damper volumes. The curve for the latter case is included in Figure 5.7. As can be seen it agrees closely with the orifice-cavity damper boundary. So the orifice-cavity damper for the present system does not provide damping. However this does not mean it will not provide damping for more complex geometries.

5.3.4 Discussion

The results presented in Figure 5.7 suggest that some of the damping seen in the more complex hinged lip model must have been related to the ability of the orifices to separate the damper bag and diffusion chamber volumes where the smaller orifices give greater separation. Greater separation should improve damping because

(i) it effectively reduces the diffusion chamber volume,

(ii) it makes the damper bag a stiffer air spring thereby reducing the effective cushion compliance by reducing the angular motions of the hinged lips.

However there are other possible sources of damping for the hinged lip model. One source is nonlinear jet formation and turbulence dissipation downstream of the orifices. Another source is the unsteady boundary layer established by the radial inflow along the walls containing the orifice (Figure 5.8). Finally there is acoustic absorption in the walls of the cavity; for the low frequencies and pressure levels involved this should be negligible here.

5.4 Conclusion

The contradiction between the theoretical analysis presented here and reported practical experience [Refs. 5.2 and 5.3] is not resolved. Although the authors have ideas for further exploration, at the time of writing, no further analysis has been undertaken owing to the pressure of other work.

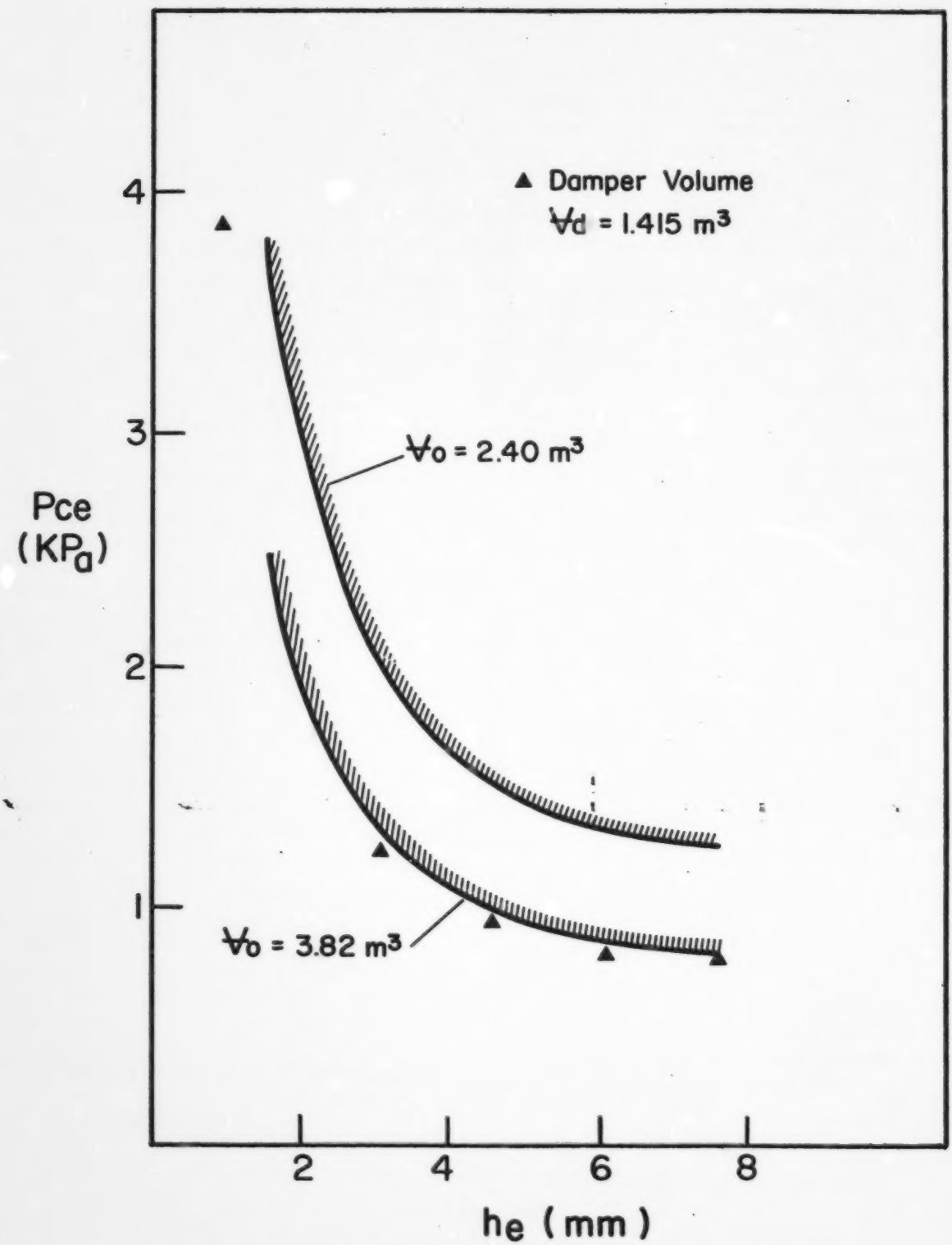

FIG. 5.7 TYPICAL THEORETICAL STABILITY RESULTS FOR ORIFICE-CAVITY DAMPER. THE HATCHED LINE RESULTS FOR V_o = 3.82 m³ ARE FOR V_D LUMPED WITH V_C

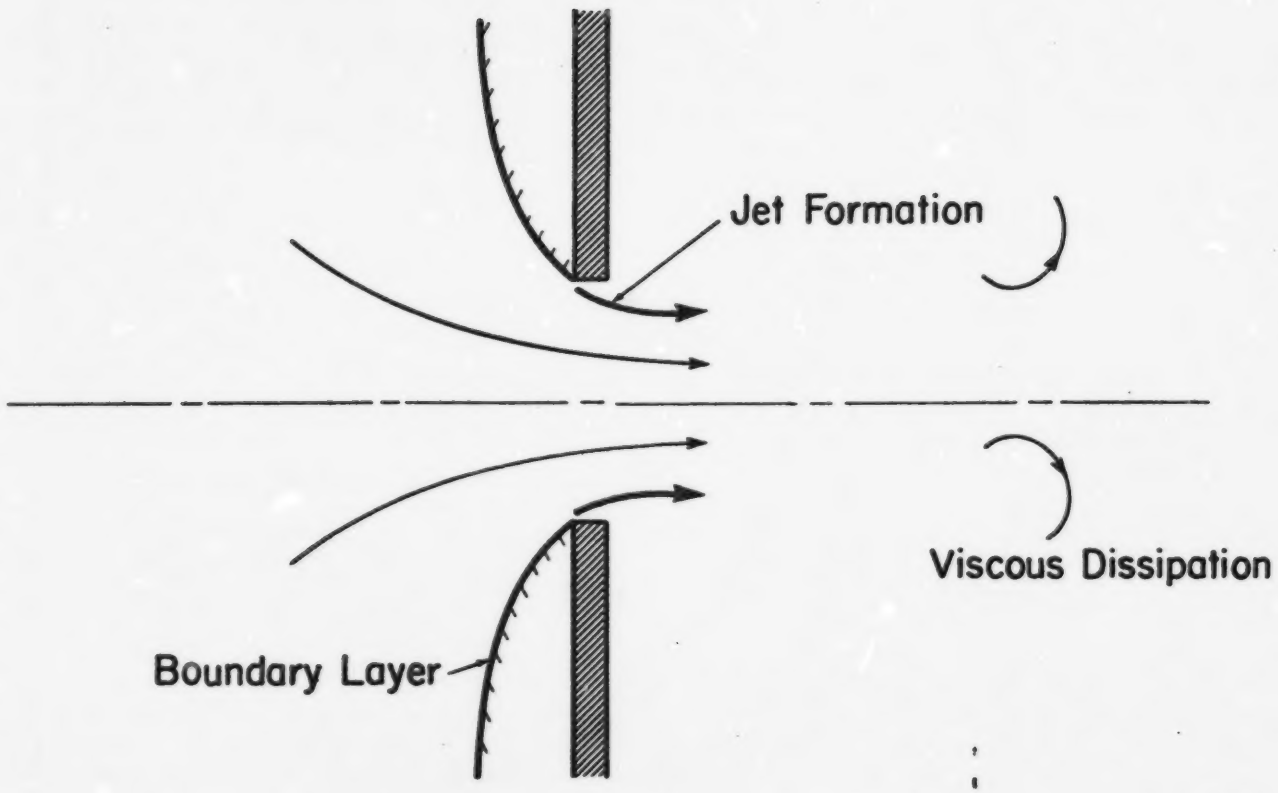

FIG. 5.8 ILLUSTRATION OF POSSIBLE DAMPING MECHANISMS THAT MAY BE IMPORTANT FOR ORIFICE-CAVITY RESONATORS.

6 COMPUTATION OF TURBULENT FLOW PATTERNS IN AIR CUSHIONS

6.1 Introduction

The lumped capacitance model of an air cushion system ignores the internal flows which occur within the air cushion volumes. Experience shows that, in many cases, this is a reasonable assumption [Ref. 6.1]. However some operating characteristics, notably those associated with dynamic stability, can be influenced by the internal flow structure. Results presented in a previous report to TDC [Ref. 6.2 figure 5.6] suggest that heave stability boundaries can be moved by as much as 50% simply by changing the cushion feed orifices from a single central hole to a ring of peripheral holes having the same total area.

To understand these effects, one must first understand the steady flow structure itself. In this regard, since a typical Reynold's number based on the diameter of the plenum and the inlet flow velocity is about 50,000, the flow is usually turbulent. Hence the analysis must take this into account. The present section shows how this can be achieved by using a finite difference technique similar to that developed by Gossman, and others [Ref. 6.3]. This section is divided into 6 major parts. Section 6.2 describes the various problem formulations, while Section 6.3 discusses the various turbulence models. Section 6.4 describes the finite difference procedure ultimately used to solve these equations. Results are presented in Section 6.5 and conclusions in Section 6.6.

Attempts to assess the effect of internal flow structure on dynamic stability were started during the tenure of the preceding TDC Contract [Ref. 6.2]. At that time, emphasis had been placed on the adaptation of the finite element method of numerical computation. This method was chosen because, in the stress analysis of structures and for the investigation of fluid flow problems that can be modelled by linear differential equations, it has been shown to be particularly suitable for computations involving the irregular geometries that occur in engineering practice. However, after a protracted effort, work on this method was finally discontinued because meaningful results could not be obtained for anything but extremely simple geometries at considerable computational expense. It is observed that the relative merits of finite element and finite difference methods applied to the computation of turbulent and other high Reynold's number flows is currently a very controversial topic.

In connection with this point, it should be noted that the work on numerical computations described in this Section formed part of a Ph.D. programme of one of the authors (MJH). This Section forms part of the thesis. Also, although it was supported mainly by the Principal Investigator's Natural Science and Engineering Research (NSERC) Grant, in general no clear-cut distinction has been made between that supported by NSERC and that supported by TDC. Readers mainly interested in the implications for ACV may wish to proceed directly to Sections 6.5 and 6.6.

6.2 Problem Formulations

There are three basic formulations for Navier Stokes flow. These are:

(i) Vorticity Transport-Stream Function (ω-ψ)

(ii) Stream Function (ψ)

(iii) Primitive Variable[1] (u, v, p)

Here, the primitive variable formulation is used. The reasons for this are outlined below.

6.2.1 Vorticity Transport-Stream Function (ω-ψ) Formulation

The primitive variable Navier Stokes-(NS) equations in two-dimensional Cartesian coordinates are:

x momentum

$$u\frac{\partial u}{\partial x} + v\frac{\partial u}{\partial y} = -\frac{1}{2}\frac{\partial p}{\partial x} + \frac{1}{Re}\left(\frac{\partial^2 u}{\partial x^2} + \frac{\partial^2 u}{\partial y^2}\right) \tag{1}$$

y momentum

$$u\frac{\partial v}{\partial x} + v\frac{\partial v}{\partial y} = -\frac{1}{2}\frac{\partial p}{\partial y} + \frac{1}{Re}\left(\frac{\partial^2 v}{\partial x^2} + \frac{\partial^2 v}{\partial y^2}\right) \tag{2}$$

Non-dimensional co-ordinates are used, that is distances x and y are divided by a reference length L, velocities by a reference speed V, and pressure by $1/2\ \rho V^2$. Then we have as usual $Re = LV\rho/\mu$. By differentiating (1) with respect to y and (2) with respect to x, and eliminating $\partial^2 p/\partial x \partial y$, one obtains the vorticity transport equation

$$u\frac{\partial \omega}{\partial x} + v\frac{\partial \omega}{\partial y} = \frac{1}{Re}\left(\frac{\partial^2 \omega}{\partial x^2} + \frac{\partial^2 \omega}{\partial y^2}\right) \tag{3}$$

where the vorticity ω is defined by

$$\omega = \frac{\partial v}{\partial x} - \frac{\partial u}{\partial y} \tag{4}$$

The continuity equation, namely

$$\frac{\partial u}{\partial x} + \frac{\partial v}{\partial y} = 0 \tag{5}$$

has been used to eliminate certain terms. By letting

$$u = \frac{\partial \psi}{\partial y} \qquad\qquad v = -\frac{\partial \psi}{\partial x} \tag{6}$$

continuity is identically satisfied. Substituting equations (6) into equation (4) gives the stream function equation

$$\nabla^2 \psi = -\omega \tag{7}$$

Equations (3) and (7), together with appropriate boundary conditions, constitute the $\omega - \psi$ formulation. As can be seen, pressure does not appear in this formul-

ation, and two, instead of three, equations have to be solved. One drawback of the formulation is it cannot be extended to three dimensions. It is also limited by the fact that boundary conditions are usually in terms of ψ only. The approaches used to obtain a solution require that the Neumann (derivative) boundary conditions on ψ be converted to Dirichlet (specified value) boundary conditions on ω by means of a Taylor series expansion. For example, typically one writes

$$\psi_p = \psi_o + h \left.\frac{\partial \psi}{\partial x}\right|_o + \frac{h^2}{2} \left.\frac{\partial^2 \psi}{\partial x^2}\right|_o + O(h^3) \tag{8}$$

where h is defined in the sketch below.

Now at the boundary, equation (7) reduces to

$$\left.\frac{d^2 \psi}{dx^2}\right|_o = -\omega_o$$

Thus, by ignoring higher order terms in equation (8), one obtains

$$\omega_o = 2 \frac{(\psi_o - \psi_p)}{h^2} + 2 \frac{\left.d\psi/dx\right|_o}{h} \tag{10}$$

As Roache [Ref. 6.4] points out, such derived vorticity boundary conditions can have a dominant effect on solution accuracy. Because of this, the $\omega - \psi$ formulation is not used for the present work. Also, the applications contimplated require that pressure be obtained accurately. Pressure can be obtained from the stream function results by first differentiating them to obtain velocities from equations (6) and then substituting the resulting expressions into the momentum equations (1) and (2). This gives equations of the form

$$\frac{\partial p}{\partial x} = R_u (x,y) \tag{11a}$$

$$\frac{\partial p}{\partial y} = R_v (x,y) \tag{11b}$$

Pressure at a point p can be obtained by integrating equations (11) along lines in the x-y plane as shown below

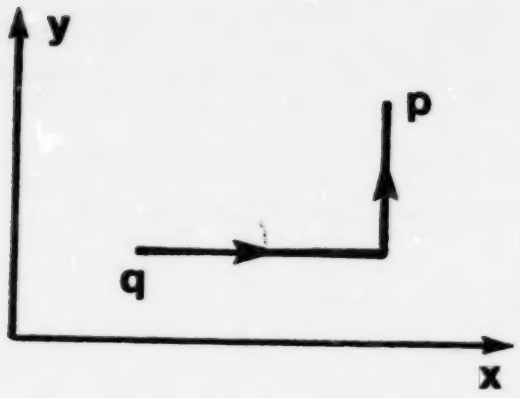

When low order finite difference or finite element interpolation schemes are used for ψ, this pressure determination will not be very accurate.

6.2.2 Stream Function (ψ)

The ψ formulation follows when equation (7) is substituted into equation (3) to obtain

$$\frac{\partial \psi}{\partial y}\frac{\partial \nabla^2 \psi}{\partial x} - \frac{\partial \psi}{\partial x}\frac{\partial \nabla^2 \psi}{\partial y} = \frac{1}{Re}\nabla^4 \psi \tag{12}$$

This formulation has a number of limitations, and these are described in [Ref. 6.5]. The formulation is not used for the present work.

6.2.3 Primitive Variable (u,v,p)

For the present work, the primitive variable equations in cylindrical coordinates are used. These are, in nondimensional co-ordinates, and with Re_{ef} and Re_t effective or equivalent Reynolds numbers defined in Section 6.3.4,

x momentum

$$u\frac{\partial u}{\partial x} + v\frac{\partial u}{\partial r} = -\frac{1}{2}\frac{\partial p}{\partial x} + \frac{1}{r}\frac{\partial}{\partial r}\left[\frac{r}{Re_{ef}}\frac{\partial u}{\partial r}\right] + \frac{\partial}{\partial x}\left[\frac{1}{Re_{ef}}\frac{\partial u}{\partial x}\right] + S(u) \tag{13}$$

r momentum

$$u\frac{\partial v}{\partial x} + v\frac{\partial v}{\partial r} = -\frac{1}{2}\frac{\partial p}{\partial r} - \frac{1}{Re_{ef}}\frac{v}{r^2} + \frac{1}{r}\frac{\partial}{\partial r}\left[\frac{r}{Re_{ef}}\frac{\partial v}{\partial r}\right] + \frac{\partial}{\partial x}\left[\frac{1}{Re_{ef}}\frac{\partial v}{\partial x}\right] + S(v) \tag{14}$$

Continuity

$$\frac{\partial u}{\partial x} + \frac{\partial v}{\partial r} + \frac{v}{r} = 0 \tag{15}$$

The quantities S(u) and S(v) are extra source terms associated with the presence of turbulence [Ref. 6.6]. They are given by

$$S(u) = \frac{\partial}{\partial x}\left[\frac{1}{Re_t}\frac{\partial u}{\partial x}\right] + \frac{1}{r}\frac{\partial}{\partial r}\left[\frac{r}{Re_t}\frac{\partial v}{\partial x}\right] \tag{16a}$$

and

$$S(v) = \frac{\partial}{\partial x}\left[\frac{1}{Re_t}\frac{\partial u}{\partial r}\right] + \frac{1}{r}\frac{\partial}{\partial r}\left[\frac{r}{Re_t}\frac{\partial v}{\partial r}\right] - \frac{1}{Re_t}\frac{v}{r^2} \tag{16b}$$

This formulation can easily be extended to three dimensions.

6.3 Turbulence Modelling

6.3.1 Fundamental Problem

Turbulence modelling is required because, although the basic Navier Stokes equations are valid for turbulent flow, important details of the turbulent motion are so small scale in character that the number of finite difference grid points or finite element nodes required to capture the detail would require the storage capacity of the computer to be orders of magnitude larger than is currently available [Ref. 6.6]. Also, the engineer is usually not interested in the details of turbulence. Because of this, models have been developed which deal only with time averaged effects. Most of these have as their starting point the Reynolds stress equations. These are obtained by integrating the Navier-Stokes equations over a time span much greater than the time scale of the turbulence fluctuations but much less than the time scale of the mean motion. The time averaging introduces the Reynolds stresses $-\overline{u_i u_j}$, and it is these which must be modelled.

6.3.2 Eddy Viscosity and Mixing Length Models

The earliest turbulence model is due to Boussinesq [Ref. 6.6]. He noted that, when a laminar wall flow becomes turbulent, the shear stress at the wall increases. As an increase in viscosity would also cause the wall shear stress to increase, he suggested in analogy with the expression for the molecular shear stress obtained from the kinetic theory of gases,

$$-\overline{u_i\, u_j} = \varepsilon_m\left(\frac{\partial u_i}{\partial x_j} + \frac{\partial u_j}{\partial x_i}\right) \tag{17}$$

where ε_m is an effective viscosity due to turbulent fluid motion.

Prandtl extended the kinetic theory analogy when he introduced the mixing length concept [Ref. 6.6]. He wrote for the effective viscosity

$$\mu_t = \rho \ell_m V_t \tag{18}$$

where ℓ_m, the mixing length, is the equivalent of the kinetic theory mean free path and V_t, the fluctuating turbulent velocity, is the equivalent of the molecular velocity. Using physical arguments [Ref. 6.6] Prandtl, in his early boundary layer work, put

$$V_t = \ell_m \left| \frac{\partial u}{\partial y} \right| \tag{19}$$

Thus

$$\mu_t = \rho \ell_m^2 \left| \frac{\partial u}{\partial y} \right| \tag{20}$$

where ℓ_m had to be specified algebraically. The major drawbacks of this model are [Ref. 6.6, p. 45]:

(i) μ_t vanishes when $\partial u/\partial y$ vanishes; this does not agree with experimental evidence.

(ii) It is not adequate for recirculating flows mainly because it takes no account of the convection or the diffusion of turbulence.

It is noted that flows inside an air cushion cell are expected to be of the latter type.

6.3.3 More Sophisticated Models of Turbulence

An important step towards the resolution of these difficulties was also made by Prandtl, who introduced the so called "one-equation" model.

$$\mu_t = \rho \sqrt{k}\ \ell_m \tag{21}$$

where k, the kinetic energy of turbulence, is obtained from a turbulence transport differential equation. However, although $\sqrt{k}$ is a much better velocity scale, the model is still limited by an algebraic specification of ℓ_m.

The next step was made by Kolmogorov [Ref. 6.6], who introduced the k-f model

$$\mu_t = \rho\, k/f \tag{22}$$

where f equals the characteristic frequency of the energy-containing motions, and

$$\ell_m = \sqrt{k}/f \tag{23}$$

This model is important because Kolmogorov suggested that both k and f should be determined from differential transport equations. Thus, with this model, the convection and diffusion of both k and f (ℓ_m) is included.

Models of this type are known as two-equation turbulence models. They have been extensively developed over the past ten years by the groups at Imperial College and elsewhere; variants include: the k-ℓ_m model, the k-ε model and the k-ω model, where ε, the turbulence dissipation rate, and ω, the fluctuating vorticity, can be expressed in terms of k and ℓ_m. They are the simplest models that can provide a realistic prediction for recirculating flows [Ref. 6.6, p.110].

One limitation of the two-equation models is they imply that when the velocity gradient is nonzero, the turbulent shear stress is also non-zero. However, experiments show that this is not necessarily so. To avoid this problem, Reynolds stress transport models have been developed; a typical one being that introduced for boundary layers by Hanjalic et al [Ref. 6.7]. In this model, an effective viscosity hypothesis is not used. Instead, $-\overline{u'v'}$ is determined from its own transport equation. It requires that transport equations for k and ε also be solved. More elaborate models along this line are also being developed.

6.3.4 Equations for the k-ε Turbulence Model

In this report, the k-ε effective viscosity model is used. The appropriate transport equations are [Refs. 6.3, 6.6]:

Turbulence Kinetic Energy k

$$u\frac{\partial k}{\partial x} + v\frac{\partial k}{\partial r} = \frac{\partial}{\partial x}\left(\frac{1}{Re_{ef}\sigma_k}\frac{\partial k}{\partial x}\right) + \frac{1}{r}\frac{\partial}{\partial r}\left(\frac{r}{Re_{ef}\sigma_k}\frac{\partial k}{\partial r}\right) + \frac{1}{Re_t}G - C_D\varepsilon \qquad (24)$$

Turbulence Dissipation Rate ε

$$u\frac{\partial \varepsilon}{\partial x} + v\frac{\partial \varepsilon}{\partial r} = \frac{\partial}{\partial x}\left(\frac{1}{Re_{ef}\sigma_\varepsilon}\frac{\partial \varepsilon}{\partial x}\right) + \frac{1}{r}\frac{\partial}{\partial r}\left(\frac{r}{Re_{ef}\sigma_\varepsilon}\frac{\partial \varepsilon}{\partial r}\right) + \frac{C_1}{Re_t}\frac{\varepsilon}{k}G - C_2\frac{\varepsilon^2}{k}$$

where

$$Re_t = \frac{\rho V L}{\mu_t} \qquad (26)$$

$$Re_{ef} = \frac{\rho V L}{\mu_{ef}}$$

are the turbulent and effective Reynolds numbers respectively. The effective viscosity μ_{ef} is made up of laminar and turbulent contributions

$$\mu_{ef} = \mu_{\ell}' + \mu_t \tag{27}$$

where

$$\mu_t = C_\mu \rho V L \frac{k^2}{\varepsilon} \tag{28}$$

Usually

$$\mu_t >> \mu_{\ell} \text{ so } \mu_{ef} \stackrel{\sim}{=} \mu_t \tag{29}$$

The function G is associated with turbulence production and is given by [Ref. 6.3]

$$G = 2\left[\left(\frac{\partial u}{\partial x}\right)^2 + \left(\frac{\partial v}{\partial r}\right)^2 + \left(\frac{v}{r}\right)^2\right] + \left(\frac{\partial u}{\partial r} + \frac{\partial v}{\partial x}\right)^2 \tag{30}$$

The universal constants σ_k, σ_ε, c_1, c_2, c_D and C_μ have been determined from a combination of dimensional arguments and an interpretation of experiments on simple geometries. Their computer-optimized values are [Ref. 6.3]

$$\begin{aligned} \sigma_k &= 1.0 \\ \sigma_\varepsilon &= 1.3 \\ c_1 &= 1.44 \\ c_2 &= 1.92 \\ c_D &= 1.0 \\ c_\mu &= 0.09 \end{aligned} \tag{31}$$

Near wall regions, where laminar effects can become important, wall formulae involving exponential damping damping factors are often used for c_μ and c_2. These are given in [Ref. 6.6]. The derivation of the k-ϵ transport equations is very similar to the derivation of the Navier Stokes equations from a kinetic theory approach. The closure modelling is also very similar [Ref. 6.6].

6.3.5 Limitations of Two-Equation Models

The two-equation turbulence models, although probably the best available for recirculating flows, have a number of limitations, one of which is mentioned above, and these are due to the information lost in the time averaging process. Another is that the universal constants are not truly universal. For example, constants determined from comparisons with plane flow experiments are not always adequate for axisymmetric flow calculations. However, some improvements have recently been made by Pope [Ref. 6.9].

A more fundamental difficulty arises because the effective viscosity hypothesis assumes that the time scales of turbulence are much smaller than the time scale of the mean motion. The time scales of turbulence are roughly proportional to the eddy sizes. Thus, if the eddies are very small, as it is usually assumed, their reaction or response times to change in the mean flow will be much less than the time scale of the mean motion. Thus, the turbulence will be approximately in equilibrium, and the assumptions used by the effective viscosity hypothesis will be adequate. However, recent work by Roshko [Ref. 6.10] has shown that large coherent eddy structures may be present even at very high values of Re and these, through interactions with each other, have a significant effect on the development of the flow. Unlike the essentially random motions of the smaller eddies, the motions of the large structures are deterministic in nature. Thus, it may not be possible to model their effect using the effective viscosity hypothesis, although some attempts have been made at this. For example, Libby [Ref. 6.11] introduced a transport equation for the level of intermittency, where intermittency is associated with the passage of large scale structures. As these move downstream, they rotate about each other and amalgamate into larger eddies while engulfing essentially non-turbulent free stream fluid. Intermittency is thus associated with the alternate passage of turbulent and non-turbulent fluid. Note that the effective viscosity hypothesis assumes turbulence to be continuous. Because the structures are large, their reaction times to changes in the mean flow could be of the order of the time scale of the mean motion. Thus, the turbulence will not necessarily be in equilibrium. The fluid could show an extra memory effect and could to some extent behave as a non-Newtonian fluid [Ref. 6.12].

One way to circumvent the large-scale structure problem is to use the subgrid eddy viscosity method, which uses the unsteady Navier-Stokes equations to calculate the large scale motions and an eddy viscosity model for the small eddy motions [Ref. 6.13]. For basic turbulence studies, such an approach is recommended but for engineering problems it is not feasible. A better approach might be to devise some corrections to the effective viscosity turbulence models which would account for the effect of the large scale structures on the mean motion. Libby's "level of intermittency" transport equation is one such approach [Ref. 6.11]. The relaxation equation for the boundary layer shear stress $-\overline{u'v'}$ proposed by Builtjes [Ref. 6.12] is another. With regard to the $k - \varepsilon$ two-equation model, it may be possible to develop relaxation equations for the production and the dissipation of k and ε. As it stands, the two-equation model implies that the production, at a particular point, depends only on the velocity gradients and the turbulent Re at that point. A relaxation equation for the production would account for the time lag, associated with the large scale structures, required for the actual production. The analogy with the fast kinetics and finite rate chemistry concepts used for combustion studies should be evident.

6.4 Finite Difference Numerical Procedure

6.4.1 Description of Teach T Programme

A finite difference solution procedure for the (u, v, p, k-ϵ) formulation is given in [Ref. 6.3]. Its distinguishing feature is a volume integration of each partial differential equation over an Eulerian subdomain or cell, and it can, to some extent, be considered as an application of the subdomain method of weighted residuals [6.14]. It uses the staggered cell arrangement shown

in Figure 6.1; the scalars p, k and ϵ are the unknowns at the intersections of the grid lines and the velocities are the unknowns at the staggered positions shown. An integration by parts is used to convert the convection, diffusion, and pressure volume integrals into surface integrals. Information at neighbouring grid points is then used to approximate the fluxes at the cell surfaces. Special attention is paid to the convective fluxes, where an upstream or upwind weighted scheme is used to ensure numerical stability. This is described in greater detail below. For the source term volume integral evaluations, it is assumed that the value of the source term at the grid point within a particular cell is a good average for the cell. This is also important for numerical stability.

A segregated approach is used in which the finite difference equations for a particular governing equation are assembled into their own global matrix. For this, each unknown is associated with a particular governing equation. For example, for the present work, u is associated with the x-momentum equation and v, p, k and ϵ are associated with r-momentum, continuity, kinetic energy of turbulence and dissipation rate of turbulence respectively. Now where v, p, k and ϵ appear in the x-momentum finite difference equations, values from the previous iteration step are inserted, and the resulting equations are then solved for u. Each governing equation is dealt with separately one after the other. This is in contrast to a coupled procedure where all governing equations are considered together.

The Semi-Implicit Method for Pressure Linked Equations or SIMPLE procedure is used to obtain a pressure correction equation [Ref. 6.3]. In this procedure the continuity equation is converted into a Poisson-like equation which allows the pressures and the velocities to be updated in an iterative manner. To start the iteration, a distribution of pressure is assumed, and the finite difference momentum equations are solved in sequence using the segregated approach. The resulting velocity field approximately satisfies momentum but not continuity and therefore must be corrected. For this, a Taylor series expansion is used to obtain for each staggered grid point

$$u_{pu} = \hat{u}_{pu} + \frac{\partial u_{pu}}{\partial(p_S - p_N)} (\delta p_S - \delta p_N) \qquad (32)$$

$$v_{pv} = \hat{v}_{pv} + \frac{\partial v_{pv}}{\partial(p_W - p_E)} (\delta p_W - \delta p_E) \qquad (33)$$

where the symbol ^ indicates the old velocity field, the subscripts 'pu' and 'pv' indicate 'u' and 'v' staggered velocity positions respectively, the subscripts N, S, E and W refer respectively to pressure grid points north, south, east and west of either the staggered point 'pu' or the point 'pv', and 'δp' indicates a pressure correction. Estimates of the slopes $\partial u_{pu}/\partial(p_S - p_N)$ and $\partial v_{pv}/\partial(p_W - p_E)$ are obtained from the finite difference momentum equations. When the expressions for u_{pu} and v_{pv} are substituted into the finite difference equations for the continuity equation, a system of equations for the pressure corrections is obtained. By solving these the pressure and velocity fields can be updated. The whole process is repeated until the pressure corrections tend to zero.

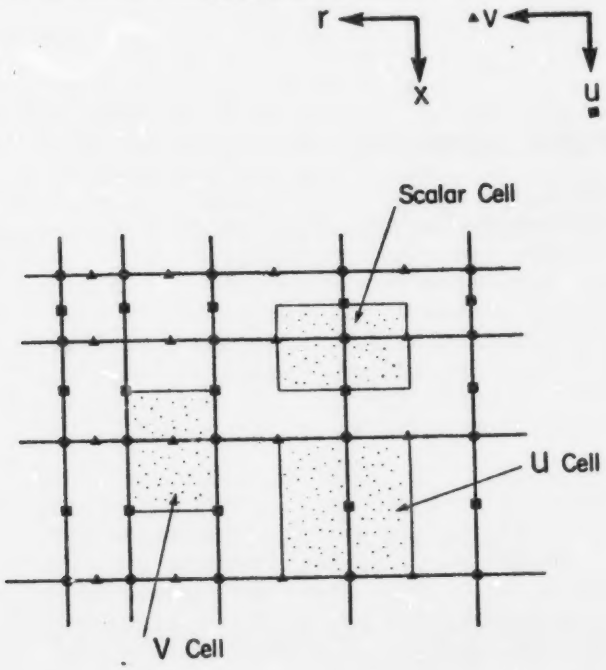

FIG. 6.1 STAGGERED GRID-CELL ARRANGEMENT FOR FINITE DIFFERENCE CALCULATIONS

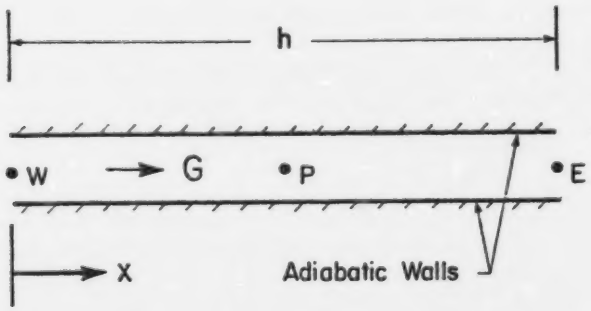

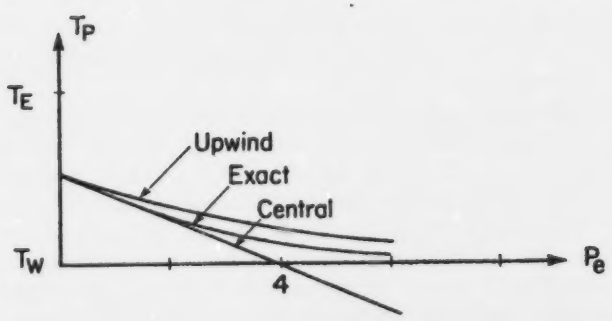

FIG. 6.2 ILLUSTRATING UPWIND DIFFERENCE SCHEMES

6.4.2 Upwind Difference Schemes

As mentioned above, an upwind weighted scheme is used for the convective terms. This ensures that the global matrices will be diagonally dominant, which is very important for the numerical stability of the tri-diagonal matrix line-by-line iterative solution procedure used. The upwind representation is said to be physically realistic in that it states that a mesh point will receive convective information only from points upstream and will transmit information only to points downstream. Spalding [Ref. 6.17] compared the central difference and upwind difference operators for a one dimensional heat conduction problem with flow as shown in Figure 6.2 for which the governing equation is:

$$C_p G \frac{dT}{dx} - k \frac{d^2T}{dx^2} = 0 \tag{34}$$

where T is the fluid temperature. For the midpoint P the exact solution, when T_W and T_E are specified, is:

$$T_P = T_W + (T_E - T_W) \frac{e^{Pe/2} - 1}{e^{Pe} - 1} \tag{35}$$

where $Pe = C_p G h/k$ is the Peclet number. Now, a central difference operator for both convective and second order terms gives:

$$\underbrace{C_p G \frac{(T_E - T_W)}{h}}_{\substack{\text{Convective} \\ \text{Term}}} - k \frac{4(T_E - 2T_P + T_W)}{h^2} = 0 \tag{36}$$

or

$$T_P = \frac{1}{2}\left[T_W \left(1 + \frac{Pe}{4} \right) + T_E \left(1 - \frac{Pe}{4} \right) \right] \tag{37}$$

whereas, an upwind difference operator for the convective term and a central difference operator for the second order term gives:

$$\underbrace{C_p G \frac{(T_P - T_W)}{h/2}}_{\substack{\text{Convective} \\ \text{Term}}} - k \frac{4(T_E - 2T_P + T_W)}{h^2} = 0 \tag{38}$$

or

$$T_P = \frac{1}{2} \frac{T_W \left(1 + \frac{Pe}{2} \right) + T_E}{1 + \frac{Pe}{4}} \tag{39}$$

The various expressions for T_P are plotted in Figure 6.2. On the basis of this plot, Spalding concluded that the central difference operator provides unrealistic values of T_P for $Pe > 4$, whereas the upwind difference operator always provides realistic values and has the same asymptote as the exact expression.

Gartling [Ref. 6.18] recently questioned the need for upwind differencing, when a direct solution procedure is used which does not require the global matrix to be diagonally dominant. He argued that, in this case, the main cause of numerical instabilities is not the use of central differencing but the use of unrealistic boundary conditions. He considered the convection-diffusion transport equation,

$$\underbrace{\sum_{i=1}^{3} u_i \frac{\partial \phi}{\partial x_i}}_{\text{Convection}} = \alpha \underbrace{\sum_{j=1}^{3} \frac{\partial^2 \phi}{\partial x_j^2}}_{\text{Diffusion}} \quad \text{on } \Omega \tag{40}$$

which is elliptic. With this classification, it follows that data must be specified at all points on the boundary of Ω. However, when the convection terms are large and streamwise diffusion is negligibly small, the transport equation takes on a boundary layer or parabolic character. In this case, specifying the outflow or downstream value of ϕ is not physically realistic. In other words, the problem is described by a differential equation which is time-like in the streamwise coordinate and, as such, does not admit a specification of ϕ at the downstream boundary, except under very special circumstances [Ref. 6.18]. A less restrictive downstream condition which is, in most cases, physically more realistic is the natural boundary condition for the problem:

$$\frac{\partial \phi}{\partial n} = C \tag{41}$$

where C is usually taken to be zero. For treating impermeable boundaries where a specified value of ϕ is physically realistic, Gartling suggested that mesh refinement be used. Recall that in developing his justification for upwind differencing, Spalding specified the downstream condition, T_E. Thus, his conclusions may be in error.

It has been observed by several investigators [Refs. 6.3, 6.4] that upwind differencing introduces a diffusion-like error when the flow is at an angle to the grid lines. Raithby [Ref. 6.16] recently presented several skew upwind schemes which attempt to take account of the cross flow gradients and thus reduce this error. Dennis and Chang [Ref. 6.19] also presented a scheme for removing the false diffusion error. Their scheme is much simpler than Raithby's scheme and consists basically of a correction to each term in the load vector (see Appendix C), which is equal to the false diffusion error. Neither of the above is used here.

6.4.3 Procedure Adopted for the Present Work

The cell finite difference procedure is not used for the present work. Instead, the closely related grid point finite difference procedure is used. In this method, Taylor series expansions are used to replace the various derivatives in the governing equations by difference quotients [Ref. 6.4]. The grid point scheme can be considered as an application of the collocation method of weighted residuals, where displaced Dirac delta functions are used as weighting functions, and the residual is effectively set to zero at particular points within the domain [Ref. 6.14]. As with the cell procedure, a staggered grid is employed, and an upwind scheme for the convective terms is used to ensure numerical stability. Also, a segregated approach is used which makes use of the SIMPLE procedure for pressure. The derivation of the finite

difference form of a typical transport equation is given in Appendix C, and a finite difference computer program listing for a simple axisymmetric air cushion vehicle is given in Appendix D.

6.4.4 Application to Single Cell Plenum Chamber

A typical air cushion vehicle geometry studied is shown in Figure 6.3. To obtain a flow pattern for this geometry, the following inlet conditions were specified. Typically, u was assumed to be uniform where $u = U_{IN}$, v was assumed to be zero, p was set equal to zero at the scalar grid point closest to the axis of symmetry, k was assumed to be given by $k = iU_{IN}^2$ where i, the intensity factor, was typically $i = 0.03$ [Ref. 6.3], and ϵ was assumed to be given by $\epsilon = k^{3/2}/\ell_m$ where ℓ_m, the mixing length, was typically $\ell_m = 0.005d$ [Ref. 6.3]. Owing to the convective nature of the flow at the outlet, u, p, k and ϵ were not specified there. However, v, the normal outflow velocity, was forced to satisfy overall flow continuity (see Figure 6.4). This was achieved by correcting the values of v at staggered grid points on the outlet plane by an amount Δv which ensured that the flow into the cushion balanced with the flow out.

Next to a wall, the flow is usually boundary layer-like, and gradients normal to the wall are usually very large (see Figure 6.5). If boundary conditions are applied at the wall, many finite difference grid points have to be used to accurately model the near wall behaviour. To avoid this, wall functions, derived from an approximate analysis closely similar to those developed for boundary layers (see Ref. 6.20), were used to relate values at the wall to values in either the laminar sublayer or the buffer layer. The analysis gives for the shear stress at a point 'p' in the buffer layer [Ref. 6.3; see also Figure 6.5]

$$\tau_w = u^{*2} = \frac{1}{R_{ef}} \frac{du^t}{dn} = \frac{C_\mu^{1/4} \hat{k}_p^{1/2} u^t}{U_p} \tag{42}$$

where u* is the so called friction velocity, u^t is the tangential velocity component, and

$$U_p = \frac{1}{\kappa} \ell n \left(E R_L C_\mu^{1/4} \hat{k}_p^{1/2} n_p \right) \tag{43}$$

The parameter $\kappa = 0.4187$ is von Karman's constant, $E = 9.793$ is a constant of integration, and $\hat{k}_p$ is a value from a previous iteration step. When

$$R_L C_\mu^{1/4} \hat{k}_p^{1/2} n_p < 11.63 \tag{44}$$

point 'p' is in the laminar sublayer. There,

$$\tau_w = \frac{1}{R_L} \frac{u^t}{n_p} \tag{45}$$

For boundary layer flows, the analysis also gives [Ref. 6.3],

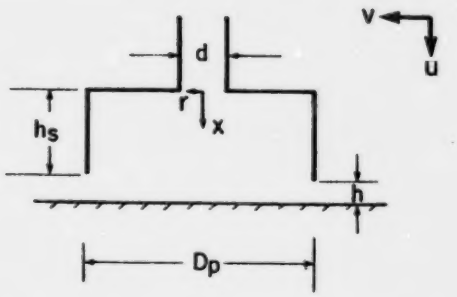

FIG. 6.3 TYPICAL AIR CUSHION GEOMETRY USED FOR INTERNAL FLOW STUDIES

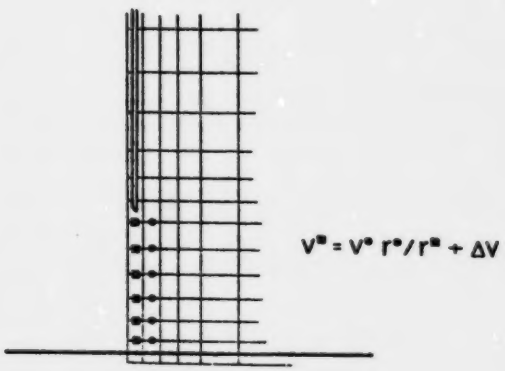

FIG. 6.4 APPLICATION OF OUTLET FLOW BOUNDARY CONDITION

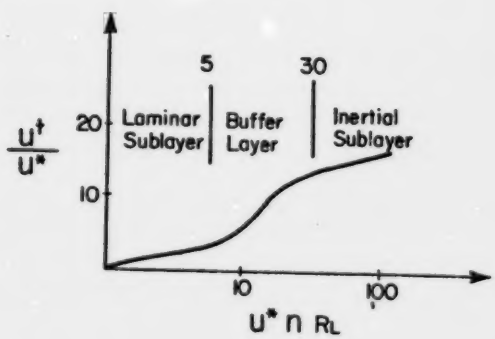

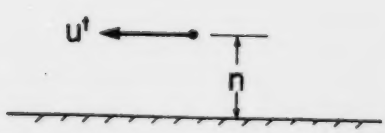

FIG. 6.5 WALL FUNCTIONS AND WALL BOUNDARY CONDITION

$$k_p = \frac{|\tau_w|}{c_\mu^{1/2}} = \frac{u^{*2}}{c_\mu^{1/2}} \tag{46}$$

and

$$\epsilon_p = c_\mu^{3/4}\, k_p^{3/2}/\kappa n_p = u^{*3}/\kappa n_p \tag{47}$$

Here, equation (47) was used for ϵ_p. However, for k_p, its finite difference equation was used with the production term modified to account for the fact that

$$\tau_w = \frac{1}{R_{ef}} \frac{du^t}{dn} \tag{48}$$

This procedure was followed owing to the recirculating nature of the flow field. It required that the dissipation term be also modified slightly [Ref. 6.3].

Finally, as noted above, pressure was specified at one point on the inlet boundary. At that point, $\delta p = 0$. For the other boundary points, the condition on δp used was the vanishing normal gradient condition

$$\frac{\partial \delta p}{\partial n} = 0 \tag{49}$$

The rationale for using this particular boundary condition is given in [Ref. 6.3]. It follows directly from equations (32) and (33).

Additional details regarding these calculations are available in [Ref. 6.22].

6.5 Results

Typical finite difference results are given for an axisymmetric plenum chamber having approximately the same geometry as that used during the previous UTIAS-TDC Contract to experimentally demonstrate the effect of internal flow structure on heave stability [Ref. 6.2, Figure 5.6].

Figures 6.6a and 6.6b are velocity vector diagrams which illustrate the main features of the flow. The individual lines located at each computational grid point are oriented in the direction of the local flow, and their length is proportional to the local fluid speed. The hovergap h is expressed as a fraction of the height h_s of the cell wall defined in Figure 6.3. The Reynolds number Re_L is based on the diameter of the inlet and the uniform inlet velocity U_{in}.

The diagram given in Figure 6.6b corresponds to a scaled hovergap representative of values used in the experiments described in [Ref. 6.2] and which would occur in practice. The two major features of the flow are: (i) radial wall-jet formed by the impingement of the inlet jet on the ground-board, and (ii) a weak viscous ring-vortex. In Figure 6.6b, the boundary layer that grows on the ground-board starting from the stagnation point at the axis of symmetry can be clearly seen, but for the flow pattern given in Figure 6.6a,

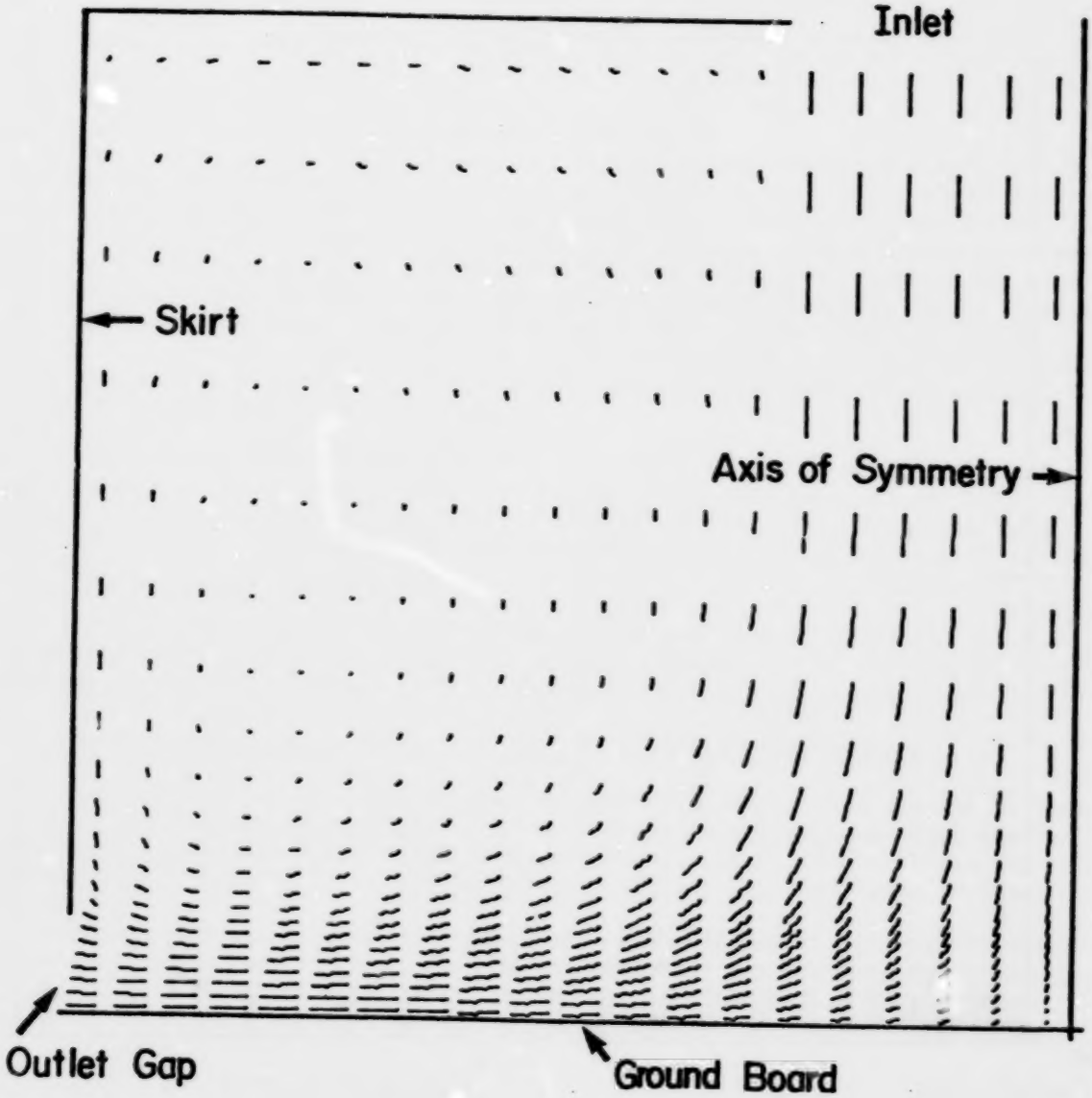

FIG. 6.6A VELOCITY-VECTOR PLOT FOR A SIMPLE AIR CUSHION GAP $h = 0.1h_s$ AND THE LAMINAR REYNOLDS NUMBER R_L BASED ON INLET DIAMETER = 10^5

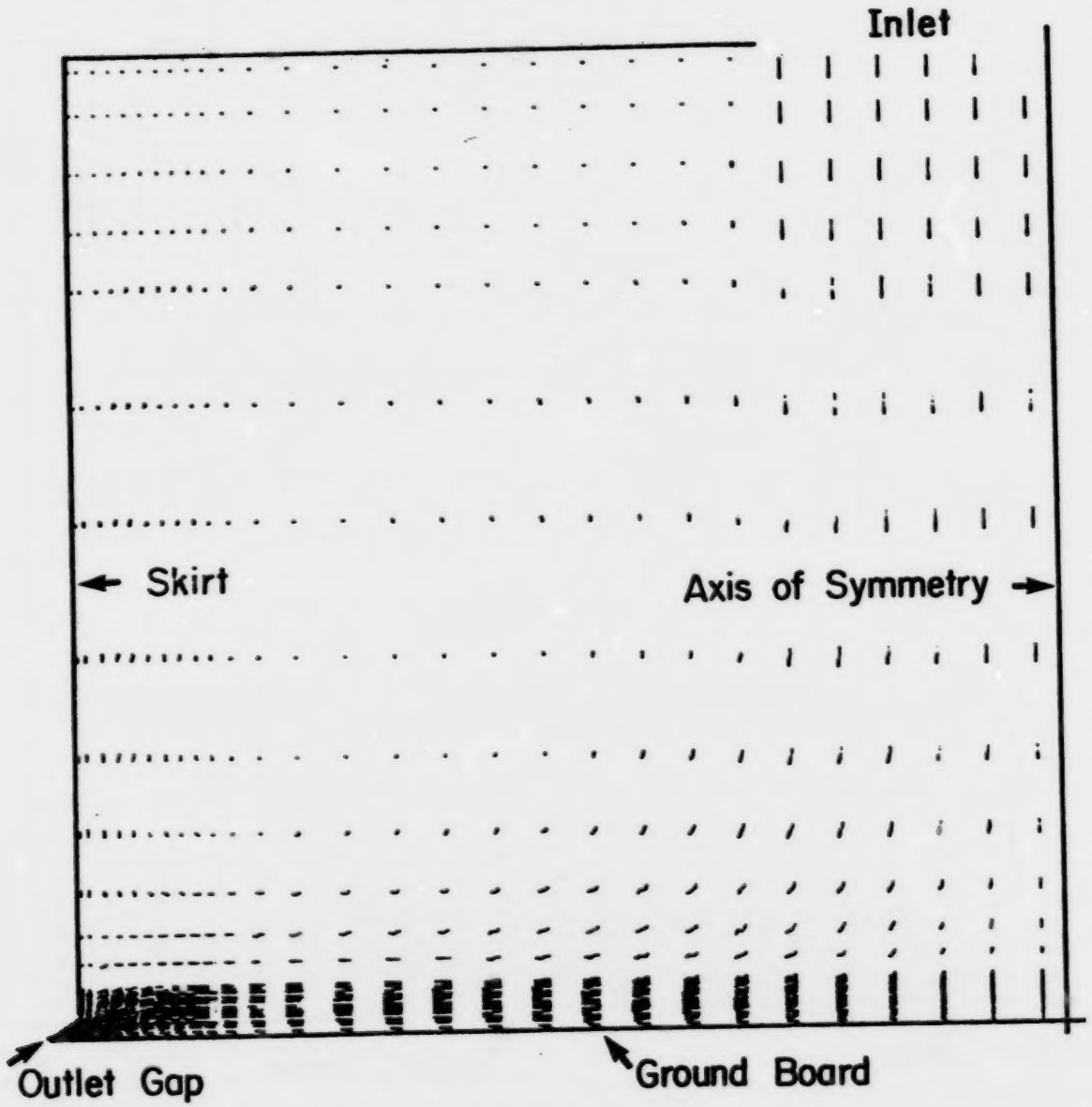

FIG. 6.6B VELOCITY-VECTOR PLOT FOR A SIMPLE AIR CUSHION GAP $h = 0.025h_s$ AND $R_L = 10^4$

it is too small to be seen. Note also that, owing to the presence of the radial wall jet, the effective fluid velocity in the neighbourhood of the gap is not zero, but can be a significant fraction of the inlet velocity. This has implications for stability calculations, as is discussed in Section 6.6.

Figure 6.7 gives the computed pressure distributions on the ground-board. The pressure is presented as a fraction of the dynamic head associated with the uniform inlet velocity, and with the datum or zero pressure taken to be that given at the inlet. The pressure on the top of the cell is effectively constant and equal to the inlet pressure. At the centre, corresponding to $r = 0$, and for the four values of h considered in Figure 6.7, the dynamic head is almost totally recovered, as might be expected for a turbulent jet directed at a wall aligned at right angles to the jet. This is qualitatively in agreement with ground board pressure measurements made during the present UTIAS-TDC Contract and given in Figure 6.8. In Figure 6.7 one can see how as the gap is decreased the pressure at the outlet becomes more and more negative due to fluid acceleration. This is illustrated in greater detail in Figures 6.9a and 6.9b which show respectively the computed pressure distributions and radial flow velocity on the outlet plane.

Figure 6.10 shows computed radial distributions of the axial component of velocity at approximately the same height above the ground plane while Figure 6.11 shows computed axial distributions of the radial component at a specific radius. Here the wall jets and boundary layers can be seen in greater detail.

Finally, Figure 6.12 shows the relatively complicated velocity vector plot obtained for an air cushion with a baffle plate. It provides a good demonstration of the versatility of the finite difference computer code.

6.6 Conclusions: Implications for Dynamic Stability Calculations

For plenum chamber cells having the geometric proportions similar to that used in the "numerical experiment" described in the previous section, the two main features of the flow, namely the radial wall-jet and the weak viscous vortex might conceivably affect dynamic stability. Consider these in turn.

First, the presence of the radial wall jet modifies the process by which the air escapes from the cushion. In the stability calculations described in Sections 2, 4 and 5 of this report it is assumed that the air in the plenum chamber is at rest so the volume flux to atmosphere is given by

$$Q_a(t) = C_m L_p h(t) \sqrt{\frac{2p_c(t)}{\rho_a}} \qquad (50)$$

But, the computations show that, at a distance of a few hovergap lengths upstream of the cushion lip, where one might expect the air to be effectively at rest, the fluid has a velocity which is essentially parallel to the ground-board and has a magnitude v_{jet} which may be as large as 75% of the inlet velocity U_{in}. This suggests that, although the air escape process is still essentially inviscid, the Bernoulli law for outlet flow should be modified to include the dynamic head due to v_{jet}, that is

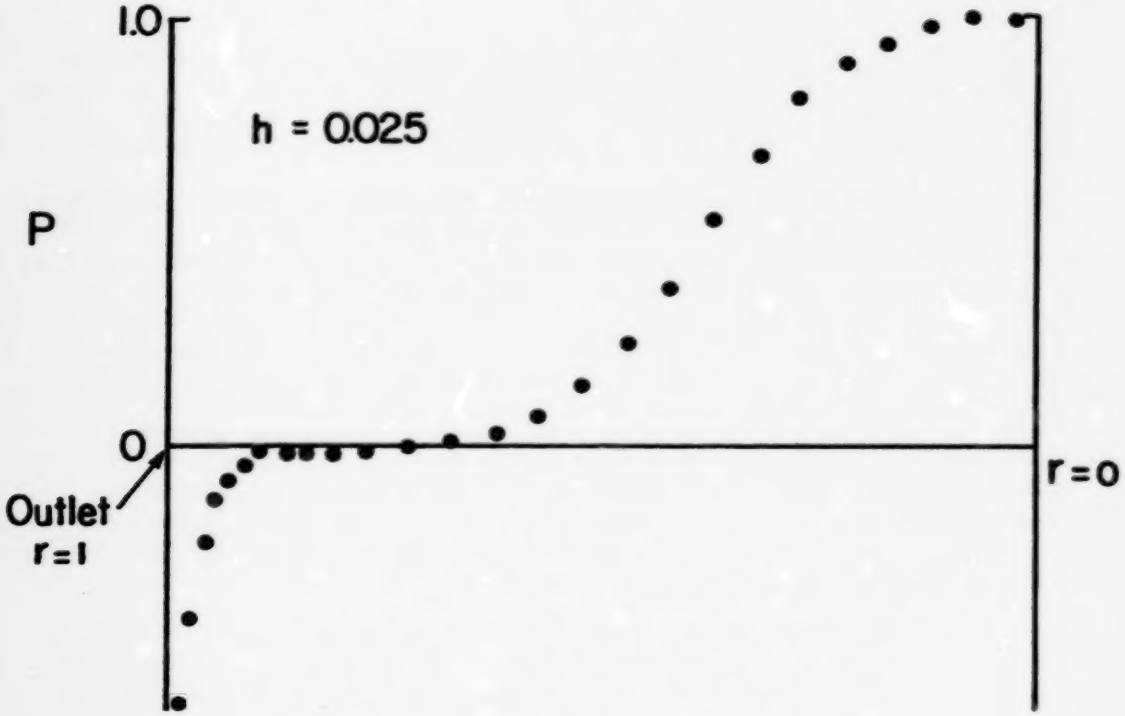

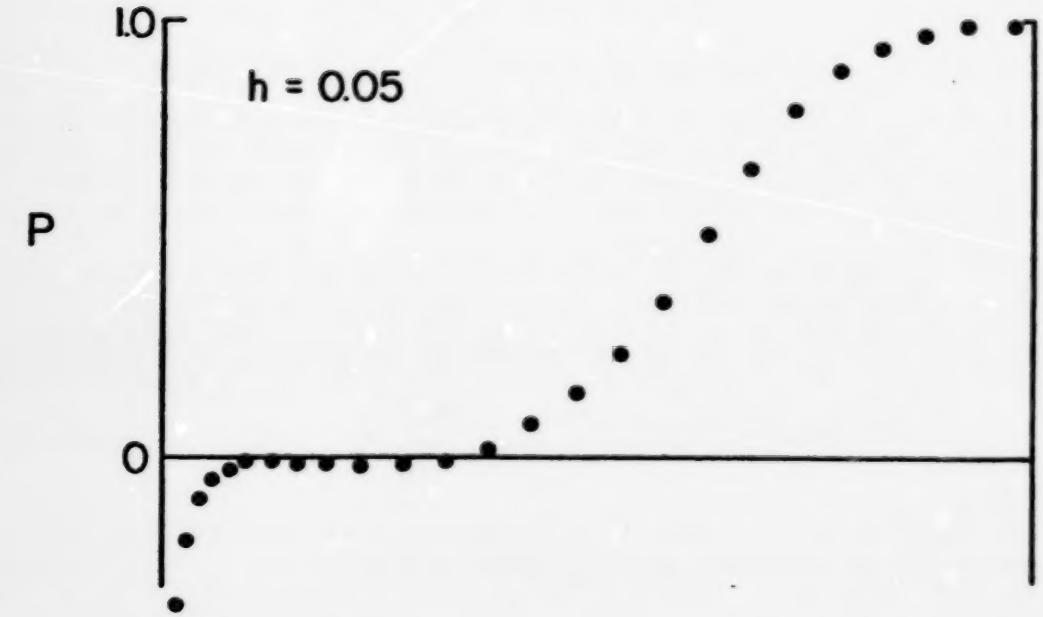

FIG. 6.7 COMPUTED PRESSURE DISTRIBUTIONS ON GROUND-BOARD FOR $R_{e_L} = 10^4$ (A) h = 0.025 and 0.05

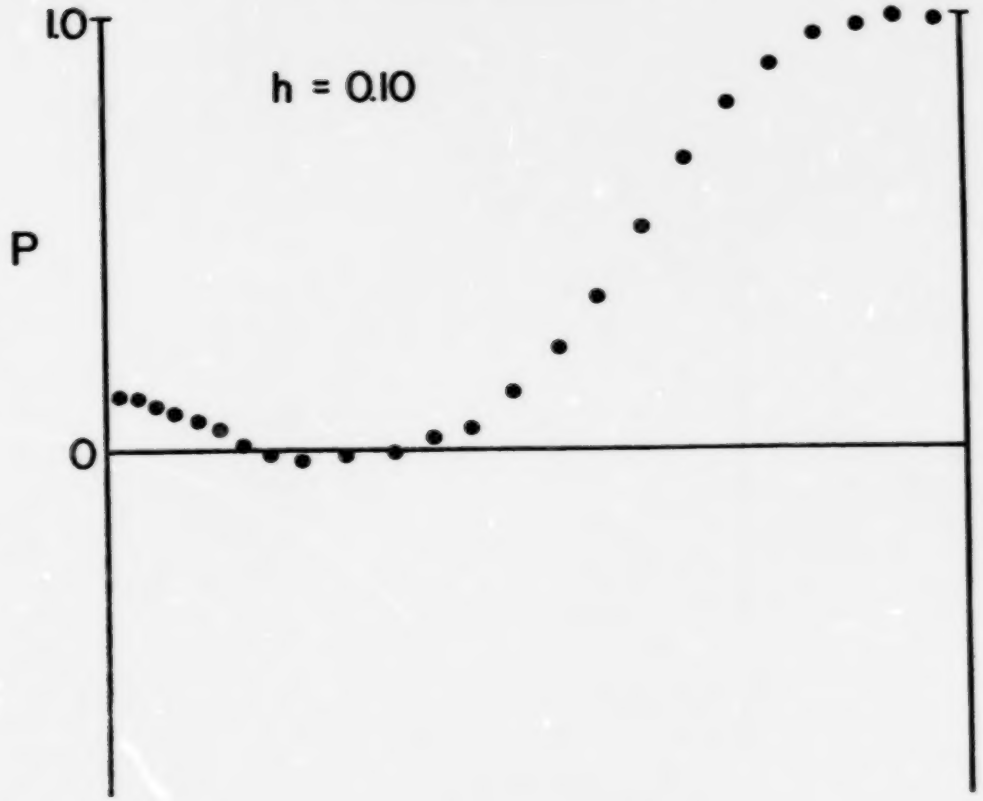

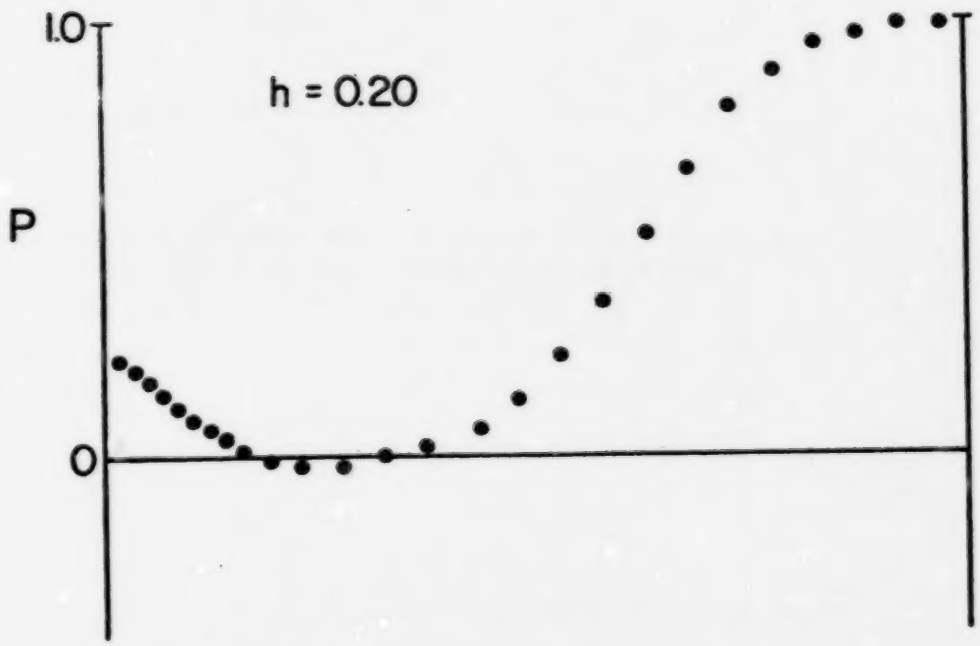

FIG. 6.7 (CONTD.) (B) GROUND-BOARD PRESSURE DISTRIBUTIONS FOR h = 0.10 and 0.20

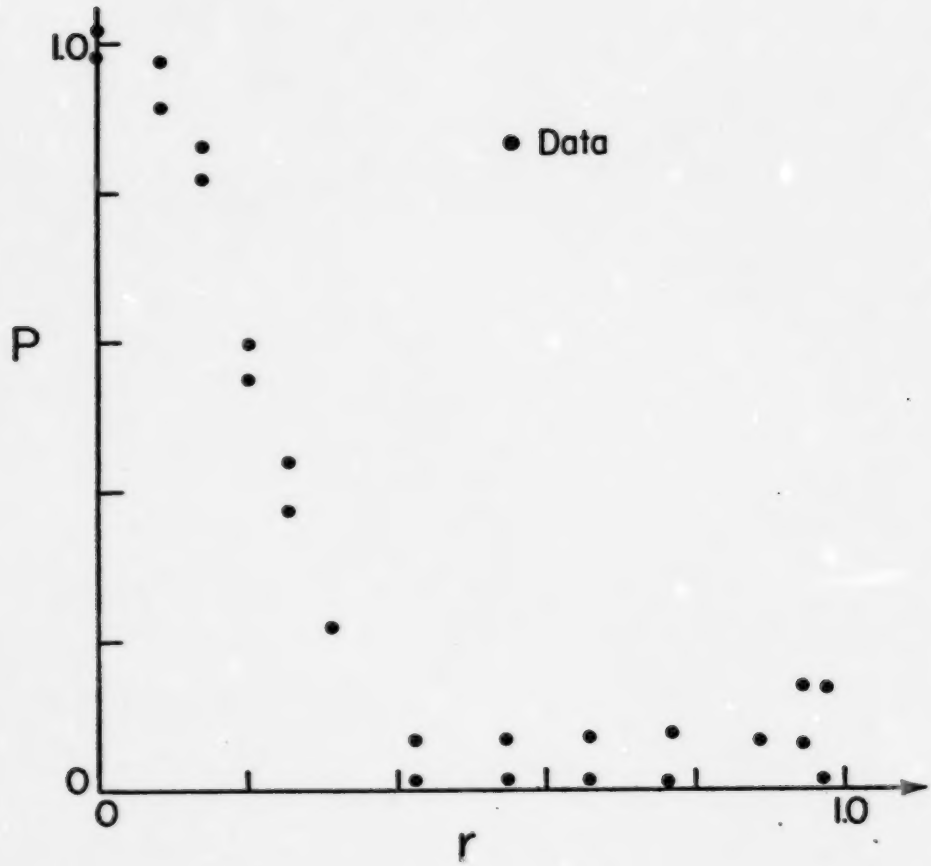

FIG. 6.8 MEASUREMENTS OF GROUND-BOARD PRESSURE DISTRIBUTIONS ON CUSHION HAVING GEOMETRY GIVEN IN FIGURE 6.3 $R_L = 2.8 \times 10^5$

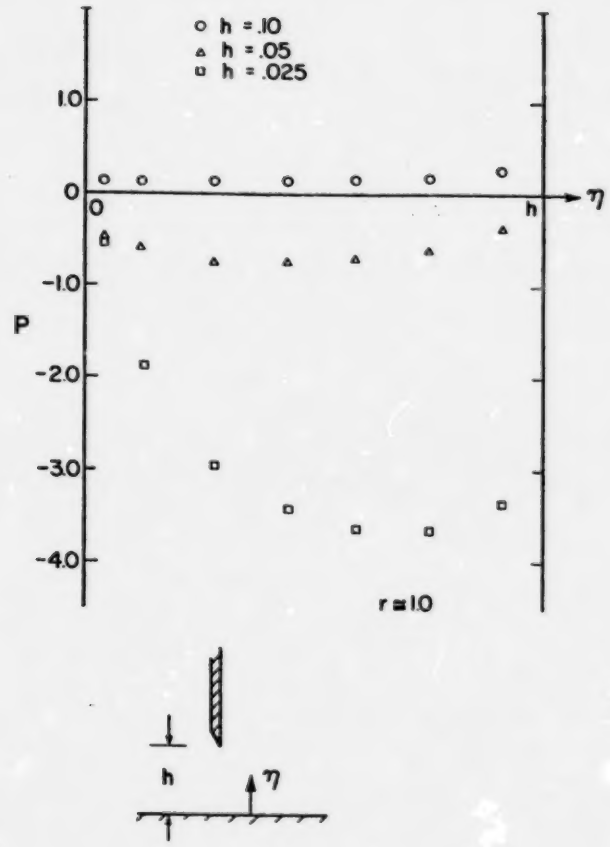

FIG. 6.9A COMPUTED PRESSURE PROFILES AT LIP FOR THREE VALUES OF h, $R_L = 10^4$

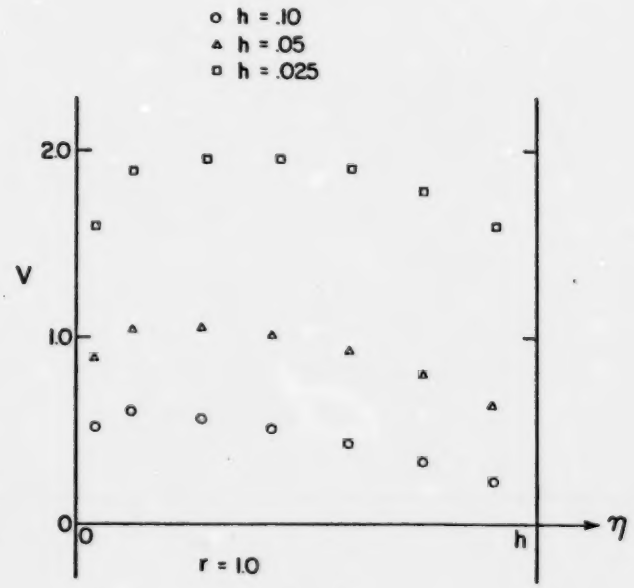

FIG. 6.9B COMPUTED RADIAL VELOCITY PROFILES AT LIP FOR THREE VALUES OF h, $R_L = 10^4$

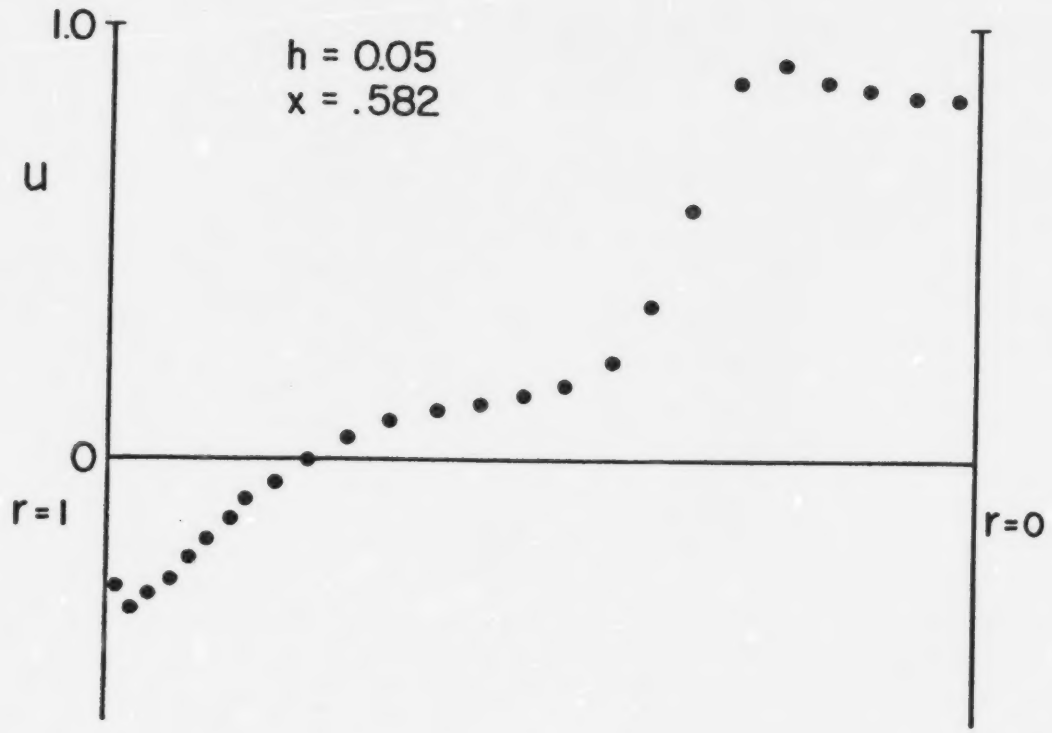

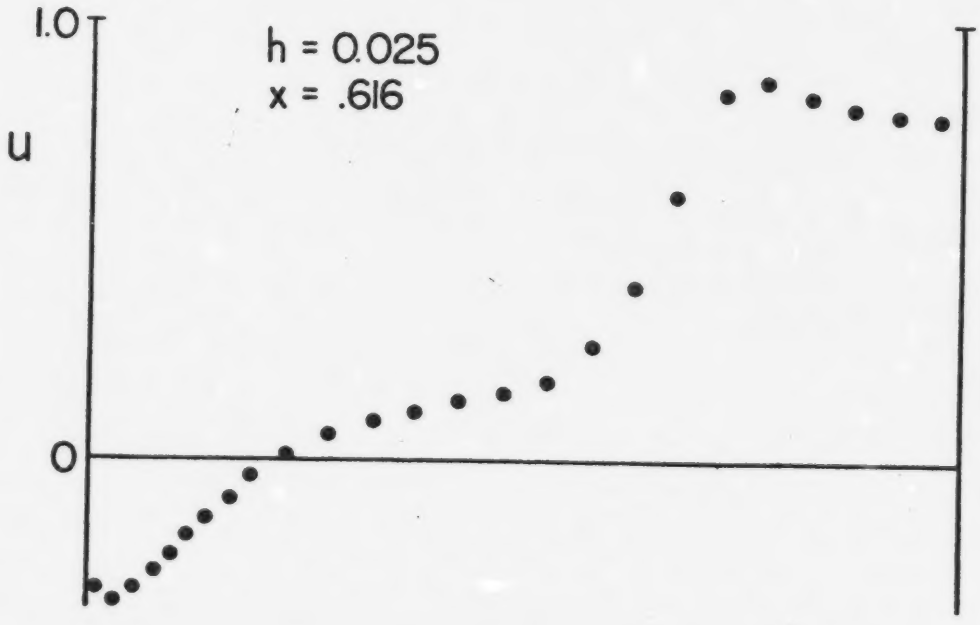

FIG. 6.10 RADIAL DISTRIBUTION OF AXIAL COMPONENT OF VELOCITY FOR h = 0.05 AND 0.025 WITH $R_L = 10^4$. PROFILES ARE LOCATED APPROXIMATELY AT $x = 0.6\ h_s$. SEE FIGURE 6.3. THE WEAK VISCOUS VORTEX IS VISIBLE.

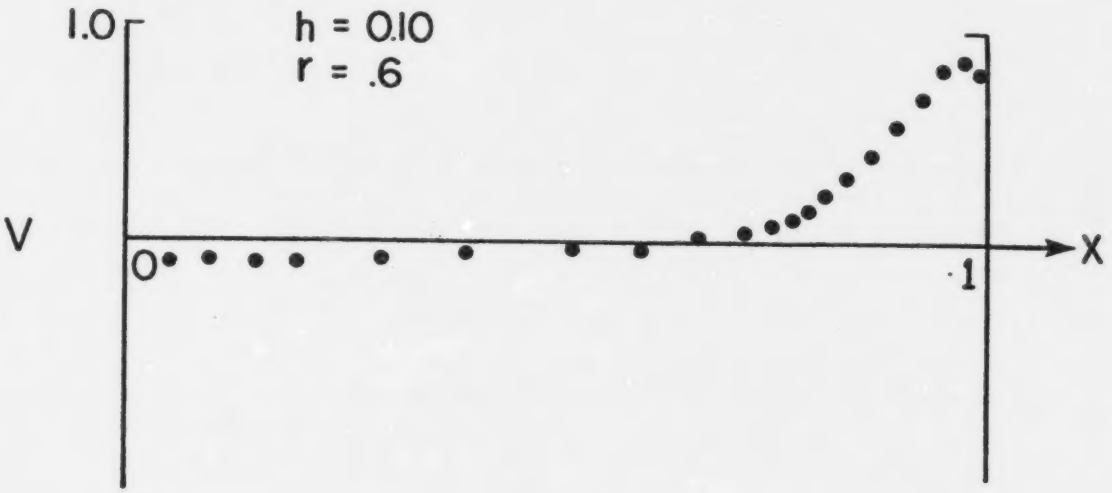

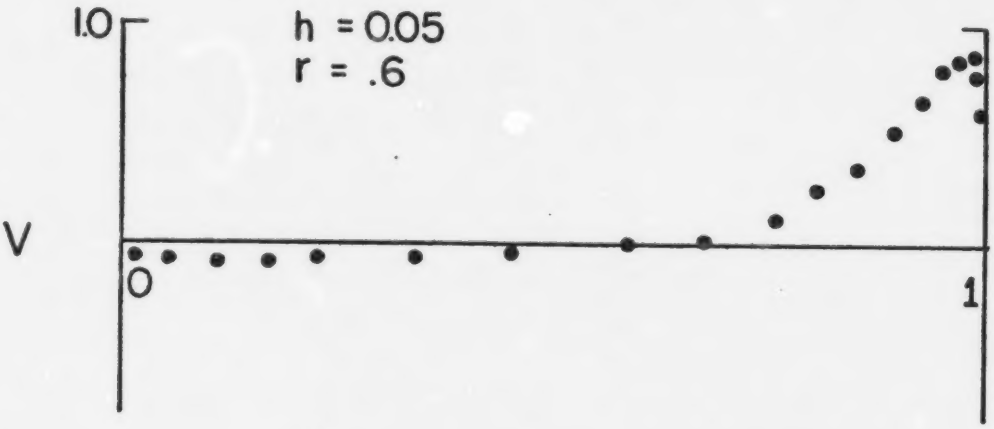

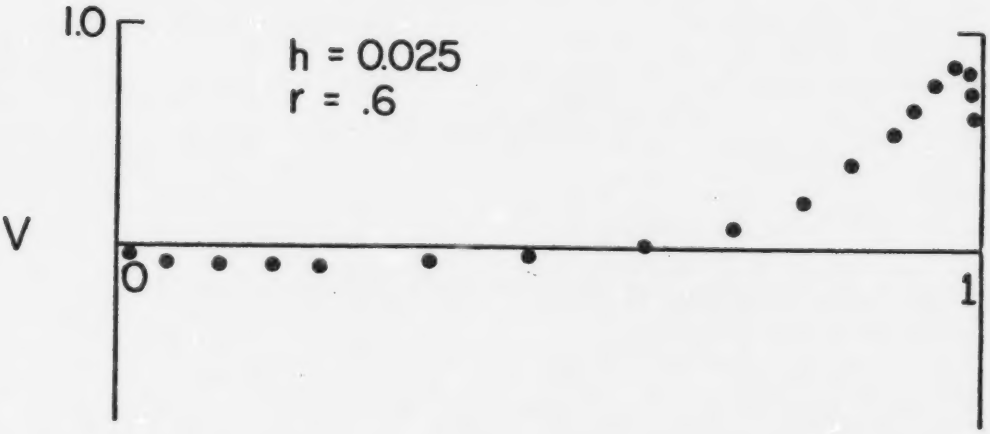

FIG. 6.11 COMPUTED AXIAL DISTRIBUTION FOR RADIAL COMPONENT OF VELOCITY FOR THREE VALUES OF h, $R_L = 10^4$

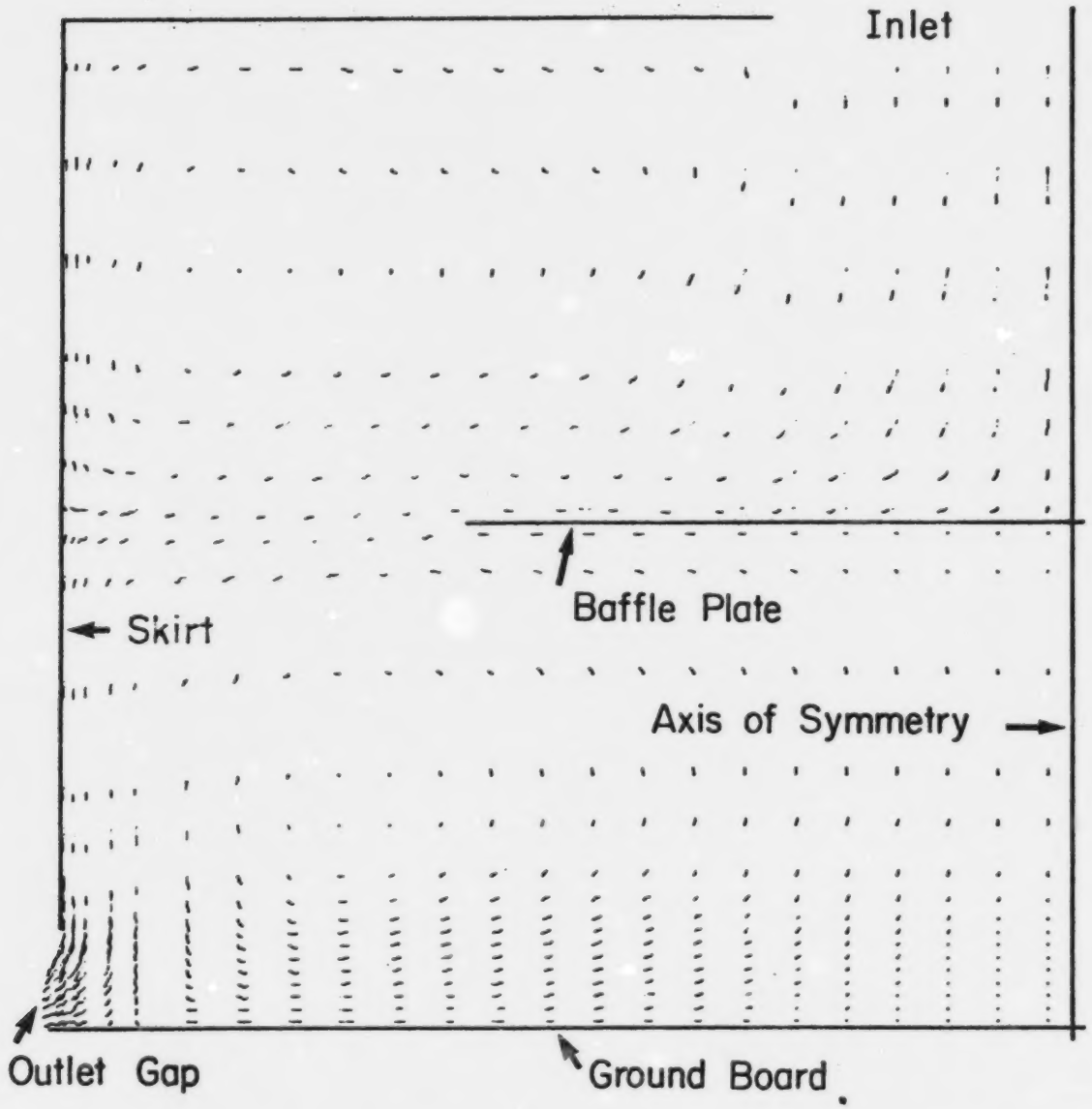

FIG. 6.12 VELOCITY VECTOR PLOT AN AIR CUSHION WITH A BAFFLE PLATE, $R_L = 10^5$, $h = 0.1$.

$$Q_a(t) = C_m \ell h \, v_o = C_m \ell h \sqrt{v_{jet}^2 + \frac{2p_c}{\rho}} \tag{51}$$

Below, the effect of the dynamic head due to v_{jet} on the stability of a duct-plenum system is considered (see Figure 6.13). For the analysis, it is assumed that the radial wall jet responds quasi-statically to the duct flow. Thus

$$v_{jet} = k_{jet} \, v_d = k_{jet} \frac{Q_d}{A_d} \tag{52}$$

where k_{jet} is a constant. With this assumption the governing equations in linearized form are:

$$C_c \frac{d\Delta p_c}{dt} = (\Delta Q_d - \Delta Q_a) - S_a \frac{d\Delta h}{dt} \tag{53}$$

$$m \frac{d^2 \Delta h}{dt^2} = S_a \Delta p_c \tag{54}$$

$$\frac{d\Delta Q_d}{dt} = - \frac{A_d}{L_d \rho} \Delta p_c \tag{55}$$

where

$$\Delta Q_a = \frac{Q_e}{h_e} \Delta h + \frac{Q_e}{\rho v_{oe}^2} \Delta p_c + \frac{v_{jet_e}^2}{v_{oe}^2} \Delta Q_d \tag{56}$$

Typical results obtained are shown in Figure 6.14, where the approximate range $0.5 < k_{jet} < 0.75$ was obtained from the numerical experiment. From Figure 6.14, it appears that the radial wall jet can have a significant effect, especially if the ducts are long. As v_{jet_e} approaches v_{oe} the system tends to behave as if it had a constant flow source. This can be seen when the perturbation in the overall cushion flow

$$\Delta Q = \Delta Q_d - \Delta Q_a \tag{57}$$

is manipulated to obtain

$$\Delta Q = \left(1 - \frac{v_{jet_e}^2}{v_{oe}^2} \right) \Delta Q_d \quad \leftarrow \text{Effective Inflow}$$
$$- \left(\frac{Q_e}{h_e} \Delta h + \frac{Q_e}{\rho v_{oe}^2} \Delta p_c \right) \tag{58}$$

As v_{jet_e} approaches v_{oe} the effective inflow perturbations tend to zero.

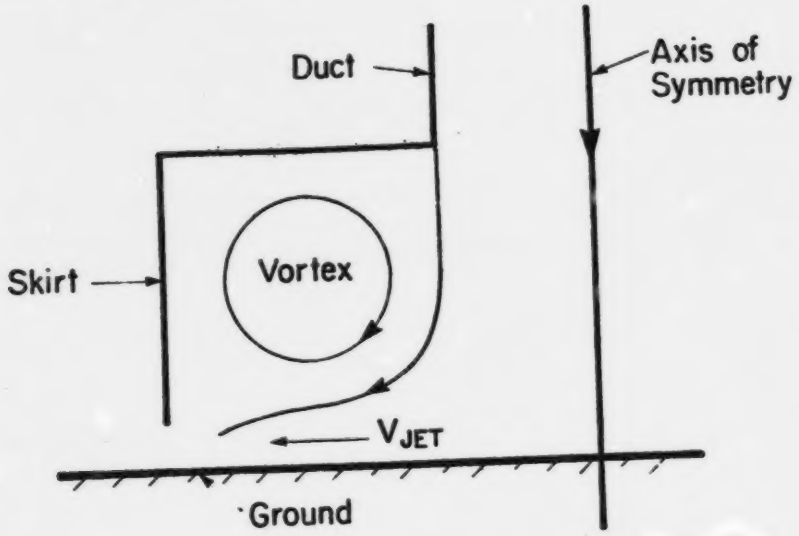

FIG. 6.13 POSTULATED SIMPLIFIED MODELS FOR INTERNAL FLOW EFFECTS

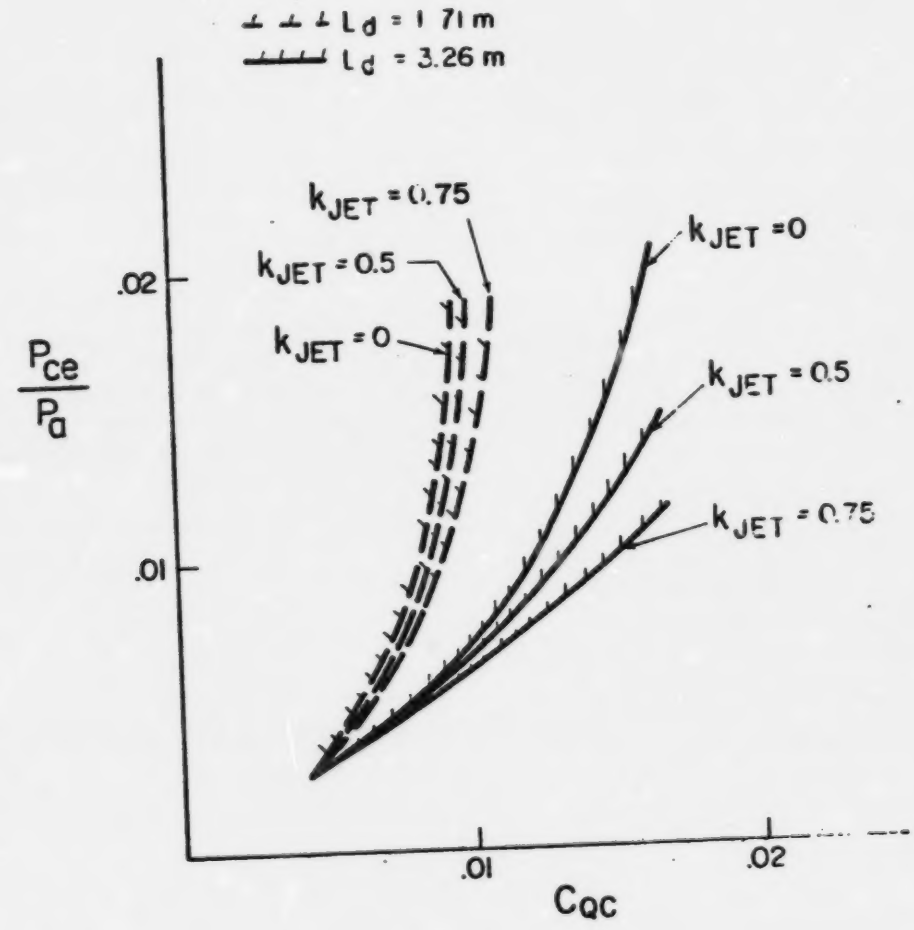

FIG. 6.14 RADIAL WALL-JET EFFECT ON STABILITY

A model of the vortex which assumed its motion to be approximately that of a rigid body rotating according to Newton's second law under the action of shear forces on its outer surface was also considered. For flow rates of practical interest, it predicted the effect of the vortex to be relatively insignificant.

7) DEVELOPMENT OF A COMPUTER PROGRAMME FOR ANALYSIS OF CIRCULAR TRACK EXPERIMENTS

7.1) Basic Purpose

As stated in the Introduction, the data to be obtained from the investigation of the dynamic response of the Circular Track Test Vehicle to various types of input or disturbance takes the form of time histories of the outputs of transducers such as accelerometers, rate gyros and trailing arm sensors. This data has to be interpreted in such a way as to obtain estimates of coefficients in the mathematical model postulated for description of the cushion being tested. This is the reverse of the way in which dynamic problems are commonly encountered. That is to say, one is usually given the differential equations and values of the coefficients, and the task is to solve the differential equations of the system in order to obtain the response to disturbance or control inputs. Here the inputs and the responses are given, and the task is to find values of the various coefficients in the differential equations which best fit the data in some sense.

The problem is, in principle at least, very simple, and it may be illustrated by using an example. Consider the classic mass-spring-damper system described by the equation

$$m\ddot{x} + c\dot{x} + kx = f(t)$$

where $x(t)$ is the time varying displacement of the mass "m" in response to an input force $f(t)$. Assume that the system is a "black box" so that there is no way of directly measuring parameters such as the damping coefficient "c" or the spring constant "k", but estimates of their value are required for some other purpose. Transducers are available to measure the quantities x, $\dot{x}$, $\ddot{x}$ and f at any instant of time $t = t_1$, t_2 and so on. Hence, using a subscript "m" to denote a measured value, given data at time t_1 and t_2 we can write

$$m\,\ddot{x}_m(t_1) + c\,\dot{x}_m(t_1) + k\,x_m(t_1) = f_m(t_1)$$

$$m\,\ddot{x}_m(t_2) + c\,\dot{x}_m(t_2) + k\,x_m(t_2) = f_m(t_2)$$

This gives two linear algebraic equations for the two unknowns "c" and "k", so that the problem is solved. Even if transducers are available only to measure accelerations "$\ddot{x}$", displacements "x", and inputs "f," no difficulty arises in principle, because we can take additional measurements at time $t = t_1 + \delta t$ and $t = t_2 + \delta t$ to estimate velocities as follows:

$$\dot{x}_m(t_1) \approx \left\{ \frac{x_m(t_1 + \delta t) - x_m(t_1)}{\delta t} \right\}$$

However, the task is greatly complicated by the fact that the transducer signals are invariably contaminated by noise, that the process of numerically differentiating the data can introduce large errors, and by other problems. Consequently, methods have to be developed to systematically treat

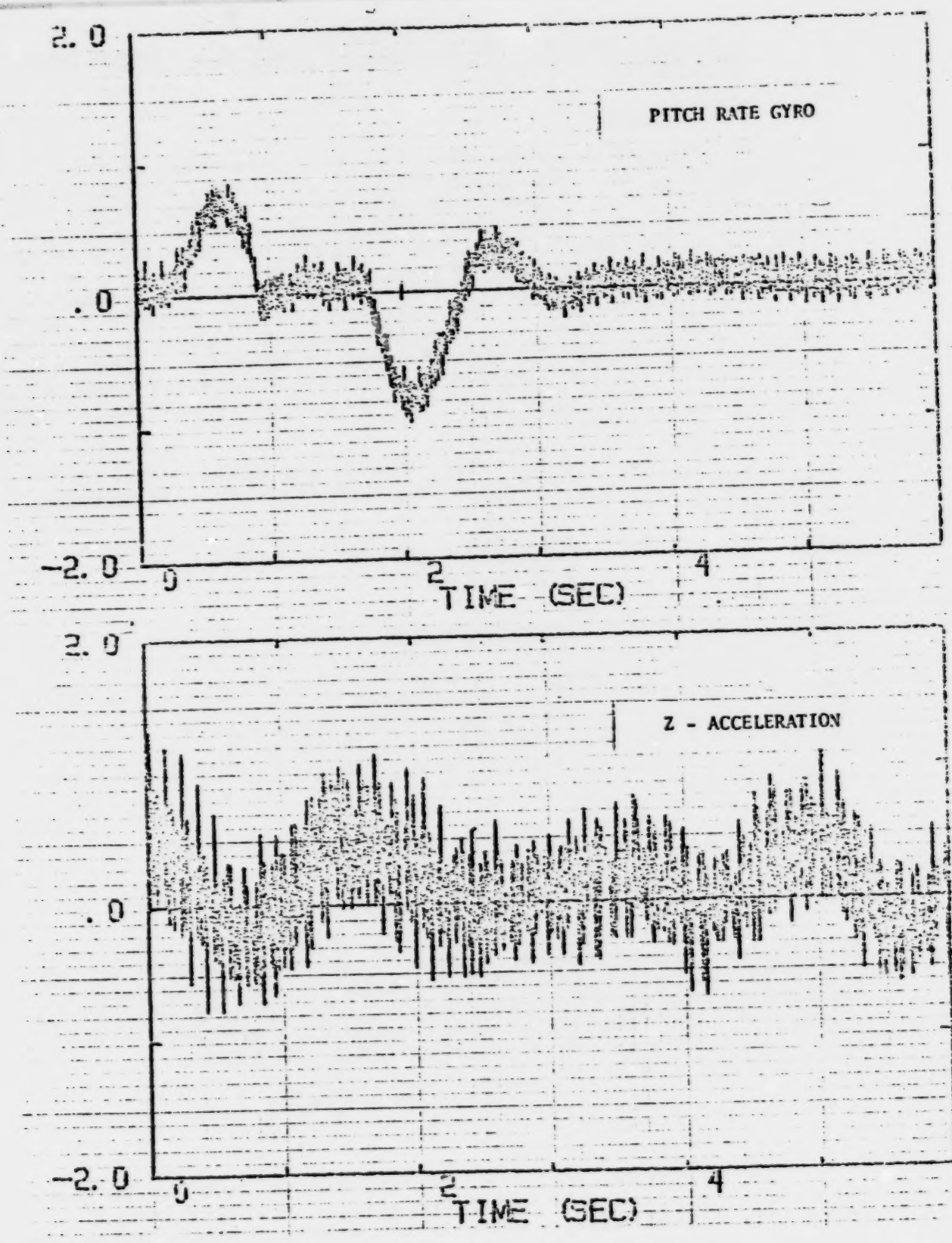

FIG. 7.1 TYPICAL OUTPUTS OF A RATE GYRO AND AN ACCELEROMETER IN VAMPIRE 1 INSTRUMENTATION PACKAGE.

large amounts of "corrupt" data in order to identify the required parameters. System parameter identification (SPI) is a particular case of the more general task of optimal estimation. Fortunately, since this optimal estimation problem has been encountered in many investigations of system dynamics, a considerable body of theory is available. Indeed, to quote but one example, the literature on attempts to analyse data from flight tests of aircraft extends back some fifty years, and the techniques that are applied today are quite sophisticated. Typically both random process theory and matrix algebra are now used to minimize the impact of measurement errors and to allow treatment of complex systems. And, as in most fields of engineering analysis, the development of large scale digital computers has had a major impact on the choice of methods and on the size and complexity of the systems that can be investigated. References 7.1 to 7.7 comprise a sample of the more recent literature appropriate to the present project.

At the time this Contract started, it was clearly understood that the data to be obtained from experiments on Vampire I would have to be analyzed by an appropriate optimal estimation procedure, and that this procedure should be based on the latest available techniques. Figure 7.1 shows typical outputs of the pitch rate gyro and an accelerometer. It is clear that the signals are noisy, indeed in this case a major source appears to be the engine vibrations. Development of the required computer programme has proceeded in parallel with preparation of the test vehicle and instrumentation system for the experiments on the HSL cushion.

One difficulty was that no data representative of the type of response to be expected from Vampire I equipped with the HSL skirt was available to use in developing the programme. Consequently it was decided that, in order to ensure minimum delay, representative data would be used from a problem which was comparable in complexity to that expected for the present experiments, but which was well understood. The problem finally chosen for development purposes was related to the lateral aerodynamics of an aircraft. It is to be noted that no special modifications would be required to apply the finally developed programme to the Vampire I pitch-heave dynamics problem, as specified for the present Contract. The use of matrix algebra ensured that the programme would be sufficiently general for this purpose.

The task has proceeded in several distinct stages:

(i) Review of the literature on optimal estimation, leading to selection of a suitable method or algorithm,

(ii) compilation of a suitable SPI computer programme,

(iii) computer-generation of the simulated response of a typical aircraft to representative control inputs,

(iv) degradation of this response by imposing suitable simulated signal noise,

(v) application of the optimal estimation programme to the noisy data generated in step (iv) to extract estimates of the derivatives used in step (iii) to generate response,

(vi) comparison of the retrieved stability derivatives with those originally specified in step (iii).

Note that if the optimal estimation or system parameter identification (SPI) procedure is perfect and the simulated data had no noise, then the exact original values of the parameters used in step (iii) should be recovered.

7.2) Description of the Selected Method

7.2.1) Overall Concept

The procedure ultimately chosen for analysis of the test data is a response matching method. The concept can be understood by reference tothe block diagram given in Figure 7.2. A time varying input vector $\underset{\sim}{u}(t)$ to the dynamic system generates an experimental response vector $\underset{\sim}{y}(t)$. This system response is assumed to be degraded by measurement noise $\underset{\sim}{n}(t)$ which results in the measured response $\underset{\sim}{z}(t)$. This measured response is the data record to be analysed by the SPI procedure. The analysis then proceeds as follows. A form of a mathematical model for the system is assumed. That is, it is postulated that the dynamical system can be described by differential equations of a given order and degree, but that certain coefficients are unknown. Then, for the control input used in the experiment, and with initial estimates of the vector of unknown coefficients $\underset{\sim}{c}$, the postulated mathematical model is used to calculate a response $\underset{\sim}{y}_e(t)$. This calculated response is then compared with the measured response, to form an error or residual $\underset{\sim}{\nu}(t) = \underset{\sim}{z}(t) - \underset{\sim}{y}_e(t)$. A criterion function J is used to assess the "goodness of fit". This criterion, which may for example be a least squares fit, is a function of the unknown parameters $\underset{\sim}{c}$. The values of the parameters $\underset{\sim}{c}$ are then adjusted - possibly by a random search, but usually by a more systematic technique - to improve the fit. Then, using the new values of $\underset{\sim}{c}$, a new response is calculated and compared with the measured response. The entire process is repeated a sufficient number of times to obtain an acceptable estimate of the unknown coefficients $\underset{\sim}{c}$.

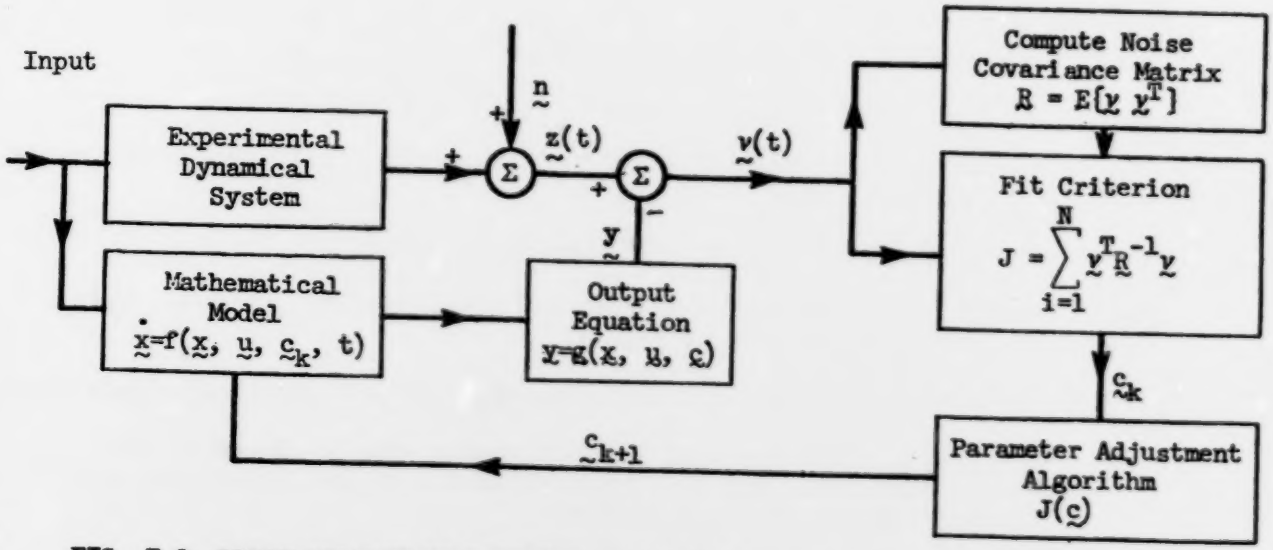

FIG. 7.2 BLOCK DIAGRAM OF RESPONSE MATCHING METHOD OF SYSTEM PARAMETER IDENTIFICATION.

It follows that the development of the method divides naturally into three parts:

(i) determination of the form of the model, that is, selection of the model differential equations, and isolation of unknown parameters,

(ii) selection of a criterion function by means of which the "goodness of fit" of the model response to the actual system response can be evaluated,

(iii) selection of an algorithm for adjustment of model parameters in such a way that the difference between the model and system responses as evaluated by (ii) are minimized.

In connection with item (i) it is known that the final estimate of the unknowns $\underset{\sim}{c}$ obtained by this scheme is very sensitive to the form assumed [Ref. 7.6]. Consequently it does not replace the task of developing a mathematical model from a knowledge of the physics of the dynamical system. On the contrary, successful use of a SPI procedure relies heavily on the availability of a physical analysis to guide the choice of form. Some of the authors who discuss this question conclude that, if a complex model is used with only a limited amount of measurement information of low quality, an unreliable result will be obtained, if the method works at all [Refs. 7.8 and 7.9]. It is also stressed that, when a parametric model is used, it is imperative that the order of the model be the same as that of the system - otherwise large errors occur [Ref. 7.9]. This basic question arises in connection with the present work.

As noted above, some of the parameters in the assumed model will be known, and it is the object of analysis to determine others. Thus, in the present project, the pitch moment of inertia of Vampire 1 has been determined from a pendulum experiment. However, there is usually sufficient data from the experiment to which the SPI procedure is to be applied to allow an independent estimate of the known coefficients to be made. This can serve as a useful check on the consistency of both the experiments and the analysis. Consequently, it is desirable to formulate the SPI programme in such a way that coefficients determined from prior experiments are still treated as unknown but that accurate initial estimates are available. This feature has been included in the programme ultimately developed.

7.2.2) Formulation of Mathematical Model

It is assumed that the system can be described by a set of differential equations:

$$\dot{\underset{\sim}{x}} = f(\underset{\sim}{x}, \underset{\sim}{u}, \underset{\sim}{c}, t); \quad \underset{\sim}{x} \text{ at } t = t_o \text{ given } (\underset{\sim}{x}_o) \qquad (1)$$

and by an output equation

$$\underset{\sim}{y} = g(\underset{\sim}{x}, \underset{\sim}{u}, \underset{\sim}{c})$$

where $\underset{\sim}{x}$ is an (n x 1) state vector,

$\underset{\sim}{u}$ is a (p x 1) input vector,

$\underset{\sim}{c}$ is a (q x 1) vector of unknown parameters,

$\underset{\sim}{y}$ is a (r x 1) vector of outputs.

If the system is linear with coefficients independent of time, equations (1) and (2) reduce a set of first-order differential equations of the form

$$\dot{\underset{\sim}{x}} = \underset{\sim}{A}\,\underset{\sim}{x} + \underset{\sim}{B}\,\underset{\sim}{u} \qquad \underset{\sim}{x}(0) = \underset{\sim}{x}_o \tag{3}$$

$$\underset{\sim}{y} = \underset{\sim}{F}\,\underset{\sim}{x} + \underset{\sim}{G}\,\underset{\sim}{u} \tag{4}$$

where the unknown parameters may in general be contained in all four matrices $\underset{\sim}{A}$, $\underset{\sim}{B}$, $\underset{\sim}{F}$, $\underset{\sim}{G}$.

If the system equations (1) and (2) are nonlinear, it is usually possible to obtain linearized equations for small perturbations about an equilibrium point and these equations can then be transformed into the canonical form (3) and (4). It is possible, however, that certain inherently nonlinear effects, such as the hysteresis phenomenon encountered both in previous TDC Contracts and for the present HSL skirt, may be present and the mathematical model will have to account for this. For the work undertaken for the present Contract, a linear model has been assumed. Consequently the SPI programme interprets hysteretic damping as an equivalent linear viscous damping.

7.2.3) Criterion Function

The criterion function J, also known as the cost or error function, depends on the unknown parameters used in the mathematical model and becomes a minimum when the model parameters equal those of the system. Note that, in the absence of measurement noise, the cost function should be zero at its minimum. The cost functions used in SPI may take several forms, such as:

(i) the least squares (LS) function,

(ii) weighted least squares (WLS) function,

(iii) maximum likelihood (ML) function,

(iv) the Bayesian function.

These are described for the case in which the data is available only at discrete time intervals. The data from the planned Vampire I experiment is in this form, since it is sampled every 1/100 of a second and then digitized.

The LS cost function J is simply the sum of squares of the errors at all time points, i.e.,

$$J = \sum_{i=1}^{N} (\underset{\sim}{z}_i - \underset{\sim}{y}_i)^T (\underset{\sim}{z}_i - \underset{\sim}{y}_i) = \sum_{i=1}^{N} \underset{\sim}{\nu}_i^T \underset{\sim}{\nu}_i \tag{5}$$

where the data has been recorded at N points in time. The LS function is not generally used. The WLS function is a sum of squares of errors at all time points multiplied by a weighting matrix, $\underset{\sim}{W}$, which expresses the confidence in the various measurements:

$$J = \sum_{i=1}^{N} \underset{\sim}{\nu}_i^T \underset{\sim}{W} \underset{\sim}{\nu}_i \qquad (6)$$

The matrix $\underset{\sim}{W}$ is usually diagonal, and the elements on the diagonal may be chosen to be inversely proportional to the relative error expected in each of the signal channels z_α of $\underset{\sim}{z}$.

It has been observed that WLS methods may be preferred when there is no basis for assigning probability density functions to the noise vector $\underset{\sim}{\nu}$ [Ref. 7.6, p. 103]. If some information about the form of the noise statistics is available, or if certain assumptions are made, one may apply the so called maximum likelihood (ML) philosophy. This takes the estimate of $\underset{\sim}{c}$, denoted by $\hat{\underset{\sim}{c}}$, to be that value of $\underset{\sim}{c}$ which maximises the probability of the measurements that were actually recorded. It is usual to assume that the noise vector $\underset{\sim}{\nu}$ has a Gaussian probability density function. One rationale for this is the well known Central Limit Theorem [Ref. 7.6, p. 39].

If $\underset{\sim}{x}$ is an r-dimensional vector of scalar random variables, then the Gaussian or normal density function $p(\underset{\sim}{x})$ is

$$p(\underset{\sim}{x}) = \frac{1}{\sqrt{(2\pi)^r |\underset{\sim}{R}|}} \exp - \left\{ \frac{1}{2} (\underset{\sim}{x} - \underset{\sim}{m})^T \underset{\sim}{R}^{-1} (\underset{\sim}{x} - \underset{\sim}{m}) \right\} \qquad (7)$$

where

$\underset{\sim}{m}$ = column vector of mean values of the elements of $\underset{\sim}{x} = E\{\underset{\sim}{x}\}$,

$\underset{\sim}{R}$ = noise covariance matrix = $E\{(\underset{\sim}{x} - \underset{\sim}{m})(\underset{\sim}{x} - \underset{\sim}{m})^T\}$,

and $E\{\ \}$ is the expected value operator; typically for a stationary ergodic process $x(t)$ which is measured at discrete time points t_i,

$$E\{x\} = \lim_{N \to \infty} \frac{1}{N} \sum_{i=1}^{N} x(t_i)$$

For the present problem, if the output at a given time t_i corresponding to the correct values of $\underset{\sim}{c}$ is $\underset{\sim}{y}_i$, then the probability density function for the measured response is simply

$$p(\underset{\sim}{z}_i | c) = \frac{1}{\sqrt{(2\pi)\ |\underset{\sim}{R}|}} \exp - \left\{ \frac{1}{2} (\underset{\sim}{z}_i - \underset{\sim}{y}_i)^T \underset{\sim}{R}^{-1} (\underset{\sim}{z}_i - \underset{\sim}{y}_i) \right\} \qquad (8)$$

Here the notation $p(\underset{\sim}{z}_i | c)$ denotes the conditional probability of $\underset{\sim}{z}_i$ given an estimate of the unknown parameters $\underset{\sim}{c}$. Note that, if as might be expected, the noise of different signal channels or elements of $\underset{\sim}{z}$ is uncorrelated, then $\underset{\sim}{R}$ is simply the diagonal matrix of the variances of the noise on each channel. If, in addition, the noise recorded at different time points is statistically independent then, since the probability of the occurrence of a sequence of independent events is simply the product of the probabilities of each event, or since,

$$p(\underset{\sim}{z}_1 \text{ and } \underset{\sim}{z}_2 \text{ and } \underset{\sim}{z}_3 | \underset{\sim}{c}) = p(\underset{\sim}{z}_1 | \underset{\sim}{c})\ p(\underset{\sim}{z}_2 | \underset{\sim}{c})\ p(\underset{\sim}{z}_3 | \underset{\sim}{c}) \triangleq p(\underset{\sim}{z} | \underset{\sim}{c})$$

one has

$$p(\underset{\sim}{z} | \underset{\sim}{c}) = \frac{1}{[(2\pi)^r |\underset{\sim}{R}|]^{N/2}} \exp - \left\{ \frac{1}{2} \sum_{i=1}^{N} (\underset{\sim}{z}_i - \underset{\sim}{y}_i)^T \underset{\sim}{R}^{-1} (\underset{\sim}{z}_i - \underset{\sim}{y}_i) \right\} \tag{9}$$

Maximizing $p(\underset{\sim}{z} | \underset{\sim}{c})$ is equivalent to minimizing

$$J(\underset{\sim}{c}) = \frac{1}{2} \sum_{i=1}^{N} (\underset{\sim}{\nu}_i^T \underset{\sim}{R}^{-1} \underset{\sim}{\nu}_i) \tag{10}$$

This is the same as the WLS criterion, except that now a statistical basis for choosing $\underset{\sim}{W}$ is given.

Now a-priori estimates of some of the parameters in $\underset{\sim}{c}$ may be available. For example, in the problem addressed in this Contract the pitch moment of inertia of Vampire 1 has been determined by a separate pendulum experiment; and this measurement is believed to be very accurate. Hence one might include in the cost function $J(\underset{\sim}{c})$ a penalty term for departure from the a-priori estimate $\hat{\underset{\sim}{c}}_o$ of $\underset{\sim}{c}$, and put

$$J(\underset{\sim}{c}) = \sum_{i=1}^{N} \underset{\sim}{\nu}_i^T \underset{\sim}{R}^{-1} \underset{\sim}{\nu}_i + \sum_{i=1}^{N} (\underset{\sim}{c} - \underset{\sim}{c}_o)^T \underset{\sim}{R}_c^{-1} (\underset{\sim}{c} - \underset{\sim}{c}_o) \tag{11}$$

where

$$\underset{\sim}{R}_c = E\{(\underset{\sim}{c} - \underset{\sim}{c}_o)(\underset{\sim}{c} - \underset{\sim}{c}_o)^T\} \tag{12}$$

It can be shown by using Bayes' Theorem of statics, that given $\underset{\sim}{R}_c$ is available, equation (11) is the correct form. This cost function has been used in the present work.

Finally it must be noted that the measurement noise covariance matrix $\underset{\sim}{R}$ is not usually available at the start of the computation, and approximations must be computed for each successive estimate $\hat{\underset{\sim}{c}}_i$ of $\hat{\underset{\sim}{c}}$. This is illustrated in the process block diagram of figure 7.2. The computation is started by simply putting $\underset{\sim}{R} = \underset{\sim}{I}$, the identity matrix.

7.2.4) Parameter Adjustment Algorithm

For the given set of model differential equations and measured data, the cost function, J, is a function of the unknown parameters, $\underset{\sim}{c}$. After calculating the cost function for a given or assumed set of parameters, $\underset{\sim}{c}_k$, we wish to adjust them in such a way that, for the new set of parameters, the cost function is reduced and a better response fit is achieved. The ultimate goal is to find a set of parameters for which the cost function, J, reaches its minimum value, and gives the best possible response fit. This procedure is an example of the task of nonlinear optimization, and a large body of

literature on the development of a variety of possible algorithms is now available. A useful introductory survey of the literature is given in Ref. 7.9.

A detailed discussion of the possibilities is out of place here, but several are described briefly to illustrate the approach chosen. They are

(i) search method,

(ii) steepest descent method,

(iii) Newton-Raphson method,

(iv) modified Newton-Raphson method.

The search method is useful when the range within which the minimum of J is located is limited and known, or when there are several minima. Various search methods, such as the random search, relaxation method s, neighbourhood search, are described in [Refs. 7.7 and 7.9]. These methods can be very time consuming and are used in special cases only.

At any value of $\underset{\sim}{c}$, the cost function $J(\underset{\sim}{c})$ decreases most rapidly in the direction of its gradient $\nabla_c J$ which is defined as

$$\nabla_c(J) = \left\{ \frac{\partial J}{\partial c_1}, \frac{\partial J}{\partial c_2}, \ldots, \frac{\partial J}{\partial c_n} \right\}^T \tag{13}$$

According to the steepest descent method, the direction taken for adjustment of the k-th estimate of $\underset{\sim}{c}$, namely $\underset{\sim}{c}_k$ is parallel to $\nabla_c J\ (\underset{\sim}{c}_k)$:

$$\underset{\sim}{c}_{k+1} = \underset{\sim}{c}_k - \lambda \nabla_c J(\underset{\sim}{c}_k) \tag{14}$$

The scalar quantity λ is chosen to minimise $J(\underset{\sim}{c}_{k+1})$. At the new point $\underset{\sim}{c}_{k+1}$, the gradient $\nabla_c J(\underset{\sim}{c}_{k+1})$ is determined again. For problems such as the present one, since $J(\underset{\sim}{c})$ is not available in given functional form, the derivatives $\partial J/\partial c_i$ must be computed by a finite difference technique at each stage. This technique is generally not recommended [Ref. 7.9, p. 31].

The Newton-Raphson technique is derived from the following considerations. The problem of finding a minimum of $J(\underset{\sim}{c})$ is equivalent to solving the set of equations

$$g_i \triangleq \partial J/\partial c_i = 0, \qquad i = 1, 2, \ldots, q \tag{15}$$

This may also be stated as $\underset{\sim}{g} = (\partial J/\partial c_1, \partial J/\partial c_2, \ldots)^T = \underset{\sim}{0}$. Given an estimate $\underset{\sim}{c}_k$ an approximate solution to the above set of equations may be obtained by using a Taylor's series expansion for the region in the neighbourhood of $\underset{\sim}{c}_k$; that is one assumes

$$\underset{\sim}{g}(\underset{\sim}{c}_{k+1}) = \underset{\sim}{g}(\underset{\sim}{c}_k) + \underset{\sim}{G}_k\, e_k + O(e^2) \tag{16}$$

where $\underset{\sim}{G}$ is a q x q matrix of second order derivatives of J:

$$\underset{\sim}{G}_k = \left[\left. \frac{\partial g_i}{\partial c_j} \right|_{c_k} \right] = \left[\left. \frac{\partial^2 J}{\partial c_i \partial c_j} \right|_{c_k} \right] \nabla_c^2 J; \quad \underset{\sim}{c}_{k+1} \triangleq \underset{\sim}{c}_k + \underset{\sim}{e}_k, \quad e^2 = \underset{\sim}{e}^T \underset{\sim}{e} \qquad (17)$$

If $\underset{\sim}{c}_{k+1}$ is the required optimum then $\underset{\sim}{g}(\underset{\sim}{c}_{k+1}) = \underset{\sim}{0}$ and, provided $\underset{\sim}{G}_k^{-1}$ exists, the above equation can be solved for $\underset{\sim}{e}_k$:

$$\underset{\sim}{c}_{k+1} = \underset{\sim}{c}_k - \underset{\sim}{G}_k^{-1} \underset{\sim}{g}_k + O(e^2) \qquad (18)$$

In the Newton-Raphson method, terms of $O(e^2)$ are ignored to give the algorithm

$$\underset{\sim}{c}_{k+1} = \underset{\sim}{c}_k - [\nabla_c^2 J(\underset{\sim}{c}_k)]^{-1} \nabla_c J(\underset{\sim}{c}_k) \qquad (19)$$

There are many difficulties associated with the use of this method, for example $\underset{\sim}{G}_k^{-1}$ may not exist at all points $\underset{\sim}{c}_k$, it does not distinguish between maxima, minima or saddle points, the computation of the matrix of second order derivatives is very cumbersome, and it can be very unstable.

However, it is known that, whenever the cost function J is the sum of square terms, as is the case here, if the noise on each of the signal channels are uncorrelated, then methods based on the Newton-Raphson concepts and matrix inversion can be particularly effective. One such method is known as the modified Newton-Raphson method or Gauss-Newton method [Refs. 7.5 and 7.9, p. 41].

Differentiate the cost function

$$\underset{\sim}{J}[\underset{\sim}{y}(\underset{\sim}{c})] = \sum_{i=1}^{N} (\underset{\sim}{z}_i - \underset{\sim}{y}_i)^T \underset{\sim}{W} (\underset{\sim}{z}_i - \underset{\sim}{y}_i) \qquad (20)$$

twice with respect to $\underset{\sim}{c}$ to obtain

$$\nabla_c J = -2 \sum_{i=1}^{N} \nabla_c (\underset{\sim}{y}_i^T) \underset{\sim}{W} (\underset{\sim}{z}_i - \underset{\sim}{y}_i) \qquad (21)$$

and

$$\nabla_c^2 J = 2 \sum_{i=1}^{N} \nabla_c (\underset{\sim}{y}_i^T) \underset{\sim}{W} \nabla_c (\underset{\sim}{y}_i) + 2 \sum_{i=1}^{N} \nabla_c^2 (\underset{\sim}{y}_i^T) \underset{\sim}{W} (\underset{\sim}{z}_i - \underset{\sim}{y}_i) \qquad (22)$$

It can be shown that the second term in $\nabla_c^2 J$ becomes $O(e^2)$ as $\underset{\sim}{e} \to \underset{\sim}{0}$. Hence the second term may be omitted in computing $\nabla_c^2 J$, and the task of computing second order derivatives of J, namely $\partial^2 J / \partial c_i \partial c_j$, can be eliminated.

With this modification the Newton-Raphson algorithm becomes

$$\underset{\sim}{c}_{k+1} = \underset{\sim}{c}_k - \left[\sum_{i=1}^{N} \left[\nabla_c(\underset{\sim}{y}_i^T)\underset{\sim}{W}\nabla_c(\underset{\sim}{y}_i)\right]\Big|_k\right]^{-1}\left[\sum_{i=1}^{N}\left[\nabla_c(\underset{\sim}{y}_i^T)\underset{\sim}{W}(\underset{\sim}{z}_i - \underset{\sim}{y}_i)\right]_k\right] \quad (23)$$

This technique was used for the present work.

7.3) Development of SPI and Test Programmes

7.3.1) Development

A computer programme based on the ideas described above has been developed, and the listing of this programme is given in Appendix A.* A useful starting point was found in the literature [Ref. 7.10] although, even with a Fortran listing available, a considerable amount of development work was required before it could be adapted toUTIAS use. The listing given in Ref. 7.10 also contained several errors; their detection and elimination consumed a lot of time.

7.3.2) Simulation Test Programme

As noted in Section 7.1, initially no Circular Track data was available for programme development purposes. Consequently a data simulation programme was also developed. To provide a well defined example, equations for the lateral dynamics of an aircraft undergoing a particular manoeuvre were used. It is worth noting that, even if experimental data is available, a data simulation programme provides a valuable check on the accuracy of the SPI programme, since the "unknown" coefficients to be obtained by SPI are, in fact, known exactly.

The simulation programme, called DATAG, is included in the main SPI programme as a subroutine. The aircraft dynamics example it uses is of fourth order. The numerical constants required for the state matrix $\underset{\sim}{A}$ and control matrix $\underset{\sim}{B}$ of equation (3) above have been taken from Ref. 7.11. Given an initial condition $\underset{\sim}{x}_o = \underset{\sim}{x}(t = 0)$ and a suitable control signal $\underset{\sim}{u}(t)$ as data, DATAG calculates the system response $\underset{\sim}{x}(t)$. The simulated data for the subsequent SPI analysis is then generated by adding to the elements of $\underset{\sim}{x}$ Gaussian stationary random noise at each interval of time. This noise is generated by a subroutine available in the U of T IBM subroutine library. The magnitude of the noise degradation is specified by assigning its variance as an input.

It is well known that the success of SPI procedure depends critically on the use of an appropriate input signal; this signal should in general excite all the modes of the system. However, in the ACV experiments planned for the Circular Track facility, only a very restricted range of possibilities is available. For example it is envisaged that the vehicle dynamics will be excited by either flying Vampire 1 over a test ramp or by dropping a weight off the rear of the vehicle. Consequently for the test programme DATAG, two cases were studied:

---

*At the time of final printing of this report it was decided to omit the computer programme description and listing because it still contained "bugs". It is to be included in the next Contract report (P.A.S.)

(i) with a continuously varying input signal u(t),

(ii) with an initial disturbance only.

7.3.3 Example of Test of SPI Programme

The matrices $\underset{\sim}{A}$ and $\underset{\sim}{B}$ used for the simulations in DATAG are given in Table 7.1 below. The parameters in the last column and last row of the $\underset{\sim}{A}$ matrix and the last two rows of the $\underset{\sim}{B}$ matrix were, for the SPI analysis, treated as known or fixed quantities so that the remaining 13 elements were the "unknowns" to be recovered. The vector of measured data is, in the absence of noise, $\underset{\sim}{z} = [x_1, x_2, x_3, x_4, \dot{x}_1, \dot{x}_2, \dot{x}_3]^T$. The input or control is $\underset{\sim}{u} = [u_1, u_2]^T$.

A total of 5 runs of the SPI program are described below. These are:

Case (i) Run 1) given continuously varying control signal, and zero noise degradation of the simulated data,

2) the same control signal, with "low" noise degradation,

3) as above, but with "high" noise,

Case (ii) Run 4) zero control input, but with initial condition $x_3 = 6$, $x_1 = x_2 = x_4 = 0$, and noise statistics as for run 2,

5) zero control input, initial conditions as for run 4 but with the noise statistics as for run 3.

The control inputs used in runs 1 to 3 are shown in Figure 7.3

System Matrix $\underset{\sim}{A}$				Control Matrix $\underset{\sim}{B}$	
-0.2740,	0.0630,	-11.400,	0	8.2230,	4.1770
0.0013,	0.2080,	2.1700,	0	-1.1400,	-3.7610
0.0830,	-1.0000,	-0.3150,	0.00790	0,	0
1.0000,	0.0	0.0	0.0	0,	0

TABLE 7.1 MATRICES $\underset{\sim}{A}$ AND $\underset{\sim}{B}$ USED IN SIMULATIONS.

Typical simulated data for case (i) are shown in Figures 7.4 and 7.5. The variables $z_1(t)$ and $z_6(t)$ are given, and the histories in Figures 7.4 and 7.5 correspond to zero noise [run (1)] and high noise [run (3)]. Figure 7.6 gives typical histories of $z_1(t)$ used in runs (4) and (5) respectively.

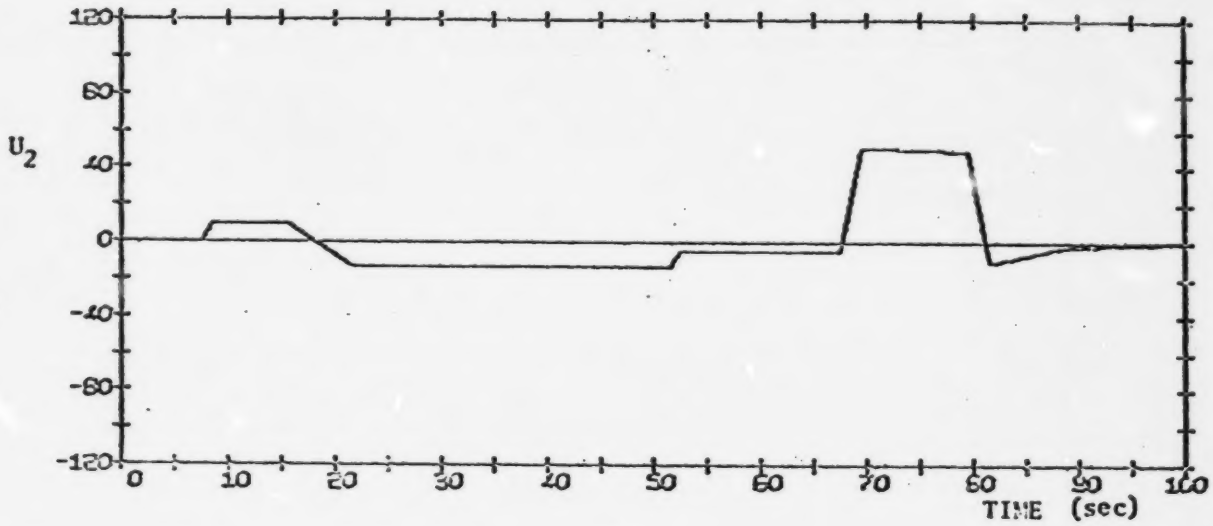

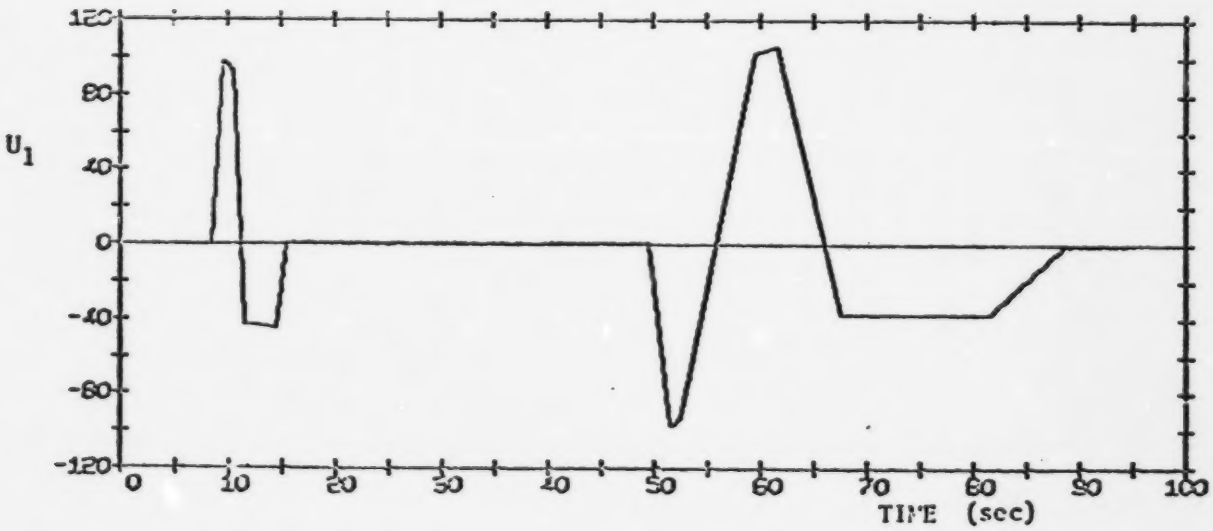

FIG. 7.3 CONTROL INPUTS USED IN SIMULATION PROGRAMME

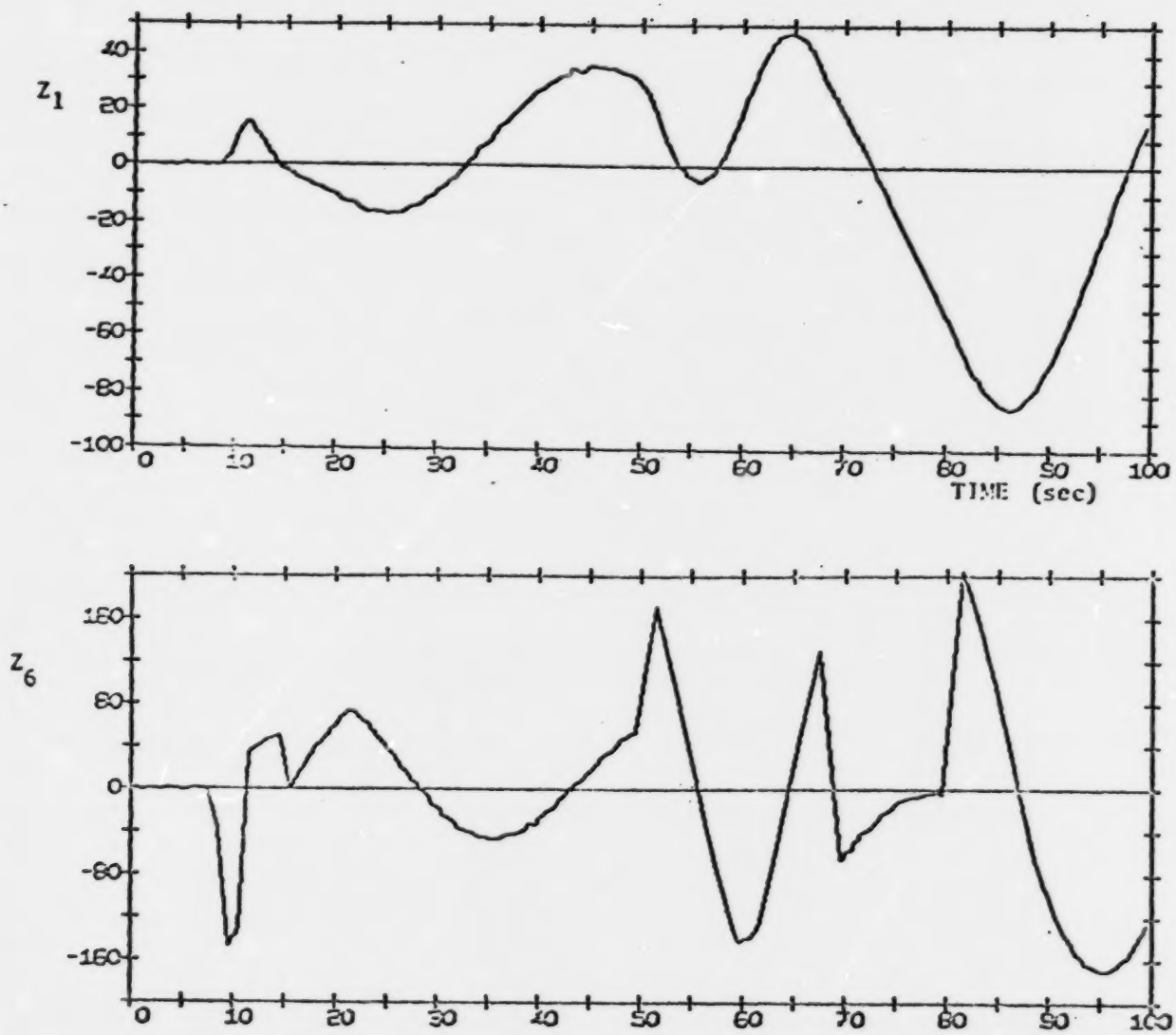

FIG. 7.4 TYPICAL OUTPUTS $Z_1(t)$ AND $Z_6(t)$ OF SIMULATION PROGRAMME IN THE ABSENCE OF NOISE, GENERATED BY THE CONTROL INPUT OF FIG. 7.3 (CASE I)

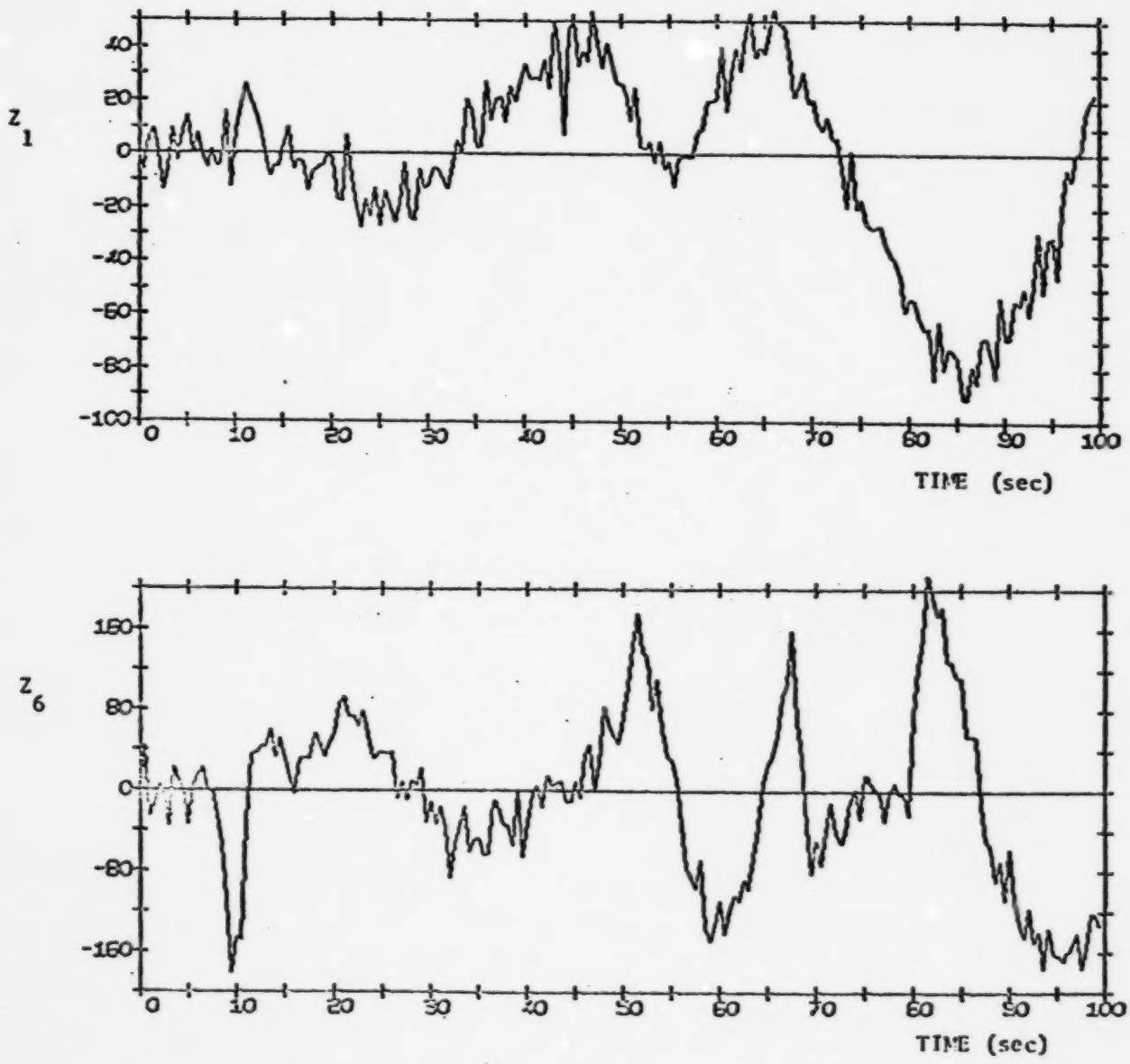

FIG. 7.5 TYPICAL OUTPUTS $Z_1(t)$ AND $Z_6(t)$ OF SIMULATION PROGRAMME FOR HIGH NOISE CASE.

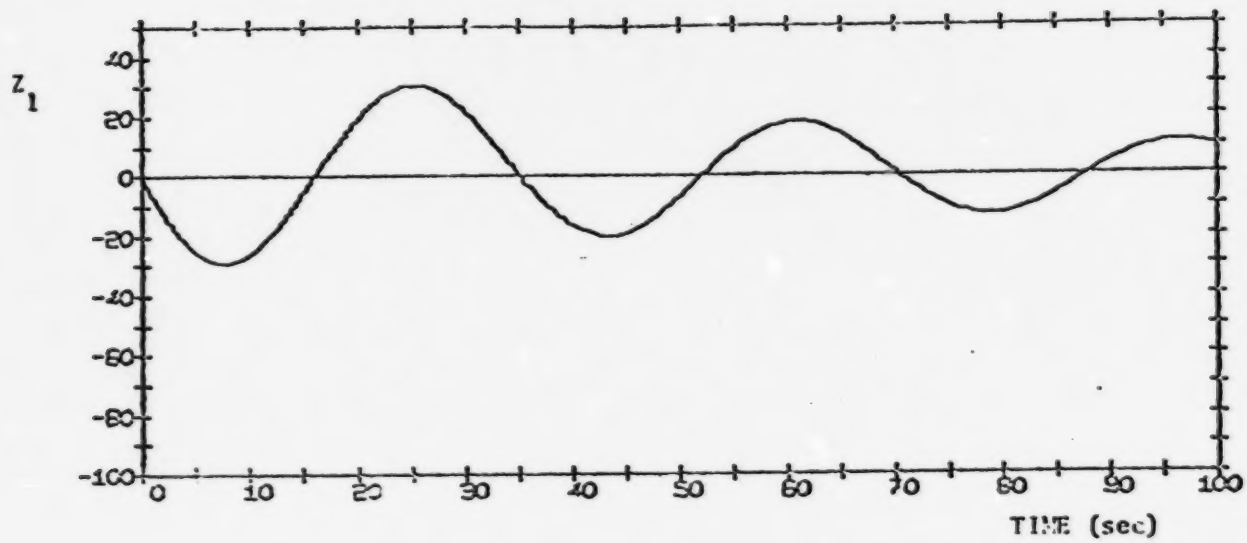

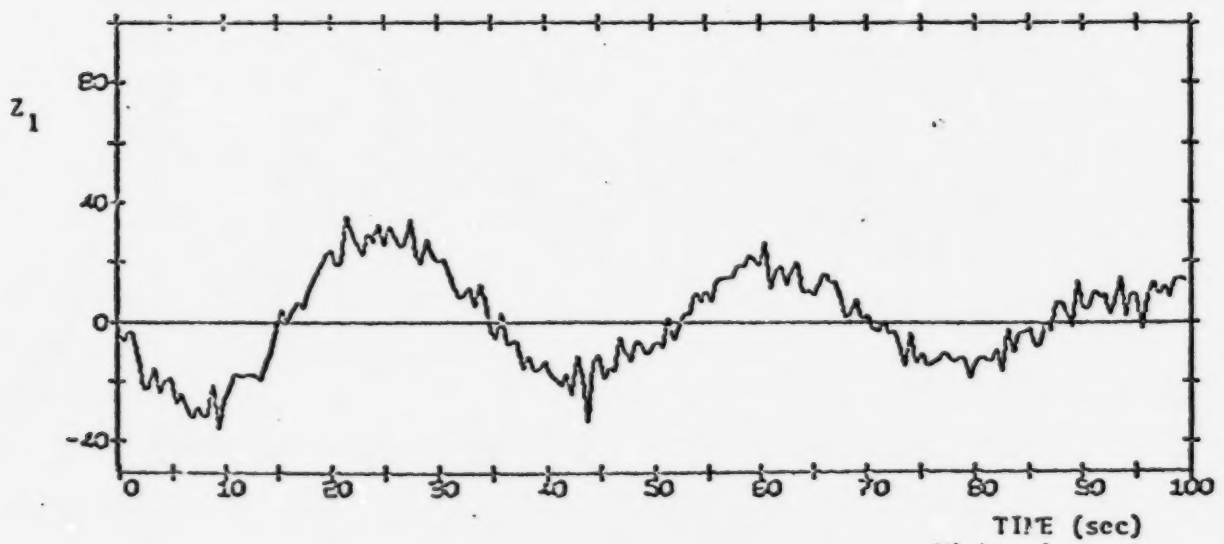

FIG. 7.6 TYPICAL OUTPUTS FOR INITIAL CONDITION INPUT (CASE II) FOR ZERO NOISE AND HIGH NOISE RESPECTIVELY.

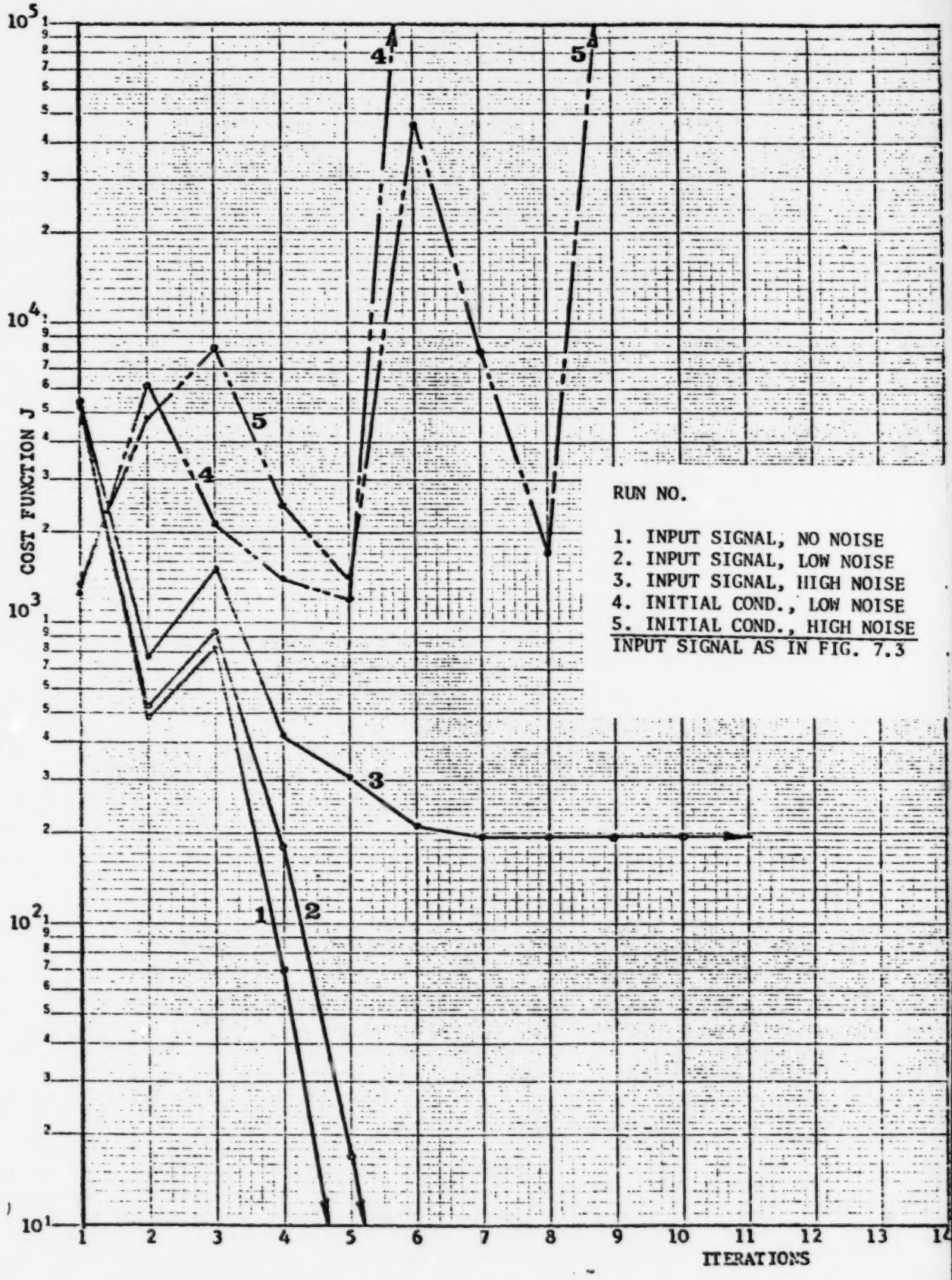
COST FUNCTION J
ITERATIONS
RUN NO.
1. INPUT SIGNAL, NO NOISE
2. INPUT SIGNAL, LOW NOISE
3. INPUT SIGNAL, HIGH NOISE
4. INITIAL COND., LOW NOISE
5. INITIAL COND., HIGH NOISE
INPUT SIGNAL AS IN FIG. 7.3

FIG. 7.7 COST FUNCTION J AS A FUNCTION OF NUMBER OF ITERATIONS FOR RUNS 1 TO 5.

The matrices $\underset{\sim}{A}$ and $\underset{\sim}{B}$ recovered for runs (2) and (3) (case i) are given in Table 7.2, and the cost function J as a function of the number of iterations is given in Figure 7.7. These results show that the recovered values for case (i) are quite good even for the high noise run, (3). No results were obtained for case (ii), corresponding to initial condition disturbance only, because, as is shown in Figure 7.7, the programme diverged.

System Matrix $\underset{\sim}{A}$				Control Matrix $\underset{\sim}{B}$	
-0.2767,	0.0477,	-11.413,		8.2770	4.1600
0.0017,	-0.2057,	2.172,	0	-1.1409	-3.7590
0.0827,	-1.0014,	-0.3147,	0.0790	0	0
1.0000,	0.0	0.0	0.0	0	0

Run (2) Control Signal Input, Medium Noise

System Matrix $\underset{\sim}{A}$				Control Matrix $\underset{\sim}{B}$	
-0.3281,	-0.2340,	-11.673,	0	8.3028,	3.8461
0.0104,	-0.1645,	2.218,	0	-1.1572,	-3.7211
0.0770,	-1.0255,	-0.3084,	0.079	0	0
1.0,	0.0	0.0	0.0	0	0

Run (3) Control Signal Input, High Noise

TABLE 7.2 MATRICES $\underset{\sim}{A}$ AND $\underset{\sim}{B}$ RECOVERED FOR RUNS (2) AND (3) CASE I ONLY.

7.4 Conclusions

The failure of the procedure to converge for case (ii) - an initial condition disturbance only - illustrates the difficulties that can be encountered. At the time of writing, a reason for this failure had not been established.

8) BUCKLING OF SKIRT MATERIAL

8.1) Introduction

8.1.1) Discussion of Previous Work

In prior work at UTIAS for TDC on the static roll stiffness characteristics of a multicell cushion system [Refs. 8.1, 8.4], the buckling characteristics of the tapered conical cell that constituted the principal element of that cushion was investigated theoretically and experimentally. It had been found that, for sufficiently large roll angles, the cells would collapse and cause a large loss of both lift and restoring moment.

The analysis reported in Ref. 8.1 proceeded on the basis of a number of key simplifying assumptions. These are:

(i) the cell is a membrane,

(ii) the material is incapable of sustaining any significant compression, so that when the loading is such as to tend to cause the lesser of the two principal stresses in certain parts of the membrane to become negative, the structure wrinkles locally,

(iii) prior to wrinkling the membrane is effectively inelastic,

(iv) the destabilizing mechanism is the internal asymmetric pressure loading associated with contact with the ground, and not skirt-ground friction,

(v) the state of stress in the cell is the same as that which would occur if the cell is cut along a line arbitrarily close to but not touching the ground; that is, the bottom of the skirt is a free edge,

(vi) for the fabric materials used in skirt models, the structure fails in buckling at the onset of wrinkling.

The assumptions lead to a remarkably simple prediction that, when the bottom of the cell is in contact with the ground plane at all points of its periphery, and the flow through the cell is said to be "shut off", the buckling angle is equal to the taper angle of the cone. Although this seemed to agree with experimental observations described in Ref. 8.4, the experiments described in Ref. 8.1 have demonstrated that the problem is not that simple.

For example, assumption (v) was motivated by the "single-wrinkle-creep" phenomenon reported in Ref. 8.1. It appeared that, for the elastomer-fabric materials used in the UTIAS model tests, the cells were unable to sustain any significant regions of wrinkling prior to buckling. This is in contrast to previously published analyses and experiments on pressurized membrane structures [see for example, Refs. 8.2 and 8.3] which show that substantial regions of wrinkling can occur. This wrinkling generally leads to significant softening of any characteristic load-displacement curve for the structure well in advance of buckling. The behaviour of the cells made from an elastomer-

fabric appears to be associated with the anisotropic properties of that material, since experimental observation of the buckling of cells made from polyethylene film, a material believed to be isotropic, showed that substantial regions of wrinkling would then occur prior to buckling. This greatly complicates the analysis, because the equations describing a partly wrinkled structure are intrinsically nonlinear. This is discussed in Section 8.1.2. It should be noted that it is not clear if the "single-wrinkle-creep" phenomenon occurs on the elastomer-fabric combinations used on the skirts of full scale vehicles.

Reference 8.1 describes an attempt made to verify the applicability of assumption (v), the so-called "cut-skirt" boundary condition. The preliminary results described in Ref. 8.1 suggested that contact with the ground actually induces a small longitudinal tension at the bottom, which in turn appeared to have a very significant stabilizing effect. The validity and significance of this finding remain to be assessed.

However some useful points were established. For example, experiments on a two-cell model reported in Ref. 8.1 gave reasonably convincing evidence that the destabilizing mechanism is in fact the internal hydrostatic pressure loading. Furthermore, the buckling angle seemed to be reasonably insensitive to manufacturing imperfections, in contrast to more classical shell buckling problems [Ref. 8.5]. And, although the experimental results reported in Ref. 8.1 indicated that the buckling angle showed a significant dependence on material thickness, which is in clear contrast to the prediction by the simplified inelastic membrane theory - in which material thickness does not enter - this does not mean that local bending must be important in the unwrinkled portions of the structure. The onset of wrinkling implies that relatively large deformations occur, so that the deformation of the unwrinkled parts of the structure must be described in some suitable fashion, and these parts must be treated as elastic. But they nevertheless remain very thin compared to the local radii of curvature describing the basic structural shape and may be treated as a membrane. Hence it appears that assumptions (i) to (iv) may still be used for the analysis of this problem.

It is important to appreciate that this problem differs in many aspects from classical shell buckling problems, so that it appears that much of the existing work is not particularly appropriate. For example, classical analyses incorporate local bending effects and that is why the resultant buckling formulae for shells (q, v, e.g., Ref. 8.5) depend on the cube of the wall thickness. In the present problem, significant bending effects occur only locally, such as at the points where a cell is clamped to the vehicle hard structure, or in the interior of wrinkled regions.

8.1.2) Effects of Wrinkling on Membrane Structures

It is important to appreciate the significance of the wrinkling phenomenon on the task of computing structural stability for air cushion skirt systems, so that the meaning of various terms used above is now explored. Some features of the process are illustrated by consideration of the "N-string beam problem" depicted in figure 8.1. In this problem a structure

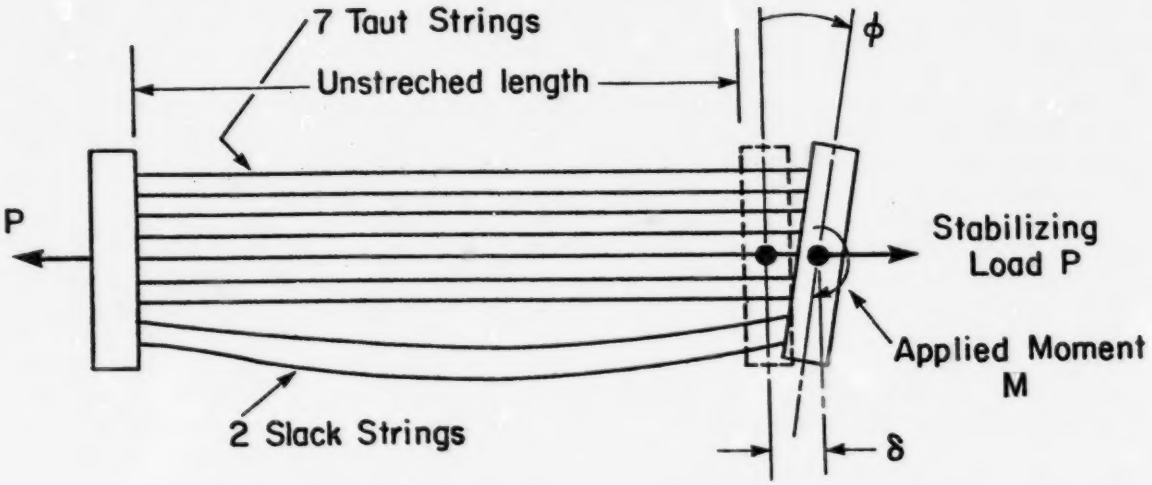

FIG. 8.1 N-STRING-BEAM ANALOGUE OF WRINKLING

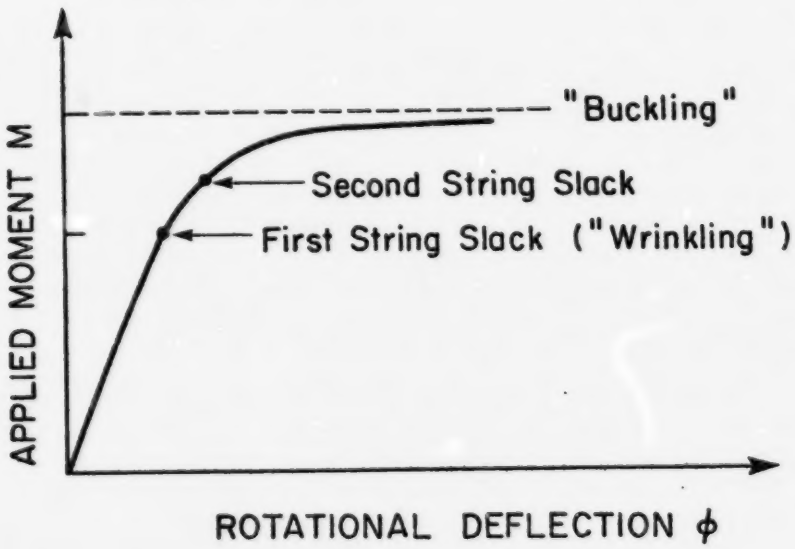

FIG. 8.2 STIFFNESS CHARACTERISTICS OF STRING-BEAM

consisting of a large number of strings clamped to two short bars is subject to a fixed tensile load P applied centrally and parallel to the string axes. This causes an extension δ. A pure moment M is applied to a bar at one end; this causes the bar to rotate through an angle θ. The strings are made from a material that has linear elastic properties, that is, the extension of the i-th string is proportional to the axial load Pi applied to that string, $\delta_i = k_s P_i$.

Now consider the process that occurs as the moment M is increased from zero. Initially, while all of the strings remain taut, the overall structural deflection θ is proportional to M. Eventually, for large enough M_w the lowest string will be subject to zero P_i. Any further increase in M causes the string to go slack; it is, in effect, removed from the structure. The slope of the curve of M as a function of θ also suddenly decreases, and the structure has become softer. Further increases in M will sequentially remove more of the strings and the structure progressively becomes even softer. This is depicted in figure 8.2. Structural failure or buckling, in the sense that a small increase in M causes an indefinitely large increase in θ, only occurs when the last string but one goes slack. However, from a practical viewpoint, the system may become unacceptably soft long before total collapse occurs.

Two important points to note are that, although the structure as a whole shows a strong nonlinear behaviour the material properties are still linear. Also, increasing the axial preload P increases the moment capacity of the system.

For the cone problem, the principal stresses act along the hoop and longitudinal or "generator" directions. The hoop stress is determined by the internal cushion pressure, and it is the longitudinal stress which is progressively reduced as the destabilizing moment is increased. Wrinkling occurs, by hypothesis, in order to prevent this stress becoming negative. In contrast to the string problem, the wrinkled region is not effectively removed, since the hoop tension still remains. It might be more useful to view the phenomenon as equivalent to that which would be obtained by using a nonlinear orthotropic materialwhich becomes extremely soft in one of its two characteristic directions as the strains go negative.

It should also be noted that the counterpart of the axial preload P which acts to stabilize the system is the internal cushion pressure. It is this which induces the longitudinal tension in the cone. However, unlike the string problem, the destabilizing condition is - according to the inelastic membrane theory - independent of cell pressure. This is because both the longitudinal tension and the destabilizing moment are proportional to the cell pressure.

8.1.3) Distinction Between Wrinkling and Buckling for the Cone Problem

It is noted above that, in the series of experiments undertaken for the previous TDC Contract [Ref. 8.1] some results were obtained for a skirt material thought to be isotropic, namely 0.127 mm thick extruded polyethylene film. This corresponds to a skirt thickness ratio C_{ST}* of about 2.5×10^{-4},

*C_{ST} is defined as the ratio of skirt thickness to a suitable reference dimension for the skirt geometry L_{ref}. Here L_{ref} is equal to the cell diameter at the point of attachment to the hard structure.

which appears to be typical for an elastomer-fabric skirt material. It was observed that, for this material, wrinkling occurred well before buckling. However, no data on this aspect of the problem was recorded.

Prior to the start of the present Contract, additional observations of the behaviour of a polyethylene cell were made and these are described briefly here. The experimental arrangement was the same as that described in Ref. 8.1; that is to say, a given fixed load was applied and a known volume flux pumped through the cell. While these quantities were held constant, the roll angle was gradually increased until first wrinkling and then buckling occurred. The term "buckling" as used here is associated with a sudden increase in cushion air escape area leading to venting of the cell followed immediately by loss of cushion pressure and collapse of the cell. The results were repeated several times for a given weight, and obtained for a range of weights. The data was also checked for any possible effects of forces due to sliding friction between the skirt and the ground.

The data obtained from these experiments is given in figure 8.3, which gives the wrinkling and buckling angles, ϕ_W and ϕ_B, as a function of load W_{eq} carried by the cell at $\phi = 0°$. Figure 8.4 is a photograph of a cell in which substantial wrinkling is present. The first point to note is that, as for previously reported tests, the buckling is not affected by any skirt-ground friction. The results obtained for the smooth surface of the basic cushion table, when the surface was covered by a rough abrasive garnet paper, and using the "rolling board" technique, were effectively the same.

The major point to note is that wrinkling occurs well before the onset of buckling, typically ϕ_W/ϕ_B ranges from 0.57 to 0.49 as W_{eq} increases from 9.1 kg to 22.7 kg. During these tests, the growth of the wrinkled region was observed as ϕ was increased, and these observations provided a useful insight into the buckling mechanism. This is depicted in figure 8.5, which shows the shape, location and size of the wrinkled region for three values of ν_W. The first corresponds to ν just after the onset of wrinkling, the second is for ν at an intermediate value, while the third corresponds to a value of ν just prior to collapse. The wrinkling starts at the point suggested by the inelastic membrane theory developed in Ref. 8.1, namely at the points at which the bottom of the fully deployed skirt intersects the ground plane [point A in figure 8.5 (i)]. The wrinkled region is approximately rhomboidal in shape, and as θ increases, it grows in size, but retains this shape. The bottom tip also remains at the point A. Two wrinkled regions occur, one each side of the cell, and failure occurs when the two tips of the rhomboidal shapes meet as shown in figure 8.1 (iii). Because of the symmetry, this occurs on the conical surface generator FF'. It is worth noting that this failure mode has a strong resemblance to that suggested for the N-string problem.

Finally it should be noted that the onset of wrinkling exhibited by the data in figure 8.4 shows a strong dependence on applied load; in the present problem this is consistent with the theory developed in Ref. 8.1. An increase in load at fixed volume flux generally results in an increase in cushion pressure. This must be associated with a reduction in air escape area; this implies that the flow aperture angle θ_c in figure 2.8 of Ref. 8.1 must decrease. The critical angle ϕ_{cr} of figure 2.11 must also decrease.

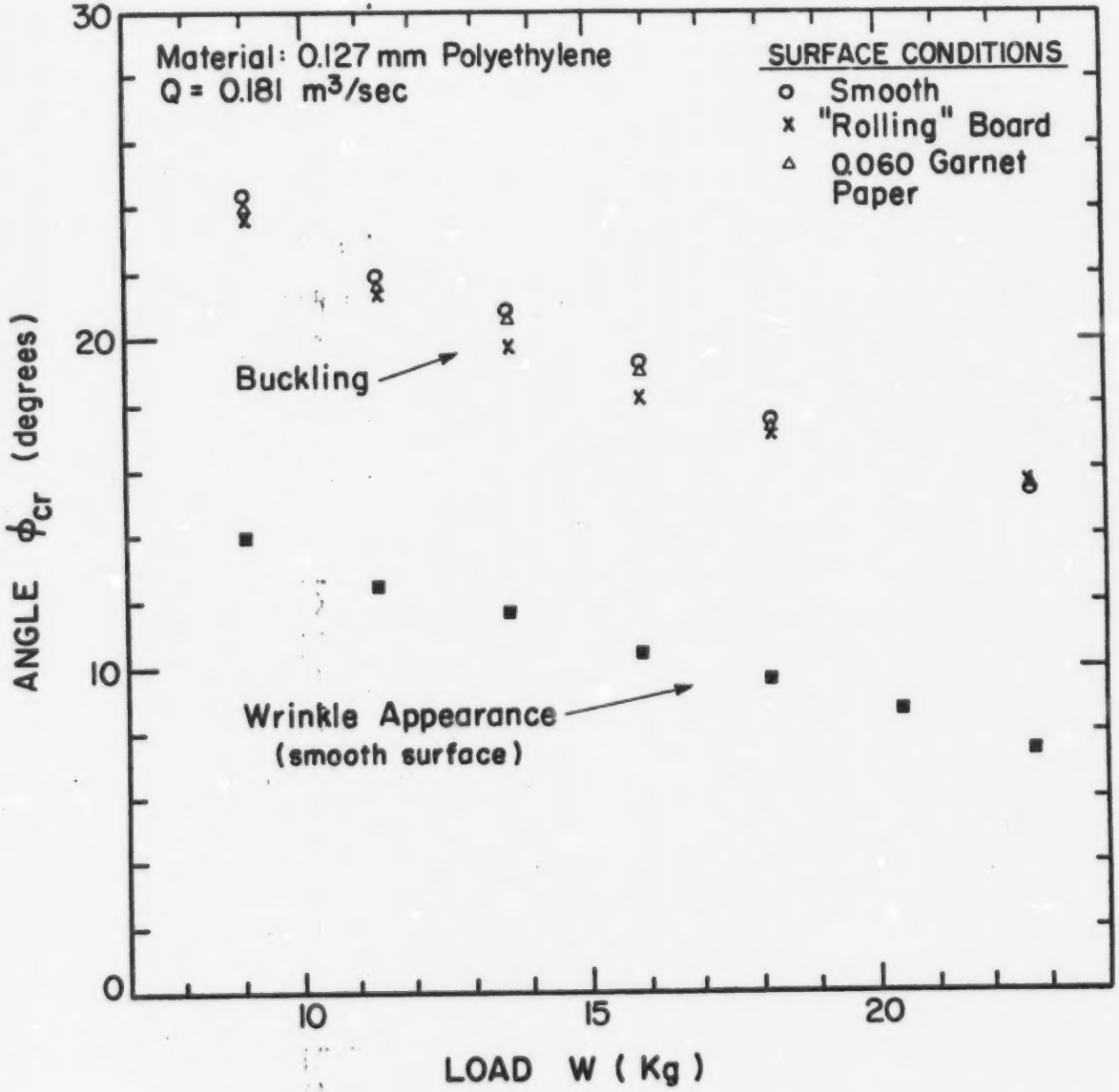

FIG. 8.3 EFFECT OF TOTAL WEIGHT ON ROLL ANGLE AT WHICH WRINKLING AND BUCKLING FIRST OCCURS

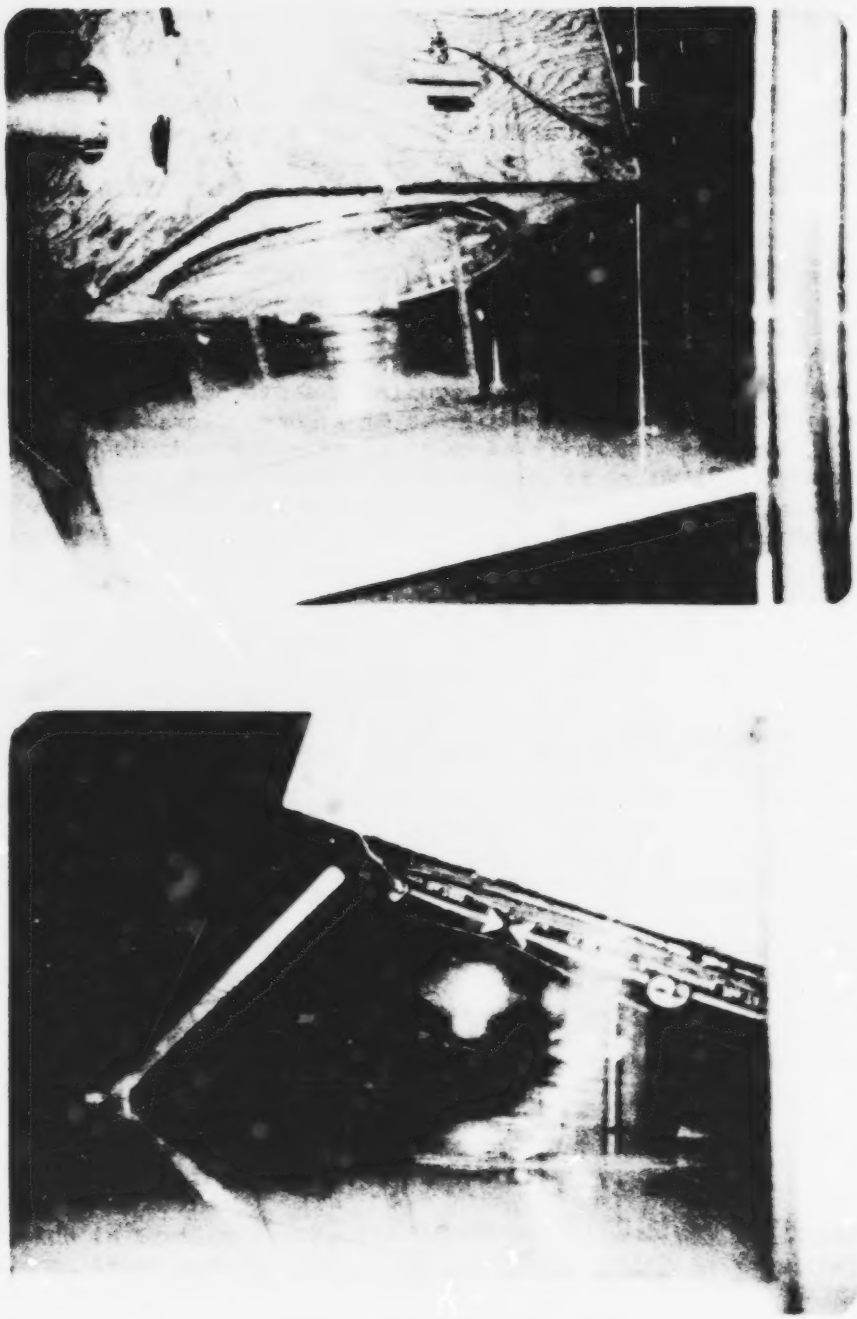

FIG. 8.4 PHOTOGRAPHS OF POLYETHYLENE CELL USED IN TESTS DESCRIBED IN FIGURE 8.3. LARGE WRINKLED REGIONS ARE CLEARLY VISIBLE.

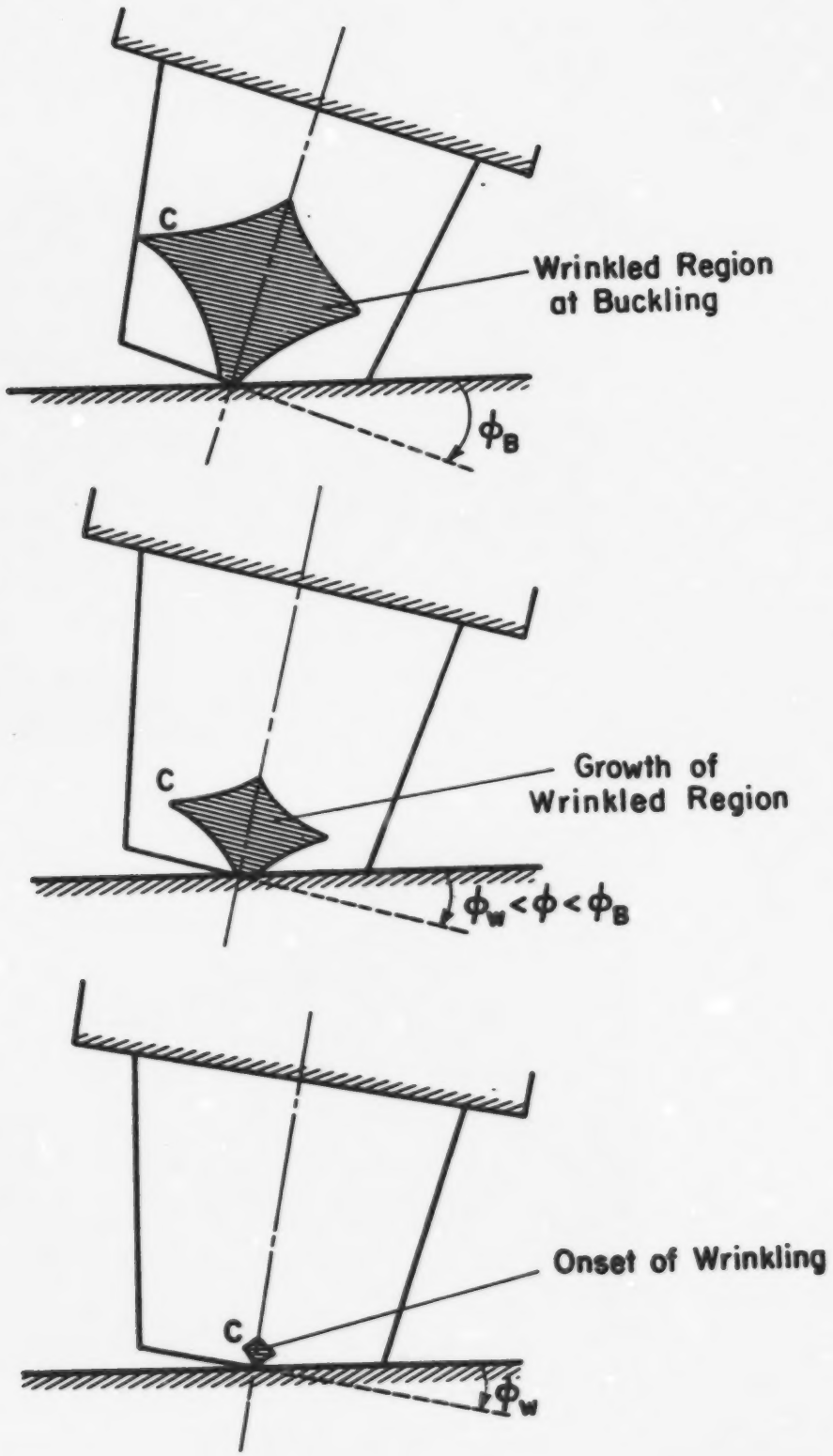

Fig. 8.5 Details of Failure Process for Conical Cell. Buckling Occurs when Points C of the two Diamond Shaped Regions Meet.

8.1.4) Comments on the Importance of Material Bending Effects

It appears that, for the cone problem and for other skirt configurations, plate-type bending effects occur in the overall structure only in certain specific locations, and may only have a secondary role to play. Typically, for the cone problem, one can identify three regions where bending effects are significant:

(i) in the immediate neighbourhood of the points where the skirt is attached to the vehicle base or "hard structure",

(ii) in the immediate neighbourhood of the points where the skirt contacts the ground,

(iii) in wrinkled regions, where bending effects determine the wavelength of the wrinkles as shown in figure 8.4.

It seems evident that bending phenomena (i) and (iii) may exert only a second order effect in the overall failure process. However, in Section 8.2 it is shown that small changes in tension at the bottom of the cone - in the neighbourhood of the region of skirt-ground contact, presumably induced by bending, can have a large effect on the onset of wrinkling. However, at the time of writing, it is not known if this is an effect peculiar to the conical geometries or indicative of what might be expected for other cushions.

8.1.5) Principal Objectives of the Present Work

As discussed in Ref. 8.1, the "single-wrinkle-creep" phenomenon encountered at one stage in the UTIAS programme raised the expectation that, for design purposes on practical cushion geometries, one might be able to bypass the complex process of analysis of a partly wrinkled structure. It was envisaged that one would simply use inelastic membrane theory to predict the initiation of wrinkling, and assume that buckling occurred soon after. However, the results given in figure 8.3 clearly indicate that, for isotropic materials at least, wrinkling can occur well before the structure may have failed.

Hence the work planned for the remainder of the present Contract is focussed on two points:

(i) exploration and development of methods for the analysis of partly wrinkled membrane structures, and

(ii) investigation of the nature of the wrinkling/buckling process for elastomer-fabric materials.

As is discussed in Section 8.1.2, the wrinkling process may be characterized by a highly nonlinear orthotropic elastic material which is very soft in compression. Because of this relationship between the two objectives it has been decided to focus attention on the development of a finite element numerical computer programme to analyse the buckling properties of shells

made from orthotropic materials. In the first instance the analysis is to be developed for cylindrical shells, but ultimately it is intended to extend this to geometries representative of cushion elements.

8.2) Effect of a Small Uniform Tension at the Bottom of a Conical Cell

8.2.1) Introduction

One complication in solving the conical cell buckling problem is the nature of the boundary condition that should be applied at the bottom. Formally this condition is that no part of the skirt material can lie below the ground surface as discussed in Ref. 8.1. To simplify the analysis, this condition was replaced by the so-called "cut-skirt" condition noted in Section 8.1.1. In a series of tests with the polyethylene material, described in Ref. 8.1, the skirt geometry in the immediate neighbourhood of the ground assumed the form shown in figure 8.6. This suggests that the effect of skirt-ground contact may be to induce a positive tension in the membrane, so that the correct boundary condition is not that the longitudinal stress be zero, but a positive tension dependent on the cushion pressure. Clearly this implies that skirt-ground contact has a stabilizing influence, but how significant is this effect? The analysis given below follows closely that given in Ref. 8.1; it is intended to include the modified boundary condition. Only the case in which the flow is shut-off is considered; that is, case A of Ref. 8.1.

As the manipulations involved in the analysis are somewhat lengthy, one may proceed directly to a discussion of the results given in Section 8.2.3.

8.2.2) Analysis

We assume that the bottom of the conical membrane is always in ground contact as shown in figure 8.6. The only forces acting on the membrane is the cushion pressure. The equations of equilibrium are [Ref. 8.1]

$$\frac{\partial}{\partial s}(sN_s) + \frac{1}{\cos\alpha}\frac{\partial N_{s\theta}}{\partial \theta} - N_\theta = 0 \qquad (1a)$$

$$\frac{\partial}{\partial s}(sN_{s\theta}) + \frac{1}{\cos\alpha}\frac{\partial N_\theta}{\partial \theta} + N_{s\theta} = 0 \qquad (1b)$$

$$N_\theta = ps\cot\alpha \qquad (1c)$$

The symbols are the same as in Ref. 8.1. The angle $\alpha = \pi/2 - \beta$ as shown in Figure 8.9. Solving for N_s and $N_{s\theta}$ we obtain

$$N_s = \frac{ps\cot\alpha}{2} + \frac{C_1'(\theta)}{s^2\cos\alpha} + \frac{C_2(\theta)}{s} \qquad (2a)$$

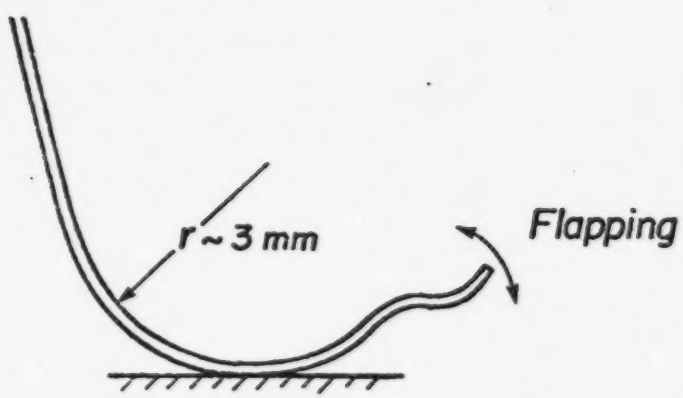

FIG. 8.6 DETAILS OF SKIRT-GROUND CONTACT

$$N_{s\theta} = \frac{C_1(\theta)}{s^2} \tag{2b}$$

where

$$C_1'(\theta) \triangleq \frac{d}{d\theta}\,[C_1(\theta)]$$

and $C_1(\theta)$ and $C_2(\theta)$ are constant along each generator of the cone. The function of integration $C_1(\theta)$ and $C_2(\theta)$ are specified by the boundary conditions applied at the bottom of the membrane. The coordinate system is shown in figure 8.7.

The latter conditions become as shown in figure 8.8

$$N_T = 0 \quad \text{and} \quad N_N = \text{given at } s = s_1(\theta)$$

where $s = s_1(\theta)$ is the equation which defines the bottom of the skirt.

To apply these boundary conditions, we consider a triangular element at the bottom of the skirt as shown in figure 8.4. Considering forces in the hoop direction, we have:

$$N_\theta \delta\ell_2 = N_{s\theta}\delta\ell_1 + N_N \delta\ell^* \sin\eta$$

or since

$$\frac{\delta\ell_2}{\delta\ell_1} = \tan\eta; \qquad \frac{\delta\ell_1}{\delta\ell^*} = \cos\eta; \qquad \frac{\delta\ell_2}{\delta\ell^*} = \sin\eta$$

$$N_{s\theta} = (N_\theta - N_N)\tan\eta \tag{3}$$

Now, if we consider forces in the s-direction

$$N_s \delta\ell_1 = N_{s\theta}\delta\ell_2 + N_N \delta\ell^* \cos\eta$$

or

$$N_s = N_{s\theta}\tan\eta + N_N \tag{4}$$

and if (3) is substituted in (4)

$$N_s = N_\theta \tan^2\eta + N_N(1 - \tan^2\eta) \tag{5}$$

Since N_θ is determined by the internal pressure, that is $N_\theta = ps\cot\alpha$, equations (3) and (5) give two boundary conditions for $C_1(\theta)$ and $C_2(\theta)$ at $s = s_1(\theta)$.

The equation which defines the bottom of the skirt is given by (see figure 8.7 and Ref. 8.1)

$$s_1(\theta) = \frac{H\sec\alpha}{\tan\alpha - \sin\theta\tan\phi} \tag{6}$$

with slope relative to a plane perpendicular to the cone axis by

$$\tan\eta = \frac{\sec\alpha\tan\phi\cos\theta}{\tan\alpha - \sin\theta\tan\phi} \tag{7}$$

Imposing these boundary conditions at $s = s_1(\theta)$ on equations (2), we obtain the following for $C_1(\theta)$ and $C_2(\theta)$.

$$C_1(\theta) = H^2\sec^3\alpha\tan\phi[p\cot\alpha\, H\sec\alpha - N_N z(\theta)]\frac{\cos\theta}{z^4(\theta)} \tag{8}$$

$$C_2(\theta) = \frac{p\cot\alpha\, H^2\sec^4\alpha\tan^2\phi\cos^2\theta}{z^3(\theta)} - \frac{p\,H^2\cot\alpha\sec^2\alpha}{2z^2(\theta)}$$

$$+ \frac{H^2\sec\alpha}{z^3(\theta)}[z^2(\theta) - \sec^2\alpha\tan^2\phi\cos^2\theta] - \frac{H\sec^3\alpha\tan\phi}{z^3(\theta)}\left[N_N\cos^2\theta\tan\phi\right.$$

$$\left. - [p\cot\alpha\, H\sec\alpha - N_N z(\theta)]\left(\sin\theta - \frac{4\cos^2\theta\tan\phi}{z(\theta)}\right)\right] \tag{9}$$

where we have written $z(\theta) = \tan\alpha - \tan\phi\sin\theta$ for convenience. If $N_N = 0$, the same results as Ref. 8.1 for $C_1(\theta)$ and $C_2(\theta)$ are obtained. Substituting these two equations in (2), it follows after some tedious algebraic manipulation

$$N_s = \frac{p\,s\cot\alpha}{2} + \frac{H^3 p\cot\alpha\sec^5\alpha\tan\phi}{s^2 z^4(\theta)}\left(\frac{4\cos^2\theta\tan\phi}{z(\theta)} - \sin\theta\right)$$

$$+ \frac{pH^2\cot\alpha\sec^2\alpha}{sz^2(\theta)}\left[\frac{1}{2} + \frac{3\sec^2\alpha\tan^2\phi\cos^2\theta}{z^2(\theta)} - \frac{\sec^2\alpha\tan\phi\sin\theta}{z(\theta)}\right]$$

$$+ N_N\left[\frac{H^2\sec^4\alpha\tan\phi}{s^2 z^3(\theta)}\left(\sin\theta - \frac{3\cos^2\theta\tan\phi}{z(\theta)}\right)\right.$$

$$\left. + \frac{H\sec\alpha}{sz(\theta)}\left(1 + \frac{2\sec^2\alpha\tan^2\phi\cos^2\theta}{z^2(\theta)} - \frac{\sec^2\alpha\tan\phi\sin\theta}{z(\theta)}\right)\right] \tag{10a}$$

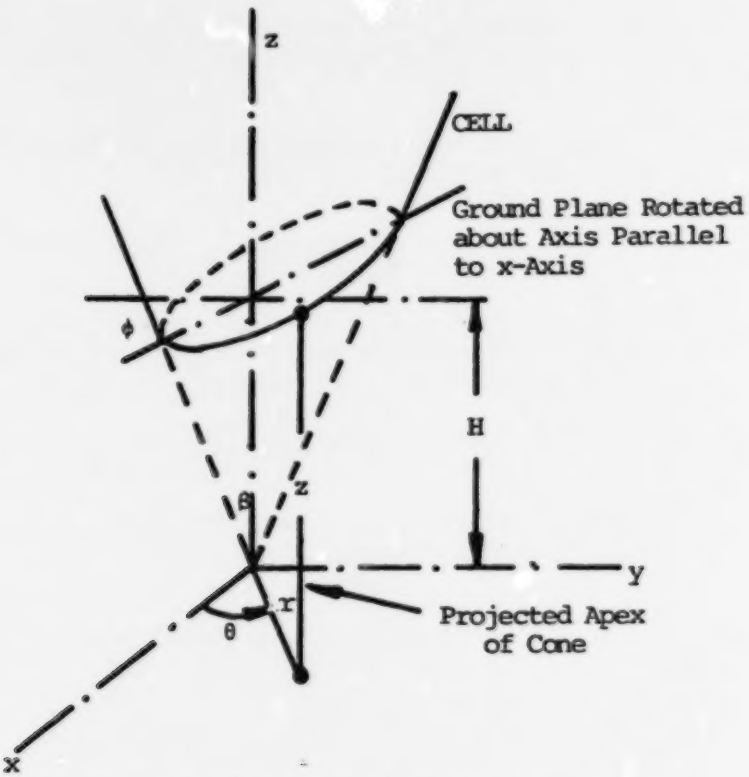

S = DISTANCE ALONG CONE SURFACE FROM APEX

S_1 = DISTANCE ALONG CONE TO GROUND PLANE FROM APEX

FIG. 8.7 COORDINATE SYSTEM FOR CONICAL CELL GEOMETRY

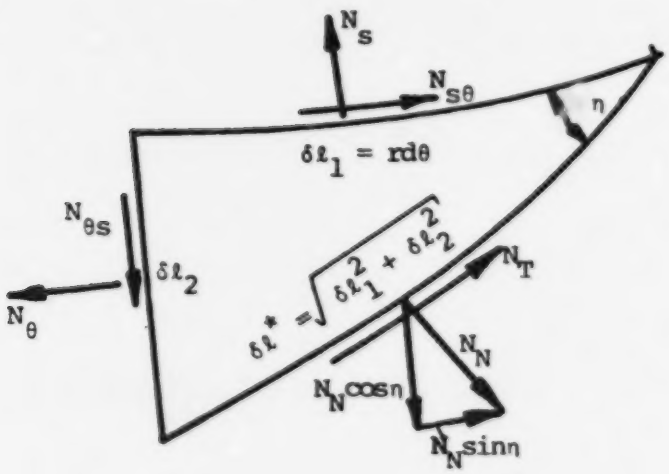

FIG. 8.8 BOTTOM EDGE BOUNDARY CONDITION WITH UNIFORM TENSION APPLIED

$$N_{s\theta} = \frac{pH^3 \sec^4\alpha \cot\alpha \tan\phi \cos\theta}{s^2 z^3(\theta)} - N_N \frac{H^2 \sec^3\alpha \tan\phi \cos\theta}{s^2 z^3(\theta)} \qquad (10b)$$

$$N_\theta = ps\cot\alpha \qquad (10c)$$

Again, if $N_N = 0$, these equations simplify to the same results as given in Ref. 8.1.

For the dimensionless form of the above equations, if the top diameter D_T, the cone angle α and the height H_1 are known, as shown in figure 8.9, then H and S_T are readily calculated. We define

$$\bar{s} = \frac{s - s_1(\theta)}{s_T - s_1(\theta)} \qquad (11)$$

so that when

$s = s_1(\theta)$, $\quad \bar{s} = 0$ (ground plane)

$s = s_T$, $\quad \bar{s} = 1$ (top of conical cell)

Rewriting (11) with the aid of equation (6),

$$\frac{s}{H} = \bar{s}\left(\frac{S_T}{H} - \frac{\sec\alpha}{z(\theta)}\right) + \frac{\sec\alpha}{z(\theta)} \qquad (12)$$

The stress-resultants are nondimensionalized with the hoop stress evaluated at the top of the cell which is $N_{\theta T} = ps_T\cot\alpha$. In particular define $\epsilon = \frac{N_N}{N_{\theta T}}$. The nondimensional stresses become

$$\bar{N}_s = \frac{1}{2}\left(\frac{H}{s_T}\right)\left(\frac{s}{H}\right) + \left(\frac{H}{s_T}\right)\frac{1}{(s/H)^2}\frac{\sec^5\alpha \tan\phi}{z^4(\theta)}\left(\frac{4\cos^2\theta\tan\phi}{z(\theta)} - \sin\theta\right)$$

$$- \left(\frac{H}{s_T}\right)\frac{1}{(s/H)}\frac{\sec^2\alpha}{z^2(\theta)}\left[\frac{1}{2} + \frac{3\sec^2\alpha \tan^2\phi \cos^2\theta}{z^2(\theta)} - \frac{\sec^2\alpha \tan\phi \sin\theta}{z(\theta)}\right]$$

$$+ \epsilon\left[\frac{\sec^4\alpha \tan\phi}{(s/H)^2 z^3(\theta)}\left(\sin - \frac{3\cos^2\theta \tan\phi}{z(\theta)}\right)\right.$$

$$\left. + \frac{1}{(s/H)}\frac{\sec\alpha}{z(\theta)}\left(1 + \frac{2\sec^2\alpha \tan^2\phi \cos^2\theta}{z^2(\theta)} - \frac{\sec^2\alpha \tan\phi \sin\theta}{z(\theta)}\right)\right] \qquad (13a)$$

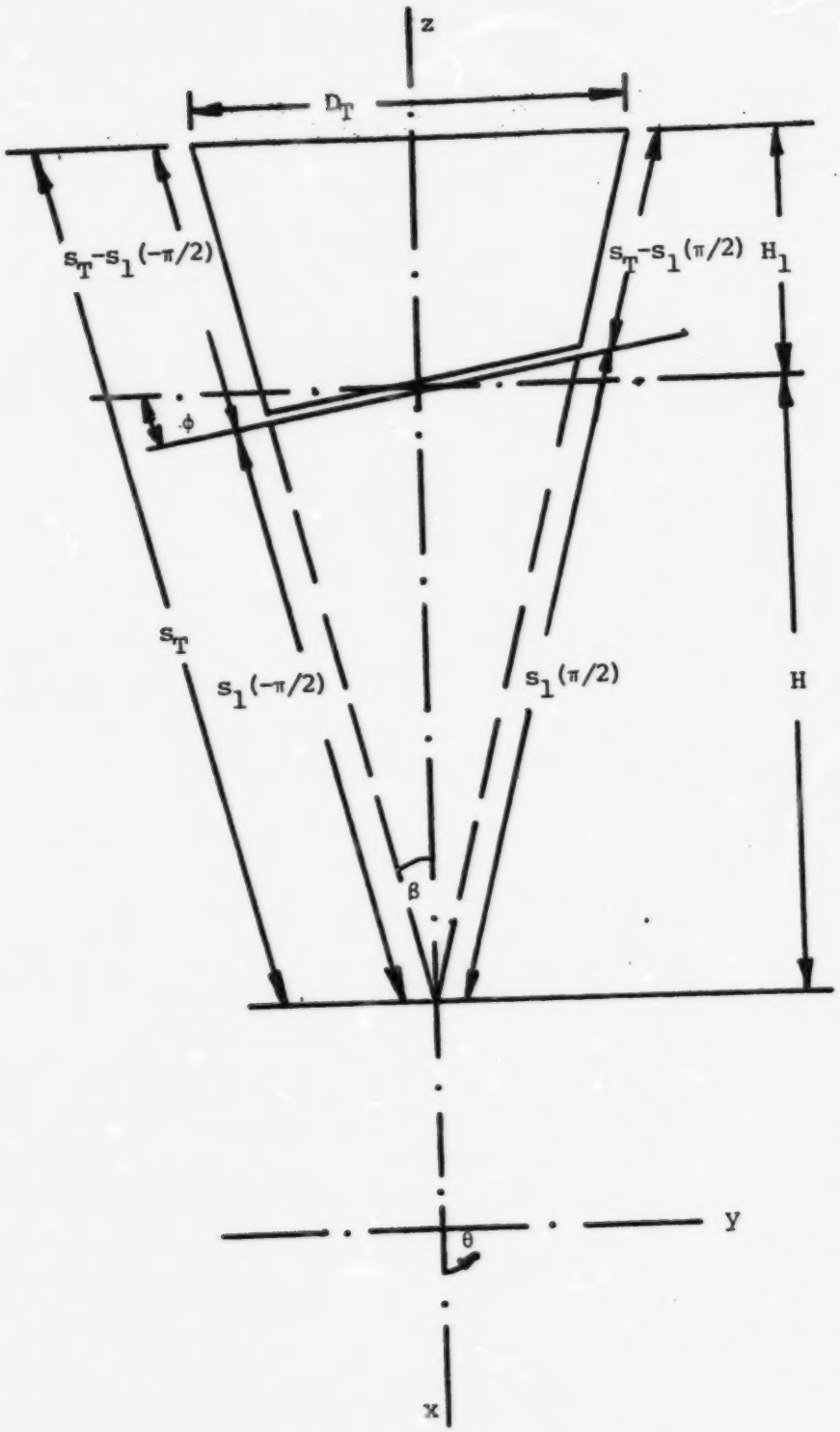

FIG. 8.9 GEOMETRICAL FEATURES OF CONICAL CELL

$$\bar{N}_{s\theta} = \left(\frac{H}{s_T}\right) \frac{\sec^4\alpha \tan\phi \cos\theta}{(s/H)^2 z^4(\theta)} - \epsilon \frac{\sec^3\alpha \tan\phi \cos\theta}{(s/H)^2 z^3(\theta)} \tag{13b}$$

$$\bar{N}_{\theta} = \left(\frac{H}{s_T}\right)\left(\frac{s}{H}\right) \tag{13c}$$

where

$$\bar{N}_s = \frac{N_s}{N_{sT}}; \quad \bar{N}_\theta = \frac{N_\theta}{N_{sT}}; \quad \bar{N}_{s\theta} = \frac{N_{s\theta}}{N_{sT}}; \quad z(\theta) = \tan\alpha - \tan\phi \sin\theta$$

The condition for wrinkling to occur is

$$\bar{N}_s \bar{N}_\theta - \bar{N}_{s\theta}^2 \leq 0$$

Let us define a function

$$\bar{F}(\bar{s}, \theta, \phi, \epsilon) = \bar{N}_s \bar{N}_\theta - \bar{N}_{s\theta}^2 \tag{14}$$

if

$$\begin{aligned} \bar{F}(\bar{s}, \theta, \phi, \epsilon) &\leq 0 \quad \text{wrinkling} \\ &> 0 \quad \text{no wrinkling} \end{aligned} \tag{15}$$

where

$$0 \leq \bar{s} \leq 1$$

$$0 \leq \theta \leq 2\pi$$

ϵ is a small positive number

8.2.3) Results

Recall that ϵ is the induced longitudinal stress imposed at the bottom expressed as a fraction of the hoop stress at the top; $z = N_N/(p s_T \cot\alpha)$ (see figure 8.9). The objective is to find ϕ_{cr}, the critical roll angle when wrinkling first occurs for a given tension at the bottom ϵ. That is

If $\phi < \phi_{cr}$ $\quad \bar{F} > 0$ the cell is in full tension

If $\phi \geq \phi_{cr}$ $\quad \bar{F} \leq 0$ the cell has a compression somewhere on the cone surface

For the special case when $\epsilon = 0$, equation (14) is always zero at $\bar{s} = 0$, which is readily seen from equations (3) and (5). We will not call this wrinkling, since for $\phi < \phi_{cr}$, for all possible values of $\bar{s}$ and θ the cell is in full tension.

With this in mind, a computer program was developed to find the critical roll angle ϕ_{cr}. The parameters for the conical membrane are those used in the tests described in Ref. 8.1 and Section 8.1.3: $\alpha = 84°$ ($\beta = 6°$); $D_T = 0.508$m (20 in); $H_1 = 0.3048$m (12 in), from which we readily have: $s_T = 2.430$m (95.67 in); $H = 2.112$m (83.15 in). The results are plotted in figure 8.10.

When there is no tension at the bottom of the conical membrane ($\epsilon = 0$), the critical roll angle is equal to the taper angle. But we have the remarkable result that, if a uniform tension of only 10% of the hoop stress evaluated at the top of the cone is applied at the bottom ($\epsilon = 0.1$), we more than double ϕ_{cr}. From figure 8.10, ϕ_{cr} grows linearly for $0.1 \leq \epsilon \leq 0.1$.

8.2.4) Conclusions

This result suggests that considerable care has to be exercised in choosing the effective boundary condition to be applied in the neighbourhood of regions of skirt-ground contact. Seide [Ref. 8.6] also mentions that for stress analysis of conical shells, the results depend strongly on the boundary conditions applied at the small end of the shell. However the implications for the stress analysis of ACV skirts is not clear. For example, it is not known if such sensitivity would occur for other skirt geometries.

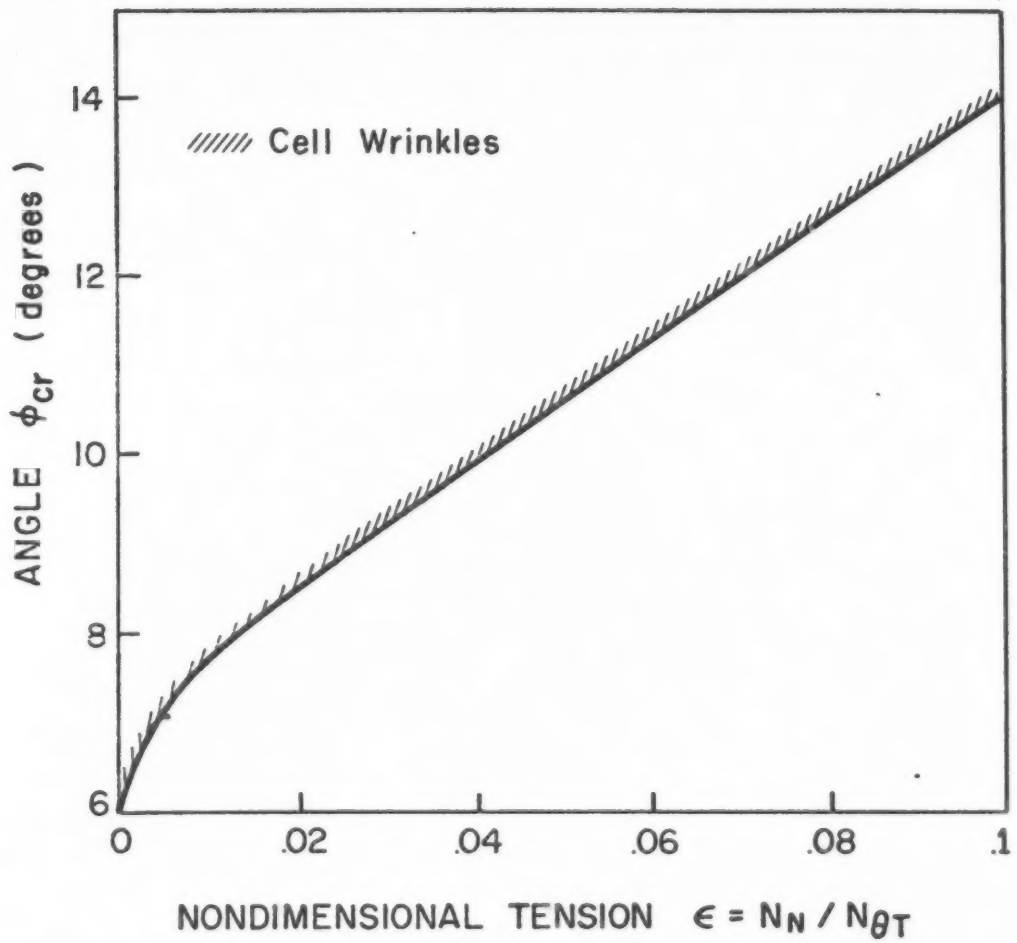

FIG. 8.10 EFFECT OF SMALL UNIFORM TENSION AT BOTTOM EDGE ON ONSET OF WRINKLING.

REFERENCES

Section 2

2.1 Richardson, H. H., and Ribich, W. A., "Dynamics Analysis of Heave Motion for a Transport Vehicle Fluid Suspension", Massachusetts Institute of Technology Report, DSR 75110-3, 1966.

2.2 Captain, K., and Richardson, H. H., "Heave Dynamics of Flexible Base Fluid Suspensions", Massachusetts Institute of Technology Report, DSR 76110-9, 1969.

2.3 Leatherwood, J. D., Dixon, G. V., and Stephens, D. G., "Heave Dynamics of a Plenum Air Cushion Including Passive and Active Control Concepts", NASA TN 5202, 1969.

2.4 Genin, J., Ginsberg, J. H., and Ting, E. C., "Fluid Suspension Model of Air Cushioned Vehicles", Journal of Sound and Vibration, 25, 1, 83-93, 1972.

2.5 Sweet, L. M., Richardson, H. H., and Wormley, D. N., "Plenum Air Cushions/Compressor-Duct Dynamic Interactions", American Society of Mechanical Engineers, Paper No. 75-WA/AUT-23, 1975.

2.6 Goodson, R. E., and Leonard, R. G., "A Survey of Modelling Techniques for Fluid Line Transients", Americal Society of Mechanical Engineers, Paper No. 71-WA/FE-9, 1971.

2.7 Streeter, V. L., and Wylie, E. B., Hydraulic Transients, New York: McGraw-Hill, First edition, Chapters 2 and 7, 1967.

2.8 Goldschmeid, F. R., and Wormley, D. N., "Frequency Response of Blower/Duct/Plenum Systems", Journal of Hydronautics 11, 1, 18-27, 1977.

2.9 Leatherwood, J. D., "Analog Analysis of the Heave Response and Control of a Plenum-Type Air-Cushion Vehicle", NASA TN D-6257, 1971.

2.10 Wormley, D. N., Garg, D., and Boghani, A. B., Massachusetts Institute of Technology Department of Mechanical Engineering Report, 1972.

2.11 Sullivan, P. A., Hinchey, M. J., Murra, I., and Paravano, G. J., "Research on the Stability of Air Cushion Systems", University of Toronto, Institute for Aerospace Studies Report No. 238, November 1979 T.D.C. File D-500-308.

2.12 Sullivan, P. A., Hinchey, M. J., and Delaney, R. G., "An Investigation of the Roll Stiffness Characteristics of Three Flexible Skirted Cushion Systems", University of Toronto Institute for Aerospace Studies Report No. 213, [T.D.C. File D-500-203-1], 1977.

2.13 Oden, J. T., Finite Elements of Nonlinear Continua, 131, New York: McGraw-Hill, first edition, 1972.

2.14 Finlayson, B. A., The Method of Weighted Residuals and Variational Principles 35, New York: Academic Press, first edition, 1972.

2.15 Huebner, K., The Finite Element Method for Engineers, 49-50, New York: Wiley Interscience, first edition, 1975.

2.16 Kinsler, L., and Frey, A., Fundamentals of Acoustics, 193, New York: John Wiley and Sons, second edition, 1962.

2.17 Pellegrin, M. T., and Bajura, R. A., "Pulsating Flow of an Incompressible Fluid Through a Sharp-Edged Orifice Meter", Department of Mechanical Engineering and Mechanics, West Virginia University, Report ENG-74-10399-A, 1976.

2.18 Sweet, L. M., Richardson, H. H., and Wormley, D. N., "Linearized Models, Stability Criteria and Experimental Verification for Plenum Air Cushions With Compressor-Duct Interactions", Massachusetts Institute of Technology, Department of Mechanical Engineering, Report DOT FR 10007, 1974.

2.19 Hahn, W., Stability of Motion, 8, New York: Springer-Verlag, 1967.

2.20 Fowler, H. S., "The Caspar Research Project, the Multicell Skirt, A Summary", National Research Council of Canada, Associate Committee on Air Cushion Technology Report 5-76, 1976.

Section 3

3.1 Wheeler, R., "Recent United Kingdon Hovercraft Development". Journal of Hydronautics, Vol. 12, No. 1, Jan. 1978, pp. 3-17.

3.2 Durkin, J., and Langhi, W., "An Investigation of the Performance of a Centrifugal Lift Fan Operating Against Sinusoidally Varying Back Pressure". Canadian Air Cushion Technology Symposium, Sept. 1974.

3.3 Streeter, V. and Wylie, E., Hydraulic Transients. 1st Edition, McGraw Hill, New York, N. Y., 1967, p.p. 32-37, p. 116.

3.4 Ohashi, H., "Analytical and Experimental Study of Dynamic Characteristics of Turbopumps". National Aeronautics and Space Administration TN D-4298, April 1968.

3.5 Hinchey, M. and Sullivan, P. A., "Duct Effects on the Dynamic Fan Characteristics of Air Cushion Systems". University of Toronto Institute for Aerospace Studies, Tech. Note. No. 211, June 1977.

3.6 Streeter, V., Fluid Mechanics. 4th Edition, McGraw Hill, New York, N. Y., pp. 466-469, 1966.

3.7 Kinsler, L. and Frey, A. Fundamentals of Acoustics. 2nd Edition, John Wiley and Sons Inc., New York, N. Y., 1962, p. 193.

Section 4

4.1 Fowler, H. S., "The Multicell Skirt, A Summary", National Research Council of Canada, Associate Committee on Air Cushion Technology, Technical Report 5/76. Caspar ACV Research Project Report No. 4, 1976.

4.2 Fowler, H. S., Private Communication, National Research Council of Canada, 1979.

4.3 Sullivan, P. A., Green, G. M. and Hartmann, P. V., "Pitch and Roll Stiffness Characteristics of a Segmented Skirt Cushion", Canadian Symposium on Air Cushion Technology, Montreal, 1979.

4.4 Ribich, W. A. and Richardson, H. H., "Dynamic Analysis of Heave Motion for a Transport Vehicle Fluid Suspension", Massachusetts Institute of Technology, Report DSR 76110-3, 1967.

4.5 Sweet, L. M., Richardson, H. H. and Wormley, D. N., "Plenum Air Cushions/Compressor-Duct Dynamic Interactions", American Society of Mechanical Engineers, Paper No. 75-WA/AUT-23, 1975.

4.6 Hinchey, M. J. and Sullivan, P. A., "Duct Effects on the Heave Stability of Plenum Air Cushions", Journal of Sound and Vibration, 60, 1, 87-99, 1978.

4.7 Hinchey, M. J., "Heave Instabilities of Amphibious Air Cushion Suspension Systems", Ph.D. Thesis, University of Toronto, 1979.

4.8 Leatherwood, J. D., "Analog Analysis of the Heave Response and Control of a Plenum Type Air Cushion Vehicle", National Aeronautics and Space Administration, TN D 6257, 1971.

4.9 Gelb, A. and Vander Velde, W. E., Multiple Input Describing Functions and Nonlinear System Design, McGraw-Hill, New York, 1968.

4.10 Sullivan, P. A., Hinchey, M. J. and Delaney, R. G., "Static Roll Stiffness Characteristics of Two Multicell Type Air Cushion Systems", Journal of Terramechanics, 15, 1, 15-49, 1978.

4.11 Sullivan, P. A., Hinchey, M. J., Murra, I. and Parravano, G. J., "Research on the Stability of Air Cushion Systems", University of Toronto, Institute for Aerospace Studies, Report No. 238, 1979.

4.12 Kinsler, L. E. and Frey, A. R., Fundamentals of Acoustics, John Wiley & Sons, New York, 1962.

4.13 Parravano, G. J. and Sullivan, P. A., "A Theoretical and Experimental Investigation of a Hinged Lip Tracked Air Cushion Vehicle Suspension System", Transport Canada, Research and Development Centre, Contract Report D-500-210, 1977.

4.14 Nayfeh, A. H. and Mook, D. T., Nonlinear Oscillations, Wiley-Interscience, New York, 1980.

4.15 Klotter, K., "An Extension of the Conventional Concept of the Describing Function", Proceedings of the Symposium on Nonlinear Circuit Analysis, Polytechnical Institute of Brooklyn, New York, 1956.

4.16 Klotter, K., "How to Obtain Describing Functions for Nonlinear Feedback Systems", Transactions of the American Society of Mechanical Engineers, pp. 509-512, April 1957.

4.17 Johansen, P., "A Numerical Formulation of Galerkin's Method and Its Application to Nonlinear Engineering Problems", Ph.D. Thesis, Purdue University, 1970.

4.18 Bergen, A. R. and Franks, R. L., "A Justification of the Describing Function Method", SIAM Journal of Control, 9, 4, 1971.

4.19 Cesari, L., "Functional Analysis and Periodic Solutions of Nonlinear Differential Equations", Contributions to Differential Equations, Vol. 1, Wiley-Interscience, New York, 1962

4.20 Finlayson, B. A., The Method of Weighted Residuals and Variational Principles, First Edition, Academic Press, New York, 1972.

4.21 Gradshteyn, I. S. and Ryzhik, I. M., Tables of Integrals, Series and Products, Fourth Edition, Academic Press, New York, 1965.

4.22 Oldenburger, R., "Signal Stabilization of a Control System", Transactions of the American Society of Mechanical Engineers, 79, pp. 1869-1872, 1957.

4.23 Oldenburger, R. and Liu, C. C., "Signal Stabilization of a Control System", Transactions of the American Institute of Electrical Engineers, 78, pp. 96-100, 1959.

4.24 Oldenburger, R. and Nakada, T., "Signal Stabilization of Self Oscillating Systems", Institute of Radio Engineers Transactions on Automatic Control, AC 6, pp. 319-325, 1961.

4.25 Oldenburger, R. and Boyer, R. D., "Effects of Extra Sinusoidal Inputs to Nonlinear Systems", Journal of Basic Engineering, 84, 4, pp. 559-570, 1962.

Section 5

5.1 Parravano, G. J. and Sullivan, P. A., "A Theoretical and Experimental Investigation of a Hinged Lip Tracked Air Cushion Vehicle Suspension System", Transport Canada, Research and Development Centre, Contract Report TDC File D-500-210, March 1977.

5.2 Fowler, H. S., Private Communication, National Research Council of Canada.

5.3 Jones, D., Private Communication.

5.4 Kinsler, L. E. and Frey, A. R., Fundamentals of Acoustics, John Wiley and Sons, New York, p. 186, 1962.

5.5 Pellegrin, M. T. and Bajura, R. A., "Pulsating Flow of an Incompressible Fluid through a Sharp-Edged Orifice Meter", West Virginia University, Faculty of Engineering, Report ENG-74-10399-A, 1976.

5.6 Hersh, A. S. and Walker, B., "Fluid Mechanical Model of the Helmholtz Resonator", National Aeronautics and Space Administration, Contractor Report CR-2904, September 1977.

Section 6

6.1 Sweet, L. M., Richardson, H. H. and Wormley, D. N., "Plenum Air Cushions/Compression-Duct Dynamic Interactions", American Society of Mechanical Engineers, Paper No. 75-WA/AUT-23, 1975.

6.2 Sullivan, P. A., Hinchey, M. J., Murra, I. and Parravano, G. J., "Research on the Stability of Air Cushion Systems", Transport Canada, Research and Development Centre, Report No. TP 1469, 1977, UTIAS Report No. 238, 1979.

6.3 Gosman, I. and Ideriah, "Teach-T, A General Computer Program for Two Dimensional, Turbulent, Recirculating Flows", Department of Mechanical Engineering, Imperial College of Science and Technology, London, 1976.

6.4 Roache, P., Computational Fluid Dynamics, Hermosa Publishers, 1972.

6.5 Heubner, K., The Finite Element Method for Engineers, Wiley-Interscience, New York, 1975.

6.6 Launder, B. and Spalding, D., Mathematical Models of Turbulence, Academic Press, London, 1972.

6.7 Hanjalic, K. and Launder, B., "A Reynolds-Stress Model of Turbulence and Its Application to Axisymmetric Shear Flows", Journal of Fluid Mechanics, 62, 609, 1972

6.8 Gosman, A., Khalil, and Whitelaw, J., "The Calculation of Two Dimensional Turbulent Recirculating Flows", Department of Mechanical Engineering, Imperial College of Science and Technology, London, 1977.

6.9 Pope, S., "An Explanation of the Turbulent Round Jet/Plane Jet Anomaly", AIAA Journal, 16, 3, 1978.

6.10 Roshko, A., "Structure of Turbulent Shear Flows: A New Look", AIAA Journal

6.11 Libby, P., "On the Prediction of Intermittent Turbulent Flows", Journal of Fluid Mechanics, 68, 1975.

6.12 Builtjes, P., "Memory Effects in Turbulent Flows", Delft University of Technology, Report WTHD, 97, 1977.

6.13 Deardorff, J., "A Numerical Study of Three Dimensional Turbulent Channel Flow at Large Reynolds Numbers", Journal of Fluid Mechanics, 41, 1970.

6.14 Finlayson, B., The Method of Weighted Residuals and Variational Principles, Academic Press, New York, 1972.

6.15 Jacobs, D., "A Corrected Upwind Differencing Scheme Using a Strongly Implicit Solution Procedure", Numerical Methods in Fluid Dynamics, Pentech Press, London, 1973.

6.16 Raithby, G., "Skew Upstream Differing Schemes for Problems Involving Fluid Flow", Computer Methods in Applied Mechanics and Engineering, 9, North-Holland, 1976.

Section 7

7.1 Liebelt, P. B., An Introduction to Optimal Estimation, Addison-Wesley, New York, 1967.

7.2 Graupe, D., Identification of Systems, McGraw-Hill, New York, 1972.

7.3 Sage, and Melsa, Estimation Theory with Application to Communication and Control, McGraw-Hill, New York, 1972.

7.4 Sage, and Melsa, System Identification, Academic Press, New York, 1971.

7.5 Denery, D. G., "Identification of System Parameters from Input-Output Data with Application to Air Vehicles", National Aeronautics and Space Administration, Tech. Note TN D-6468, August 1971.

7.6 Gelb, A., [Editor], Applied Optimal Estimation, Massachusetts Institute of Technology Press, Cambridge, Massachusetts, 1974.

7.7 Bekey, G. A., "System Identification - An Introduction and a Survey", Simulation, pp. 151-166, October 1970.

7.8 Stephner, D. E., and Mehra, R. K., "Maximum Likelihood Identification and Optimal Input Design for Identifying Aircraft Stability and Control Derivatives", National Aeronautics and Space Administration, Contractor Report CR 2200, 1973.

7.9 Dixon, L. C. W., Nonlinear Optimization, Crane, Russak and Company, New York, 1972.

7.10 Taylor, L. W., and Iliff, K. W., "System Identification Using a Modified Newton-Raphson - A Fortran Program", National Aeronautics and Space Administration Technical Note TN D-6734, 1972.

7.11 Iliff, K. W., and Taylor, L. W., "Determination of Stability Derivatives from Flight Data Using a Newton-Raphson Minimization Technique", National Aeronautics and Space Administration Technical Note TN D-6579, 1973.

Section 8

8.1 Sullivan, P. A., Hinchey, M., Murra, I., and Parravano, G. J., "Research on the Stability of Air Cushion Systems", TDC File D-500-308, UTIAS Report No. 238, November 1979.

8.2 Stein, M., and Hedgepeth, J. M., "Analysis of Partly Wrinkled Membranes", National Aeronautics and Space Administration Technical Note TN D-813, 1961.

8.3 Miller, R. P., "Experimental Bending Strength of an ATLAS LV-3C Booster, Beyond Compression Skin Wrinkling", National Aeronautics and Space Administration Technical Note TN-D-5156, April 1969.

8.4 Sullivan, P. A., Hinchey, M. J., and Delaney, R. G., "An Investigation of the Roll Stiffness Characteristics of Three Flexible Skirted Cushion Systems", TDC File D-500-203-1, UTIAS Report No. 238, November 1979.

8.5 Tennyson, R. C., UTIAS, Private Communication.

8.6 Seide, P., "A Survey of Buckling Theory and Experiments for Circular Conical Shells of Constant Thickness", National Aeronautics and Space Administration Technical Note TN D-1510, 1962, pp. 401-426

7.9 Dixon, L. C. W., Nonlinear Optimization, Crane, Russak and Company, New York, 1972.

7.10 Taylor, L. W., and Iliff, K. W., "System Identification Using a Modified Newton-Raphson - A Fortran Program", National Aeronautics and Space Administration Technical Note TN D-6734, 1972.

7.11 Iliff, K. W., and Taylor, L. W., "Determination of Stability Derivatives from Flight Data Using a Newton-Raphson Minimization Technique", National Aeronautics and Space Administration Technical Note TN D-6579, 1973.

Section 8

8.1 Sullivan, P. A., Hinchey, M., Murra, I., and Parravano, G. J., "Research on the Stability of Air Cushion Systems", TDC File D-500-308, UTIAS Report No. 238, November 1979.

8.2 Stein, M., and Heigepeth, J. M., "Analysis of Partly Wrinkled Membranes", National Aeronautics and Space Administration Technical Note TN D-813, 1961.

8.3 Miller, R. P., "Experimental Bending Strength of an ATLAS LV-3C Booster, Beyond Compression Skin Wrinkling", National Aeronautics and Space Administration Technical Note TN-D-5156, April 1969.

8.4 Sullivan, P. A., Hinchey, M. J., and Delaney, R. G., "An Investigation of the Roll Stiffness Characteristics of Three Flexible Skirted Cushion Systems", TDC File D-500-203-1, UTIAS Report No. 238, November 1979.

8.5 Tennyson, R. C., UTIAS, Private Communication.

8.6 Seide, P., "A Survey of Buckling Theory and Experiments for Circular Conical Shells of Constant Thickness", National Aeronautics and Space Administration Technical Note TN D-1510, 1962, pp. 401-426

POOR

QUALITY

ORIGINAL